UNIVERSITÀ DI TRENTO | Department of Industrial Engineering

XXXV Cycle

Doctoral School in Materials, Mechatronics and System Engineering

Modeling and Simulation of Vehicle Emissions for the Reduction of Road Traffic Pollution

Mostafa Rahimi

January 2023

Modeling and Simulation of Vehicle Emissions for the Reduction of Road Traffic Pollution

Mostafa Rahimi

Email: mostafa.rahimi@unitn.it

Approved by:

Prof. **Daniele Bortoluzzi**, Advisor
Dept. of Industrial Engineering
University of Trento, Italy

Prof. **Jens Wahlström**, Co-tutor
Dept. of Mechanical Engineering
Lund University, Sweden

Ph.D. Commission:

Dr. **Yezhe Lyu**
Dept. of Mechanical Engineering
Lund University, Sweden

Prof. **Giuseppe Loprencipe**
Dept. of Civil, Construction and Environmental Engineering
University of Roma La Sapienza

University of Trento

Department of Industrial Engineering

January 2023

University of Trento – Department of Industrial Engineering

Doctoral Thesis

Mostafa Rahimi – January 2023

Published in Trento (Italy) – by University of Trento

ISBN: ----------

Abstract

The transportation sector is responsible for the majority of airborne particles and global energy consumption in urban areas. Its role in generating air pollution in urban areas is even more critical, as many visitors, commuters and citizens travel there daily for various reasons. Emissions released by transport fleets have an exhaust (tailpipe) and a non-exhaust (brake wears) origin. Both exhaust and non-exhaust airborne particles can have destructive effects on the human cardiovascular and respiratory systems and even lead to premature deaths. This dissertation aims to estimate the amount of exhaust and brake emissions in a real case study by proposing an innovative methodology. For this purpose, different levels of study have been introduced, including the subsystem level, the system level, the environmental level and the suprasystem level. To address these levels, two approaches were proposed along with a data collection process. First, a comprehensive field survey was conducted in the area of Buonconsiglio Castle and data was collected on traffic and non-traffic during peak hours. Then, in the first approach, a state-of-the-art simulation-based method was presented to estimate the amount of exhaust emissions generated and the rate of fuel consumption in the case study using the VISSIM traffic microsimulation software and Enviver emission modeler at the suprasystem level. In order to calculate the results under different mobility conditions, a total of 18 scenarios were defined based on changes in vehicle speeds and the share of heavy vehicles (HV%) in the modal split. Subsequently, the scenarios were accurately modelled in the simulation software VISSIM and repeated 30 times with a simulation runtime of three hours. The results of the first approach confirmed the simultaneous effects of considering vehicle speed and HV % on fuel consumption and the amount of exhaust emissions generated. Furthermore, the sensitivity of exhaust emissions and fuel consumption to variations in vehicle speed was found to be much higher than HV %. In other words, the production of NOx and VOC emissions can be increased by up to 20 % by increasing the maximum speed of vehicles by 10 km/h. Conversely, increasing the HV percentage at the same speed does not seem to produce a significant change. Furthermore, increasing the speed from 30 km/h to 50 km/h increased CO emissions and fuel consumption

by up to 33%. Similarly, a reduction in speed of 20 or 10 km/h with a 100% increase in HV resulted in a 40% and 27% decrease in exhaust emissions per seat, respectively. In the second approach, a novel methodology was proposed to estimate the number of brake particles in the case study. To achieve this goal, a downstream approach was proposed starting from the suprasystem level (microscopic traffic simulation models in VISSIM) and using a developed mathematical vehicle dynamics model at the system level to calculate the braking torques and angular velocities of the front and rear wheels, and proposes an artificial neural network (ANN) as a brake emission model, which has been appropriately trained and validated using emission data collected through more than 1000 experimental tribological tests on a reduced-scale dynamometer at the subsystem level (braking system). Consideration of this multi-level approach, from tribological to traffic-related aspects, is necessary for a realistic estimation of brake emissions. The proposed method was implemented on a targeted vehicle, a dominant SUV family car in the case study, considering real driving conditions. The relevant dynamic quantities of the targeted vehicle (braking torques and angular velocities of the wheels) were calculated based on the vehicle trajectory data such as speed and deceleration obtained from the traffic microsimulation models and converted into braking emissions via the artificial neural network. The total number of brake emissions emitted by the targeted vehicles was predicted for 10 iterations route by route and for the entire traffic network. The results showed that a large number of brake particles (in the order of billions of particles) are released by the targeted vehicles, which significantly affect the air quality in the case study. The results of this dissertation provide important information for policy makers to gain better insight into the rate of exhaust and brake emissions and fuel consumption in metropolitan areas and to understand their acute negative impacts on the health of citizens and commuters.

Keywords

Traffic Modeling; Traffic Microsimulation; VISSIM; Enviver; Non-exhaust Emissions; Exhaust Emissions; Emission Modeling; Brake Emission; Brake Wear; Airborne Particles; Minidyno; Reduced-scale Dynamometer; Vehicle Longitudinal Dynamics; Artificial Neural Network-based modeling.

Contents

List of Figures

List of Tables

List of Abbreviations

AI	Artificial Intelligence	EF	Emission Factor	NAO	Non-Asbestos Organic pads
ANN	Artificial Neural Network	ELPI+	Electrical Low-Pressure Impactor	OPS	Optical Particle Sizer
APS	Aerodynamic Particle Sizer	FAST	Friction Assessment Screening Test	PIV	Particle Image Velocimetry
BLCF	Brake Linings' coefficient of friction	FEA	Finite Element Analysis	PM	Particulate Matter
CA	Cellular Automaton	FMPS	Fast Mobility Particle Sizer	PM_{10}	Particulate Matter 10μm or less in diameter
CFD	Computational Fluid Dynamics	GDP	Gross domestic product	$PM_{2.5}$	Particulate Matter 2.5μm or less in diameter
CMB	Chemical Mass Balance	HDV	Heavy-duty Vehicle	R&D	Research and Development
CVS	Constant-volume Sampling	HEPA	High Efficiency Particulate Air	RDE	Real Driving Emission
DMS	Differential Mobility Spectrometer	LDV	Light-duty Vehicle	SEM	Scanning Electron Microscopy
DLPI	Dekati Low Pressure Impactor	MCA	Movable Cellular Automata	TEM	Transmission Electron Microscopy
Dyno	Dynamometer	ML	Machine Learning	TRAKER	Testing Re-entrained Aerosol Kinetic Emissions from Roads
EDXS	Energy Dispersive X-ray Spectroscopy	MLR	Multiple Linear Regression	VAPI	Vehicular Air Pollution Inventory
EEA	European Environment Agency	MOUDI	Micro-orifice Uniform Deposit Impactor		

List of Symbols

m	vehicle mass	h	center of mass height	l_f	longitudinal distance between front axle and center of mass
$\ddot{x}$	vehicle acceleration	k_f	front tire longitudinal stiffness	l_r	longitudinal distance between rear axle and center of mass
F_{aero}	aerodynamic drag force	k_r	rear tire longitudinal stiffness	h_{aero}	height of aerodynamic drag force
F_{xf}	longitudinal force of front tire	σ_f	Front longitudinal slip ratio	T_r	rear braking torque
F_{xr}	longitudinal force of rear tire	σ_r	Rear longitudinal slip ratio	T_{rf}	front wheel resistance torque
R_{xf}	front tires rolling resistance force	ω_f	front wheel angular velocity	T_{rr}	rear wheel resistance torque
R_{xr}	rear tires rolling resistance force	ω_r	rear wheel angular velocity	k_b	brake distribution coefficient
g	gravity acceleration	r_{ef}	Front wheel effective radius		
ϑ	road slope	r_{er}	Rear wheel effective radius		
f	rolling resistance coefficient	r_0	undeformed tire radius		
F_{zf}	normal force on front tire	k_t	vertical tire stiffness		
F_{zr}	normal force on rear tire	$\dot{\omega_f}$	front wheel angular acceleration		
ρ	air mass density	$\dot{\omega_r}$	rear wheel angular acceleration		
C_w	aerodynamic drag coefficient	J_f	front wheel inertia		
A	vehicle frontal area	J_r	rear wheel inertia		
$\dot{x}$	vehicle speed	T_f	front braking torque		

Acknowledgements

Foremost, I would like to express my sincere gratitude to my supervisor **Prof. Daniele Bortoluzzi** for the continuous support of my Ph.D. study and research, for his patience, motivation, enthusiasm, wisdom, immersion knowledge, and trust in me. He has always been a key-person for me in inculcating the learning attitude towards cutting-edge research since the beginning of my Ph.D. degree. His guidance helped me in all the time of research and writing of this thesis. I also like to give my warmest thanks to my co-supervisor, **Prof. Jens Wahlström**, for his consistent support throughout my research activities at Lund University, Sweden, which oriented and boosted my Ph.D. studies. Also, it a genuine pleasure to express my deep sense of thanks to the dissertation committee: **Dr. Yezhe Lyu** and **Prof. Giuseppe Loprencipe**, for their encouragements, insightful comments, and brilliant suggestions. A debt of my gratitude is also owed to the **Department of Excellence** for providing funding for this research, without which completion of this research was impossible. Many thanks also to the **Department of Industrial Engineering** for letting me fulfill my dream of being a researcher here.

In addition, I would like to express my most profound appreciation to my father, **Ahmad**, and my mother, **Tahereh**, as I grew up cocooned in their love, comforted by their hugs, and motivated by their lives. They have been the impetus I have ever needed to succeed and the reason behind my successes, and the inspiration behind my endeavors. I should also thank my sisters, **Elnaz** and **Reyhaneh**, who take the time to always be in the right places and right times throughout my life and guide me to do big things in life.

Last but not least, I would like to give special thanks to my lovely wife, **Fatemeh**, who helped me regain hope after despair, resume life after obstructions, restart journeys after detours, revive strength after defeat and resurrect dreams after rejection. My deepest thanks to her for tolerating the difficulties of living in a foreign country to let me follow my academic ambitions. All I know is that I'm incredibly fortunate to have such a down-to-earth and loving wife to lean on and share my thoughts with.

Trento, January 2023,

Mostafa Rahimi

Chapter 1

Introduction

1. Chapter 1: Introduction

1.1. Background

The transportation sector plays a crucial role in enabling the mobility of people, which has been interwoven with the life quality and economy development [1]. Considering the wide range of services to various industries and providing dynamic life for urban infrastructures, it has been reported that almost 7% of the government's income comes from the transportation sector [2]. Also, this sector has a 5% share in reducing the unemployment rate of the communities [2]. Based on various profitability, many European societies consider the transportation sector to be the backbone of country developments [3]. Despite its potential merits, it is known as the biggest contributor in air pollution, accounting for the major emission-related health issues worldwide. Approximately 25% of European Union's greenhouse gas emissions is related to the transportation sector [4]. It was also reported that the rate of carbon dioxide generation released by the transportation sector in Europe has increased from 32% to 45% [5]. Since the past decade, the total amount of transport-origin emissions is elevating unceasingly; reached 7866.01 Mt in 2016 [1], [6].

Many studies have emphasized on the harmful effects of air pollution on human health. In addition to increasing rate of morbidity and mortality mostly due to cardiovascular and respiratory diseases, air pollution can also be one of the cause of asthma, lung cancer, ventricular hypertrophy, Alzheimer's and Parkinson's diseases, psychological complications, autism, retinopathy, fetal growth, and low birth weight [7]. Eye irritations , throw-ups, and odour were also counted as the immediate impacts of vehicular emissions on human body [8]. In the long-term, they may also make tremendous problems for the central nervous and reproductive systems [9]. It has been reported that all these transport-related problems can eventually cause the death of 17,000 to 20,000 people annually [10]. Given such remarkable fatalities and due to increasing worldwide environmental concerns, the reduction of transport-origin emissions has become a key priority at all government levels, especially in developed countries. Fuel standards promotion, fleet efficiency, novel approaches for vehicle emission estimation, eco-driving behaviors, road network improvements, and preventive

rules for the rate of emission generation are all being conducted as an answer to the above concerns.

All the mentioned problems have convinced the policy makers to define preventively rules to reduce air pollution in congested and non-congested areas and provide more sustainable zero-emission transportation systems. In 2011, an integration action was initiated by the European Commission (EC) for terminating the barriers for a sustainable transportation system and boosting mobility in Europe [11]. Regarding this roadmap, a 60% reduction in greenhouse gases was predicted by 2050 in the European Union (EU). Overall, the European Union aims to decrease emissions by 80-95% below 1990 levels by 2050 [11]. Furthermore, considering new technologies for vehicles and traffic management was also introduced in the EC roadmap as one of the critical elements which can significantly help the reduction of transport-related emissions. These technologies include the innovative ideas about emission estimations using more efficient and modern methods to achieve more accurate proportions of generated vehicular pollutants. Furthermore, the EU is planning to introduce limits for brake wear as part of the upcoming Euro 7 emissions standard. The working group of the Particle Measurement Program (PMP) of the EU is currently developing the technical cornerstone for measuring brake wear, which will then be examined by the responsible bodies in the EU Commission [12].

The emissions produced by the transportation sector may have different sources [13]. Emission originated from the non-ideal and/or incomplete combustions of fuel in the vehicle's engine and, accordingly, emitted from the vehicles' tailpipe is called "Exhaust emission" or "tailpipe emission". On the other side, the one which is called "Non-exhaust emission" includes particles generated during the vehicle's brake system operation, the particles generated by the wear of the tire and road contact surfaces due to slip, road dust resuspension, and dry clutches [14].

To provide a better insight for the vehicular emissions features, they can be investigated in three main categories: Subsystem Level, System Level, and Environmental Level. The emission generation rate, both for exhaust and non-exhaust emissions, is directly influenced

by the parameters in these investigation levels. Those dealing with the features of the braking system components in the laboratory environment are categorized in the Subsystem Level whereas the studies in which all the data collection and the investigation of brake wear particles are implemented on-road or in laboratory ambient by using real cars, chassis or brake wear tracers are categorized in System Level. Finally, those in which the sampling is directly performed on the environment, such as roads, rivers, agricultural farms, and runoffs, are categorized in the third level entitled "Environmental Level". In addition to these main categories, there is also another level of investigation called "Suprasystem level", which rules how vehicles (referred to as "systems") behave in the network. The interaction of different individuals with various driving activities can be monitored in this level. Therefore, it can be considered as an investigation level between System Level and Environmental Level. Figure 1-1 presents the relationships between all these investigation levels.

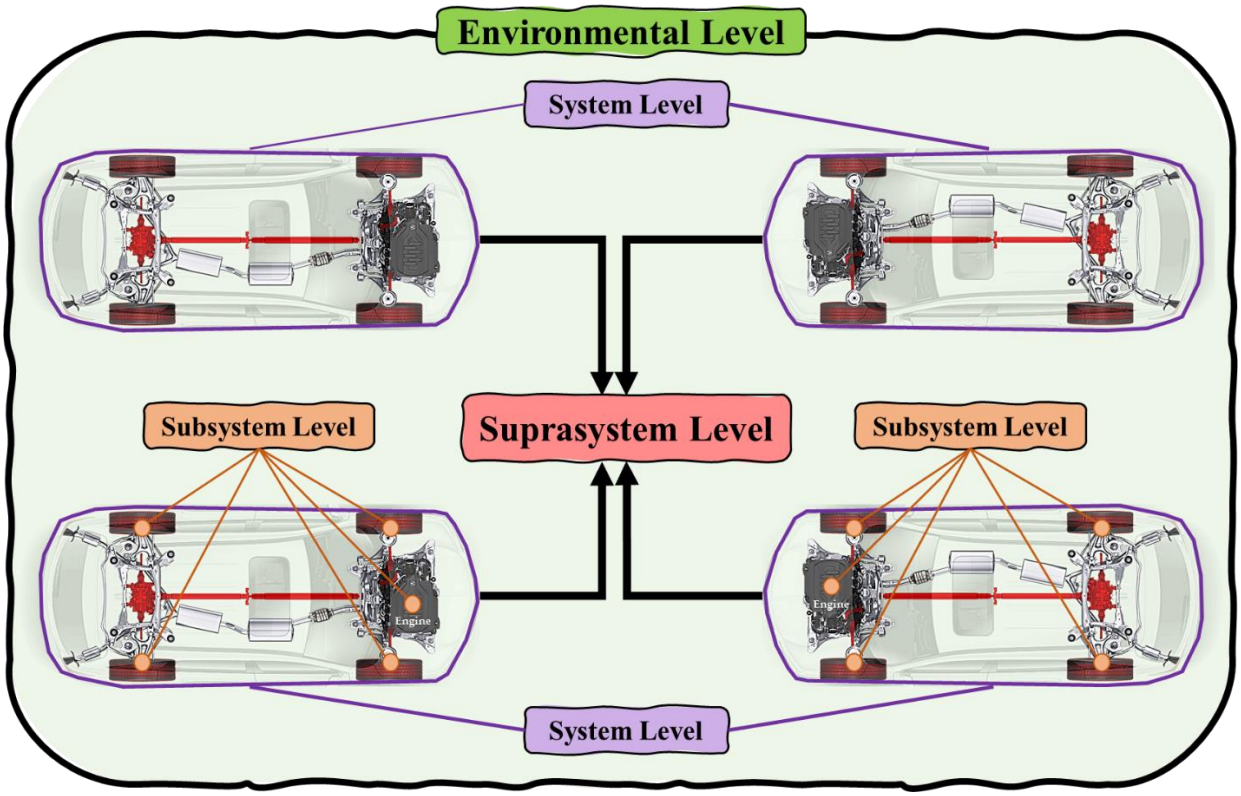

Figure 1-1. Investigation levels of vehicular emissions and their relationships

Brake wear, one of the most essential sources of non-exhaust emissions, is counted as a considerable part of traffic-related emissions accounting for the 55% by mass of total non-exhaust emissions in urban areas [15]–[17]. It was estimated that 30%-50% of brake wear is

exposed as airborne, removed wear particles which disperse and suspend in the air with aerodynamic diameters less than 10 μm [18]–[20]. However, Wahlström declared that this percentage could be up to 50%-70% [21]. Brake wear, based on their size, can be generated in four phases: gaseous, volatiles, semi-volatiles, and solid. The most momentous factor that highly designates the type of brake wear is temperature [22]. In previous studies, various tests were implemented on different type of discs and pads using distinct testing machines to find a critical temperature considered as wear volatile boundary. For instance, Perricone et al. reported that a significant amount of volatile brake wear is produced at temperatures above 200°C, identified as critical temperature [23]. However, among literature, this critical temperature was identified in the range 120-300°C regarding the test-determined features [24]–[27]. According to Perricone et al. [23], the particles with the size less and above 200nm were considered as semi-volatile and non-volatile, respectively. The gaseous part consists of volatile materials and, depending on the particle size, may remain in the air or be altered to solid particles. Solid emission produced by wear, which, in some cases, can be seen with naked eyes, is affected by tribological, mechanical, thermal, chemical, and fluid-dynamics phenomena and its result is characterized by various indices, especially the number and distribution of particles [28].

Several studies showed that the vehicle's braking system is one of the most relevant sources of PM particles [29]–[33]. Furthermore, the previous investigations showed that the particles generated by the cast iron discs are an important fraction of PM particles, which exposed the average size below 20μm [18], [34]. Furthermore, there are some influential parameters that can increasingly affect the amount of brake wear debris. Friction materials [25], the quality of brake system compositions [35], driving styles [36], and the severity of braking [37] are some parameters which may be counted. The release rate of PM particles can also be different regarding the vehicle parameters. For instance, the weight of a vehicle is one of the critical features that may influence the rate of brake wear, as it was shown in electric vehicles [38]. As traffic congestion corresponds to enhancements in the frequency of stop-and-go driving cycles causing more generation of brake wears.

The efficiency of integrating different investigation levels to estimate vehicular emissions, either exhaust or non-exhaust, is crystal clear regarding its comprehensive capabilities. However, no remarkable effort can be found in the literature taking the development of such integrated models into account due to their complexity and inaccessibility of necessary tools. Furthermore, no one can deny the drawbacks of lab-restricted experiments as they are mostly crippled in considering influential elements such as traffic conditions, road geometry, and driving styles. Third, new modern technologies and complex AI-based models have solved the drawbacks of using traditional statistical modeling techniques for emission estimation by proposing non-linear dependencies corresponding to brake wear.

In response to previous studies' limitations and to obtain more reliable exhaust and non-exhaust estimation models, this research aims to predict tailpipe and brake emissions by proposing two approaches. First, the exhaust emissions influenced by the fluctuations of the vehicle speed and heavy vehicle percentage, released by the motor vehicles around a sensitive location (case study), will be estimated using a traffic microsimulation model at the suprasystem level. Second, a novel approach will be presented for the brake emission estimation by proposing a downstream approach, starting from the suprasystem level (microscopic traffic simulation models) using a vehicle dynamics model at the system level and proposing an Artificial Neural Network (ANN) brake emission model appropriately trained and validated by means of emission data collected by the experimental tribological tests on a reduced-scale dynamometer machine (hereafter "minidyno") at the subsystem level (braking system). Through more than 1000 configured tests in minidyno, increasing the diversity of data to boost the robustness of analyses and inferences is targeted. By implementing full-HD cameras in a case study, the field surveys were conducted for both exhaust and non-exhaust emission estimations to collect as realistic data as possible instead of using dummy data. All emission calculations, both exhaust and brake emissions, were finally represented.

1.2. Motivations

Air pollution is one of the most significant environmental risks to health. By reducing air pollution levels, countries can reduce the disease burden from stroke, heart disease, lung cancer, and chronic and acute respiratory diseases, including asthma. Understanding the behaviors of airborne particle resources and their generation rates can illustrate ways of improving air quality. No study can be found in the literature focusing on the estimation of non-exhaust emissions in a real case study considering the real behavior of vehicles' movements, driving styles, traffic conditions, and road geometries. Real estimating vehicles' non-exhaust emissions requires penetrating different investigation levels and using various experimental tools, mathematical models, and simulation-based approaches.

By making all exhaust and non-exhaust emission modeling efforts in the present study, it is hoped that avenues be opened to the development of simulation-based emission models usable for diminishing project costs and promoting the accuracy of results. In addition to traffic microsimulation, the efficiency of Machine Learning models for brake emissions estimation is crystal clear as it paves the way to reaching reality.

1.3. Objectives

The main objectives of this study could be summarized as follows:

- Traffic and non-traffic data collection in a real case study in Trento, Italy.
- Conducting a comprehensive literature review over the history of research about vehicular emissions, both exhaust and non-exhaust, at various investigation levels and identifying the gaps and major shortcomings of previously-proposed modeling methodologies.
- Evaluating the simultaneous effects of vehicle maximum speeds and heavy vehicles contribution on exhaust emission generation in a real case study.
- Conducting a set of verification approaches on the exhaust emission estimations obtained by traffic microsimulation models.

- Introducing a novel approach for brake emission estimation using traffic microsimulation, vehicle system dynamics, tribology, and machine learning modeling.
- Estimating the brake emissions generated by dominant vehicles in a real case study based on their route choices.
- Predicting the amount of brake wear particles generated by dominant vehicles in the whole transportation network.

1.4. Structure of the Thesis

This thesis is structured as follows: In Chapter 2, first, the previous studies conducted on evaluating emissions in various investigation levels, including subsystem level, system level, suprasystem level, and environmental level, and the attempts to develop emission models are comprehensively reviewed. In this review, the history of research about vehicular brake emission, from the use of tribological experimental tests to the recent attempts to use on-road tests, is discussed.

The experimental procedure and proposed research methodology for the exhaust and non-exhaust emissions estimations, as well as vehicle dynamics and traffic microsimulation modeling, are explained in Chapter 3. To be more precise, data requirements of the research, data collection process, preparation of field-measured data, execution of different speed and HV%-based scenarios for exhaust emissions evaluation, and the novel and efficient ANN-based brake emission model for brake emission estimation were introduced in this Chapter. In Chapter 4, the case study chosen for the field surveys and traffic data collection is introduced in detail. The results of obtained data collected in the field are also presented in this Chapter. Then, in Chapter 5, the outcomes of the exhaust (together with the results of verification tests) and non-exhaust emissions (combined traffic microsimulation + vehicle system dynamics + ANN-based brake emission models) estimations are visually and statistically discussed. Finally, in Chapter 6, conclusions are drawn, and possible future research topics following this study are explained.

Chapter 2

Literature Review

2. Chapter 2: Literature Review

Throughout the interaction of brake disc and pads, there are several factors that may considerably influence the amount of brake wear generation [39]. Contact pressure, rotating speed, friction materials, and contact temperature are among some of these factors, which were regarded in previous studies [32], [40], [41]. However, by far, some of these factors are more influential in this phenomenon than others [42].

In the literature, previous studies focusing on airborne emissions are investigated in four main categories: Subsystem Level, System Level, Suprasystem Level, and Environmental Level. Figure 2-1 shows an overview scheme of the emission categories in the simulation and testing approaches performed throughout the literature [14].

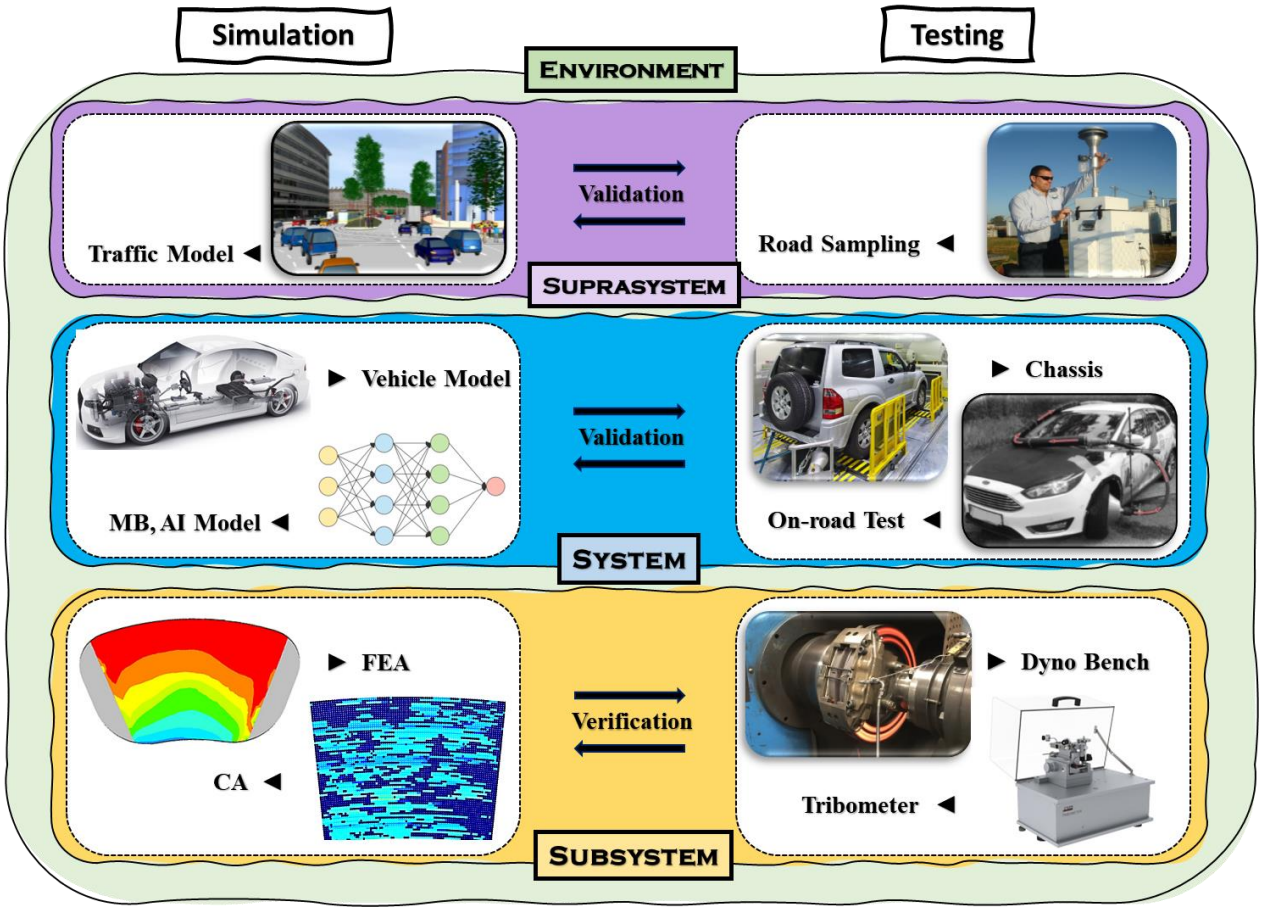

Figure 2-1. An overview scheme of different investigation levels

The majority of previous studies focused on subsystem level (component level) by which the tribological parameters can be obtained. In line with this, dynamometer and pin-on-disc

machines have been regarded remarkably due to their reliability, accuracy, and compatibility with other emission capturer devices like Optical Particle Sizer (OPS).

2.1. Subsystem Level

The subsystem level is the fundamental category that is introduced as the first level of the investigation, dealing with the smallest components of the existing system in microscopic analysis of the brake system. This level is based on the reproduction and deep study of some key aspects of the braking action. A remarkable advantage of implementing the studies at this level is the possibility to keep the test under control and make a deep study of the basic physical phenomena. There are some limitations to this level. The vehicle dynamic is reproduced by its equivalent inertia. Moreover, the operative conditions (intensity and duration of the braking action) may be relatively representative. Therefore, it is necessary to consider effective strategies to overcome these restrictions. The main metrics applying into this level are the coefficient of friction, wear of pads and disc, emission rate in terms of mass/time and traveled distance, and emission factor.

To provide and develop the air quality management and a reasonable estimation of the emissions generated by the vehicles, validated models, and emission estimators are needed. In some cases, these models may be restricted to the modeling of the parameters that have direct impacts on the rate of brake wear generation. For instance, the models established on brake linings' coefficient of friction (BLCF) to monitor the brake operation [43], [44].

Basically, the brake system inherently operates stochastic. The main problem of measuring the brake airborne wear in the field is that distinguishing the original sources of the particles is overwhelming. They may be originated from the braking pads or disc, resuspended road dust, tires, and other sources. Thus, a reliable environment is needed to provide the different scenarios and circumstances during the braking operations in different driving conditions. In the subsystem level, the evaluation of the characters of brake wear particles is implemented in the laboratory environment. There are many studies investigating brake particle features by using well-known tribometer machines such as pin-on-disc and dynamometer. Speed, acceleration, deceleration, pads wear, disc wear, continuously

changing temperature by the friction of pads and disc, and noises are the most influencing parameters of the interaction of brake pads and disc in the subsystem level. Philippe et al. [45] suggested that the best option to examine the brake wear is the use of pin-on-disc and dynamometer tests. The particle's properties, like size distribution, are similar between these two tests. However, the emission rates obtained from these two tests are not compatible because of the different testing temperatures.

Laboratory methods used for estimating the brake wear emissions enhance the potency to implement determined testing programs [46]. One of the benefits of implementing such tests in labs is to provide comparisons between brake emissions from the different types of brake components and evaluate their value in the market. Furthermore, the results obtained from different tests may allow scholars to identify the pads which generate an unacceptable amount of wear, either airborne or sedimental, from the environment-friendly pads.

There are several instruments employed to assess the different brake wear parameters in the lab-based measurements. Scales are commonly used to measure the weight of the test samples before and after testing. Instruments like Scanning Electron Micros-copy (SEM), Transmission Electron Microscopy (TEM) together with Energy Dispersive X-ray Spectroscopy (EDXS), are used to characterize the wear debris captured on filters after testing. Particle instruments based on different measurement techniques are available such as Fast Mobility Particle Sizer (FMPS), Optical Particle Sizer (OPS), Differential Mobility Spectrometer (DMS), Electrical Low-Pressure Impactor (ELPI+), Micro-orifice Uniform Deposit Impactor (MOUDI), Electrical Aerosol Analyzer, Aerodynamic Particle Sizer (APS), Dekati Low Pressure Impactor (DLPI) and Image Analysis) [14].

2.1.1. Material Level

2.1.1.1. Pin-on-disc test

The pin-on-disc tribometer test is one of the most popular tests that many scholars benefited from in studies focusing on brake pads and disc wear particles [28], [47]–[55]. This test is validated by previous investigations and named as an authentic experiment for inquiring the airborne particles from vehicles' disc brake contact [56], [57].

In this test, all airborne wear particles, which are generated by the friction at the sliding contact between a dead-weight or a hydraulic system loaded a pin manufactured from pad material and a horizontal rotating disc, are collected. Due to the simplicity of the pin-on-disc tribo-meter test, it cannot totally represent the real condition of the vehicle braking system. To make a real condition, further considerations are needed in addition to the steady interaction of pressure and sliding velocity [58]. However, the scholars introduced the pin-on-disc test as reliable equipment for evaluating the brake pad's wear and its friction behaviors sliding against a cast iron disc [59], [60]. As claimed in [47], at least, the pin-on-disc test can be beneficial in Research and Development (R&D) objectives, especially in the initial phase of the development of new materials. Moreover, its lower costs and operation times, compared to other tests, may be essential in projects dealing with many problems in providing budgets [61].

For brake wear testing by pin-on-disc tribometer, the ambient air will be passed through the HEPA (High Efficiency Particulate Air) filter to control the cleanness of the outlet air. The outlet air will be led through an inlet pipe to a chamber. A closed climate chamber should be used to ensure the particles measured are all generated from the pin-disc contact. To prevent errors (leakages) and increase the accuracy of results, all the connections must be sealed. Otherwise, the airflow rate conveyed in the chamber varies and causes the mismatch of the particle concentration measurements [62]. In 2020, this procedure was performed by Gomes et al. [63] to investigate the particle size and mass of particles released from a pin-on-disc machine. However, they reported the non-correlation of emissions and the friction coefficient.

In 2015, Chandra Verma et al. [64] perused the different aspects of braking pad wear in terms of their behavior during sliding on a rotating iron disc by implementing lab studies on a pin-on-disc machine.

2.1.2. Component Level

The component level of investigation of airborne brake emissions implements an experiment which involves sliding surfaces characterized by more representative

dimensions. At this level, the instrument developed for the experimental characterization of the braking behavior of the components under test is the dynamometer.

2.1.2.1. Dynamometer test

Innumerable studies investigated emissions of brake wear with dynamometer testing (with the abbreviation of "Dyno"), which can simulate the real conditions (driving in urban or suburban areas) of a braking system of a vehicle in the lab environment [23], [30], [65]–[70]. A brake dynamometer provides a more representative and controlled environment for the disc and pad test. Like the pin-on-disc machine, using a chamber is necessary to determine the airborne particles during the braking process [71]. A dynamometer machine usually has a blower that provides a constant flow of air passing through the braking system that simulates the reality and carries the particles to a tunnel known as Constant-volume Sampling (CVS) [72].

One of the substantial differences between the pin-on-disc and dynamometer test is the provision of the appropriate power per unit area or mass of samples to realize the correct temperature on the area of friction contact. Although the pin-on-disc tribometer can be able to provide sufficient power to the pin sample, it is common to load the powers which can simulate the common braking power in cities, that is why the maximum mass wear of the dynamometer is two times more than the pin-on-disc tribometer results [73]–[75].

Scholars classified dynamometers into two major types: the inertia dynamometer and the CHASE dynamometer. The inertia dynamometer is used to investigate full-sized brakes. Although it may be either time consuming or expensive, it shows more accurate results in comparison to the CHASE dynamometer. The CHASE dynamometer, despite the low capital expenditure and shorter test time, can be used only for the quality control or similar non-essential subjects [76].

2.1.2.1.1. Inertia Dynamometer

Inertia dynamometers are the dynos that incorporate a full or reduced-sized brake. Compared to other dynamometers, these dynos can reproduce the braking system operating

conditions in a reasonably reliable way [77]. Based on the literature, there are two types of inertia dynamometers: Full-scale and Reduced-scale.

2.1.2.1.1.1. Full-Scale Dynamometer

One of the tribological tools that can be used for the investigation of these new achievements is the full-scale dynamometer [78]. The rotating body used for the full-scale dynamometers is relatively large, which simulates the vehicle's total mass during the brake operation.

In 2019, Hagen et al. studied the brake wear particle emissions using a full-scale brake dynamometer by presenting a novel measurement setup to reduce particle transport losses [79]. In this research, the brake wear particles were calculated during either braking or driving to expose more realistic results. Mamakos et al. designed a dilution tunnel aimed at making a more accurate and reliable measurement of the brake wear in a brake dynamometer. This dilution tunnel provided the minimization of the particle losses in the sizes of less than 10μm [80]. In 2020, Matějka et al. investigated the amount of airborne wear particles generated by the braking system by means of a full-scale dyno-bench [81]. By investigating the data obtained by utilizing the PM_{10} and electric low-pressure impactors, they found that the maximum disc temperature and brake duration had the most significant impacts on the rate of brake wear generation.

2.1.2.1.1.2. Reduced-Scale Dynamometer

The reduced dynamometer is known as a tool to decrease the cost of time and un-necessary expenses which exist in full-scale dynos. Previous studies introduced the reduced-scale friction testing for investigating the quality of friction materials, assessing their property, and the linings. For instance, Sanders et al. used a reduced-scale inertia brake dynamometer to determine the frictional characteristics of lining materials [82]. Anderson et al. also investigated the brake lining materials in a brake disc in terms of friction stability [83]. In this research, they claimed that their test, named Friction Assessment Screening Test (FAST), was reproducible and could highly correlate with vehicle performance. However,

Kermc et al. discussed the inability of the FAST test in presenting the quantitative values of the coefficient of friction [84].

In the literature, the reduced-scale dyno is also known as a small-scale dynamometer. Although a reduced dynamometer is benefited by the simple pads and disc assembly, it has a reasonable and acceptable correlation with the full-scale dynamometers. Recent studies showed the reliable approximation of collected data obtained by evaluating the temperature tests of the sliding surface for the reduced and full-scale brake discs [85]. Thus, it can be a useful tool for screening the brake linings and calculating the friction coefficients [82]. The small scale of these kinds of machines helps the scholars prevent the negative effects of the brake pad geometry and implement a uniform distribution of pressure on pads and disc during the braking operation. This uniform distribution leads the brake system acceptably perform even in severe conditions like high temperatures [84]. Beyond all these merits, reduced-scale dynos cannot provide 100% realistic performance of the braking system regarding its less realistic simulation of operating conditions [86].

Furthermore, it is necessary for the full-scale dynamometers to respond dynamically to the vast surrounding systems. Because of that, they may show less accuracy of results due to the existence of caliper and bracket deflection and pressure fluctuations in comparison to the reduced dynamometers [84]. One the other hand, some issues increase the complexity of designing of the reduced-scale dynos such as cooling rates of brake system configuration. Therefore, tuning of scaled parameters is mandatory when using this type of dynamometers [85]–[87].

2.1.2.1.2. CHASE Dynamometer

Differently from the inertia dynamometer, which provides a full-scale of friction materials, the CHASE dynamometer simulates the braking system by implementing a small number of friction materials which are rubbing against a drum. In 1980, Liu et al. measured the wear rates of a drum lining and a disc pad [88]. However, regarding the significant changes in pads and disc materials and the development of the vehicle's braking system in recent years, the recent results on the braking wear using the previous approach are not fully reliable.

Inherently, regarding its design, the CHASE dynamometer cannot simulate the realistic state of the braking system in terms of the physical and chemical state of the friction contact during system operation. Thus, Tsang, by comparing the results of both inertia and CHASE dynos, proved that the CHASE dynamometer could not be reliable for the prediction of materials' performance on the inertia dyno and for the screen of automotive friction materials [76].

The running time of sample evaluation using the CHASE dyno is much less than the inertia dyno. An inertia dyno needs an appropriate number of the full-size braking systems, including pads, rotor, disc, linings [89] together with proper inertial capacity, therefore the analysis of the results requires a time-consuming procedure of disassembling the pads and evaluating the samples. Also, testing by the CHASE dynamometer can be carried out by using small samples, while the inertia dyno needs the appropriate number of linings and other segments [76].

To investigate the brake emissions, simulation-based models in subsystem level were introduced by scholars as reliable state-of-the-art approaches. In 2009, Wahlström et al. introduced a simulation-based Finite Element Analysis (FEA) approach as a possible and reliable method of predicting the number distribution of airborne brake wears [90]. This approach was also regarded by the other researches. For instance, Riva et al. developed an FEA approach to simulate airborne brake wears in the condition of various contact pressure and sliding speed using pin-on-disc tribometer tests [50]. Their findings showed 19% error between the simulated and measured results, representing a promising approach for brake wear estimation. This approach was also implemented for finding the correlation between the non-uniform contact pressure and uneven brake wear [91].

2.2. System Level

Hierarchically, the next level will be the level that deals with the full vehicle, named "System Level". When the amount of emissions generated by the brake system of the whole car is considered, it will be defined as the emissions at the system level. It means that a single car, as a confined ambient, is considered an ensemble of devices that interact and therefore

constitutes an "emitting system". These emissions can be evaluated by assessing cars in either laboratories or on-road environment. It addresses the emission in real driving conditions, therefore the vehicle dynamics (including the drivetrain), the driving style, road geometry, and slope are enabled. Regarding the inherent feature of this level, the emissions which are continuously emitted by the system, even in conditions that the deceleration and speed reduction are carried out by engine, can be estimated. One limitation of the system level is that it does not allow the deep study at the microscopic level since the brake is installed on the vehicle and a limited number of instruments may be installed. The main metrics applying into this level are emission rate in terms of mass/traveled distance, emission factor, and loss of performance when over-heated [92].

Despite the advantages of the subsystem level tools like dynamometer or pin-on-disc in scrutinizing the brake-related emissions, they cannot present a more realistic perspective of the parameters influencing the amount of generated brake wear. For elevating the accuracy of the results, in addition to the speed, temperature, acceleration, and the other parameters of the subsystem level, some other key factors can lead to more realistic results. The vehicle dynamics, the geometry of the road, the effects of the weather, and the driving styles can be counted as some well-known instances lying in this issue.

At the system level, there are two ways to study the brake wear particles. First, it can be done in the real-world conditions on the road, which is called "On-road Driving Tests", and second, it can be implemented in the laboratory through a relatively con-trolled ambient conditions. One of the approaches that provide this controlled environment is the use of a single car on a CHASSIS Dynamometer in the lab (as an agent). Although each of these ways can provide reliable results, for making a comparison, they can also be used simultaneously. For instance, in 2020, Beji et al. compared the non-exhaust emissions obtained from the testing of a similar instrumented vehicle and collected samples in three distinct environments, including a full-controlled laboratory (CHASSIS dyno), semi-controlled test track, and on-road urban areas [93]. In addition to brake wear particles, they calculated the tire-road contact and resuspension particles and specified their features. Due to one of the

main achievements of this research, over 70% of brake wear particles originated from brake pads. Furthermore, the speed variations influenced the amount of wear generated by brake and tires. Thus, regardless of the driving conditions, Beji et al. suggested that the rate of wear would be remarkably reduced in various speeds and braking force frequency.

2.2.1. Emission Factor

Emission factors (EFs) are representative values chiefly implemented for quantifying the emissions generated by vehicles, i.e. they relate the vehicle's activity to the amount of pollutions emitting in the air [94], [95]. There are plenty of factors, such as vehicle characteristics, fuel consumption, fuel type, and quality of the fuel, and driving conditions directly affecting the EFs [15]. As a result, the level of emissions in numerous regions with various traffic conditions can be easily predicted by EFs. EFs can be calculated directly by performing laboratory tests, on-road measurements, or receptor modeling [96].

2.2.2. Laboratory (CHASSIS Dynamometer)

The CHASSIS dynamometer can be conducted using a full vehicle, which leads to ground-truth data and provides a reproduction of the real braking condition. Although there are a lot of previous works on the subsystem level-related laboratory tests, the studies in the system level are scarce. That may be related to the high costs and overwhelming methodology that the scholars should inherently deal with.

A CHASSIS dynamometer can evaluate various parameters related to the brake wear in the laboratory ambient. Humidity and its effects on the rate of pad or disc wear is one example of such a parameter that was comprehensively studied by [97], [98].

In 2018, Chasapidis et al. estimated the brake wear particles generated by running a minivan in a CHASSIS dynamometer under various initial speeds, deceleration rates, and ambient temperatures [99]. In this research, the authors declared that dealing with a system facing with different sources of particles like brake and tire under the custom configurations is challenging. They also showed that the ambient temperature had trivial effects on the generation of brake wear particles.

In 2019, Mathissen et al. used an instrumented passenger vehicle together with a novel approach for collecting brake wear particles in the laboratory environment [100]. This CHASSIS dynamometer was instrumented by a big vacuum hose, a cone-shape capturer, and the sampling modules in the vehicle's trunk. Although the brake cooling was one of the limitations of this study (brake emissions are temperature de-pendent), they showed a remarkable amount of total brake PM_{10} emissions (up to 30%) generated by the particles emitted from the braking system in the time that the brakes are not applied.

To summarize, regarding the influential variety of advantages, it seems that the measurements obtained by implementing the CHASSIS dynamometer are reliable for the investigation of brake wear particles. In addition to its capability to prevent the interventions of environment parameters, the CHASSIS dynamometer can be assessed as a reasonable tool to evaluate the impact levels of the phenomenon like particle loss. Furthermore, this approach has some restrictions and disadvantages. The main problem of using a CHASSIS dynamometer is the limited representativeness of the ventilation rate that produces a low level of cooling for the brake system. As shown in [100], besides the remarkable advantages of CHASSIS dynos such as the evaluation of changes in a vehicle's chassis, this problem causes the accumulation of particles in the chamber causing the use of artificial brake ventilators.

2.2.3. On-road Driving Test

In comparison to laboratory tests, on-road driving tests are more expensive and complicated. Because of that, there are few studies related to the on-road driving test in the literature. In 1983, Cha et al. measured the asbestos emissions of the vehicle's braking system by implementing field studies [101]. By performing a computer-based emission test, they collected the brake wear emitted from a front-wheel disc brake during passenger car driving in the city downtown and simulated the brake wear dynamics.

Sanders et al. investigated the emissions on-roads by using some sampling tubes installed on the vehicle's wheels to minimize sampling losses [18]. They calculated the on-road emissions both in traffic and a high-speed test track and reported the correlation between

them and dynamometer tests using a wind dilution tunnel. The results of this research showed that the half proportion of the wear obtained by vehicle tests be-came airborne. In addition, similar elements such as Fe, Cu, and Ba were observed in both dynamometer and on-road samples. In 2013, Kwak et al. calculated the physical and chemical properties (like mass distribution) of the non-exhaust sources such as brake, tire, and road dust on-road and in the laboratory by using a mobile instrument-ed sampling vehicle and considering isokinetic sampling design under different driving conditions [37]. In this research, they installed some sampling inlets in front of the vehicle, close to the tire and brake pads to collect the on-road data and compare them with the data obtained from the laboratory tests. A similar approach was carried out by Kwak et al. to investigate the physical and chemical characteristics of non-exhaust ultrafine particles generated by non-exhaust origins, driving an equipped vehicle on-road [102].

By presenting a novel approach, Mathissen et al. successfully investigated the non-exhaust PM emissions, which were generated by brake system and resuspension of road dust, obtained with an instrumented mobile trailer attached to a light-weight passenger vehicle [103], similar to the procedure introduced by Fitz et al. in 2002 [104]. They implemented their survey studies by driving more than 800 kilometers on un-paved and dust loaded agricultural paved roads. The scholars also investigated the particles dispersing in the wake of the vehicle by implementing a tracer gas test. Emission factors calculated in this research showed lower results on motorways.

In 2015, Wahlström et al. presented a field study measurement of the brake wear by collecting data in the outer of Stockholm, Sweden [105]. They mounted two sampling tubes close to brake pads and also installed two tubes in front of an instrumented car. By mounting pressure and speed sensors in the sampling vehicle, simultaneous measurement of the vehicle's speed and brake pressure was provided. The results of this research showed a reliable correlation between the brake operation and the in-creased particle concentrations.

Despite the remarkable results of sensor installation in the braking system, they can only partially sample the brake dust. Farwick zum Hagen et al. introduced an innovative

sampling approach retrieved from the dynamometer test [36]. In this re-search, they collected entire brake wear emissions by a semi-closed vehicle setup. This setup helped the scholars to collect the entire brake aerosol. In this research, they com-pared the obtained results of conventional and novel materials for the pads with different coatings. They concluded that the novel composition presented almost 18 per-cent lower PM_{10} particles.

In 2020, Perricone et al. conducted a field road test by using a LDV equipped with temperature and pressure sensors on the brake system [106]. By calculating the emission factors, they showed that the brake system temperature during the urban driving changed in the range of 100-170^{o}C. In addition, they made a comparison between the brake number and mass emissions factors and the regulations of Euro 6 and 4. As shown in this research, having a cycle that can act as a representative of the real-world is crucial to get accurate results.

2.2.4. Wheel Sampling

Puisney et al., by sampling the brake system of a passenger car under different driving conditions, investigated the nanoparticle characterization and their toxic effects in the environment and on human body cells [107]. They also got samples from a dynamometer bench to make a comparison between the results. They concluded that the brake wear has adverse effects on the human lungs due to its notable amount of metallic nanoparticles, which accounted for 26% of the total brake wear particle mass. Varrica et al. investigated the airborne Sb particles generated by the brake system with sampling from the wear residues on vehicle's wheels, brake linings, road dust, and the atmospheric particles [108]. By specifying the type of different Sb existing in various samples, they introduced Sb as a good tracer of emission classification in studies.

2.3. Environmental Level

Naturally, the environment collects the emissions and produces further modifications of their distribution. The environmental level is the level where all the emissions are finally collected. It does not constitute just a passive level, as many complex phenomena act and produce further re-distribution of the emissions with relevant implications on the local

pollution and related risk for health. In order to implement the experiments on wear generated by the brake system, it is necessary to collect samples from the surfaces and areas supposed to be subjected to the emissions. These prone areas include road surfaces, vehicles' surfaces, plants' leaf, oceans, rivers, agricultural farms, soils, and runoffs. Since the origin of particles is unknown as they can be generated from various sources, it is necessary to use experimental-based methods to distinguish them. The study at this level cannot address the details of the emission sources but rather focuses on the external phenomena like resuspension, weather, wind, the morphology of the environment (valleys, mountains, etc.). Large scale statistical models are also developed at this level.

No one can cast a shadow of doubt on the fact that the automobile industry is developing each year new materials as the environmental restriction rules are updated by the legislators. Since 1978, more than 100 formulations related to the friction material which are used in the brake system have been introduced, and nowadays according to [109], it is difficult to count the number of existing materials in brake components. Thus, this makes it much more difficult to evaluate the chemical compositions of the samples.

2.3.1. Sampling Place

Non-exhaust particles, including tire and brake wear, are one of the substantial sources of road dust contamination. However, tunnels can be counted as important places where the particles, dusts, and brake wears are carried and accumulated by wind or runoffs originated by precipitations. As shown by Wang et al. [110], tunnels are one of best places where the real-world emissions can be obtained. However, data collection and sampling from the tunnels should be done regularly to update the emission models [110]. The size distributions of particles can be also measured by the samples collected from the tunnels. Abu-Allaban et al. showed that the contributions of HDVs dominated the particles generated by the LDVs in the ultrafine particle distribution [111]. However, the impressive contributions of these emissions to PM concentrations should not be neglected [112].

As it was shown in previous studies, the dominant sources of PM particles are due to the generation of non-exhaust emissions by the transportation fleets [113]–[115], especially in the

countries located in the north of Europe [116]. The main source of the road dust is the wear generated by the studded tires [117], especially in the countries where using these kinds of tires is common [118].

A lot of studies can be found in the literature that investigated the existence of tire wear in road dust samples [119]–[121]. Furthermore, the brake system is another source of road dust. These wears are generated by the occurrence of friction between pads and disc while the temperature during brake operation goes up. In urban areas, some places such as intersections and traffic lights are prone to show an excessive amount of sedimental wear due to the repeatedly braking.

As it was shown in several previous studies, the emissions of road dust can be evaluated by Testing Re-entrained Aerosol Kinetic Emissions from Roads (TRAKER) system [122]–[124]. In 2009, Pirjola et al. presented an innovative road dust measurement system by carrying out a mobile laboratory SNIFFER to find out the level of emissions on various streets [125]. Adamiec et al. identified the dust from brake linings and tires in the motorway, urban, and mountain roads [109]. In cities, additional contamination of wear dust exists due to the resuspension of the pre-sedimented particles on the surfaces. Therefore, it is likely to report a greater amount of emission in cities in comparison to mountain areas. Based on the results of this research, the diameters of the non-exhaust particles will not be greater than 250 μm, the same as the results presented in [126]. They also concluded that the finest fraction of the Pd element was much lower in mountain roads in comparison to urban areas.

In 2016, Gonzalez et al. studied the atmospheric PM particles by sampling from two major European cities at the street level [127]. They implemented their field studies at sites with variable traffic density. They found that the Zn and Cu isotope are mostly generated by non-exhaust emissions.

2.3.2. Non-exhaust emission models

Over the years, non-exhaust emission models, which are mainly used to estimate the emissions in various applications by implementing the observed data on a distinct spatial and temporal scale, have been improved from a primary model introduced by the US-EPA

in 1984 to the more developed models in emissions measuring approaches and the size of data used to validate [128]–[132]. To make a comparison between the emission models available in various European countries, emission factors were used by [133].

In 2003, Abu-Allaban et al. used two techniques, Chemical Mass Balance (CMB) receptor modeling and SEM, to estimate the emission factors of various vehicle modal splits, the contribution of different type of vehicles in the total number of transportation fleets, by implementing survey studies on-road and getting samples directly [134]. A high amount of brake wear in freeway exit sites in comparison to other locations was one of the results of their research.

The different variables that the scholars implemented in their non-exhaust emission models are controversial. Kukkonen et al. presented a semi-empirical model to estimate the PM10 concentration based on a linear regression approach between emissions [135]. Besides the road dust, road surface moisture is also essential to be considered into the emission models, because it can influence the dispersion of particles re-suspended from the road surface. In order to investigate this variable, scholars introduced a non-exhaust emission model to predict the main features of the particles by considering both surface moisture and dust variables [116], [130]. They used ground-truth data to calibrate their model with real conditions. This local measurement de-pendency of their model has been reduced in the model presented by Berger et al. [136].

Denby et al. presented a comprehensive model of non-exhaust emissions entitled "NORTRIP" considering the road surface moisture, road wear, surface dust, sand, and salt loading and their suspension together with the wear of road, tire, and brake [117]. The model was applied in the 7 years of data collected from two locations exposed to the moisture. But they declared the uncertainty of their model to approximately ±40% for the long-term means. A similar model has been used for the modeling of the road dust emission abatement by [137], and it was shown that the NORTRIP model could be performed as a reliable model for air quality planning.

In 2015, Mawdsley et al. introduced a novel method to calculate the non-exhaust emissions based on the SIMAIR model, an internet-based coupled model system that was built in Sweden to calculate the air quality [138]. It could provide comprehensive data related to the parameters influencing the amount of annual reported non-exhaust emissions like the use of studded tires. Database of the emission factors related to the road and vehicle, together with a model calculating the non-exhaust emissions, are the main parts of the SIMAIR model covering all the transportation networks of Sweden. The SIMAIR model was successfully validated by Gidhagen et al. [139]. Furthermore, Mawdsley et al. utilized the NORTRIP non-exhaust model to make a comparison be-tween the results of two approaches [138]. Investigation of the resuspension model in the SIMAIR and NORTRIP was another strategy of their project. Regarding the operational production condition of the SIMAIR model in Sweden, they concluded that this model could present regular calculations of emission in comparison to the NORTRIP model.

Nagpure et al. estimated the exhaust and non-exhaust emissions simultaneously by deploying the Vehicular Air Pollution Inventory (VAPI) model in Delhi city [140]. VAPI model can estimate the emissions generated by vehicles in terms of their age and technology based on the econometric Gompertz equation tool [141]. Their emission analysis consisted of the investigation of emissions in the period of 1991 to 2020 implementing GDP (Gross Domestic Product) and per capita based econometric model. The results of this research indicated the drastic enhancement of PM_{10} emissions produced by non-exhaust sources.

Chapter 3

Methodology

3. Chapter 3: Methodology

3.1. Traffic Data Requirements

Based on the defined objectives of the research (presented in Section 1.3), a comprehensive field data collection in a real case study is essential. Trento, located in the northeast of Italy, is found quite appropriate city to conducting the field surveys. The Buonconsiglio Castle area, located in Trento city center and surrounded by different two-way and one-way roads and signalized intersections, is selected as the case study. All the details of the case study and related data collection process in the field are explained in a separate Chapter. Please refer to Chapter 4 for the details.

3.2. Traffic microsimulation

Traffic microsimulation models have been widely used in the last decade to facilitate traffic analysis and develop agents' activity data. Obtaining the vehicles' movement records is essential for developing emission and fuel consumption agent-based models as they depict the details of agents' activity in a time domain. To make the traffic microsimulation models more accessible and provide an ambient for the users to shape their own thoughts throughout the simulation models, traffic microsimulation software has been introduced in recent years. These tools are able to provide detailed and more precise information on the likely evolution of traffic in various contexts. As the demand for using such software is increasing day-to-day, many companies around the world have tried their entire attempt to introduce a feature-oriented product to promote their position in the market. PTV-VISSIM, TransModeler, TSIS-CORSIM, Cube Dynasim, LISA+, SiAS Paramics, Simtraffic, Aimsun, and MATSim are some examples of traffic microsimulation software packages available in the market.

3.2.1. PTV-VISSIM

Among all available traffic microsimulation software, PTV-VISSIM has extensively attracted scholars', scientists', and engineers' attention in recent years due to its unique features. Vissim is a microscopic multi-modal traffic flow simulation software package developed by PTV- Group in Karlsruhe, Germany. It was first developed in 1992 and is

known as a leader in the global market [142]. One of the distinctive features of this software is its flexibility in analyzing non-default applications. On the microscopic level, VISSIM can simulate complex vehicle interactions realistically, together with actual driving behavior considerations [143]. Having an efficient and user-friendly interface, VISSIM is an effective tool to accurately simulate the interactions between vehicles and pedestrians in a defined transportation network. According to all these merits, PTV-VISSIM, version 2022, is selected as the main microsimulation software for traffic modeling in the present dissertation.

3.2.2. Exhaust Emission Estimation

Many studies can be found in the literature emphasizing the reliability of VISSIM in calculating exhaust emission and fuel consumption [144]–[148]. By default, VISSIM can estimate the amount of exhaust emission and fuel consumption in the nodes (areas) defined by the user. However, it is crippled to report the emissions and fuel consumption throughout the entire trip agent-by-agent. The cornerstone for node emission calculation in VISSIM is formed by standard formulas for vehicles' consumption values from TRANSYT 7-F (Traffic Network Study Tool version 7-F), a program for signal timing design and optimization, as well as data on emissions of the Oak Ridge National Laboratory of the United States Department of energy [149].

Many studies can be found in the literature, which have used VISSIM for estimating the rate of exhaust emission generation in urban areas. In 2021, Ziemska investigated the impacts of changes in the number of heavy goods vehicles (HGVs) in a port city on exhaust emissions and fuel consumption using VISSIM microsimulation software [146]. The results of Ziemska's research showed that a 40% increase in HGVs percentage significantly increased the generation of exhaust emissions in the port transportation network. Having the feature of traffic control optimization, VISSIM has also been used in previous studies to find the best strategy to reduce the amount of exhaust emission generation and fuel consumption in urban areas [147], [150], [151]. VISSIM was also employed to investigate the effects of instantaneous vehicle speed and acceleration on emission generation and rate of fuel consumption [152]. All these investigations support the reliability of using VISSIM in exhaust emission and fuel

consumption prediction in urban areas, which convinced the author to employ this versatile software as the main microsimulation tool.

3.2.3. Non-exhaust Emission Estimation

In contrast to exhaust emission and fuel consumption functional models embedded in the software by default, currently, VISSIM has not been equipped with particular modules which can present the rate of non-exhaust emission generation in a transportation network. Even though VISSIM does not possess this feature, it can provide the individuals' activity records in time-series. Monitoring vehicles' movements millisecond-by-millisecond in a one-hour simulation running time can make millions of records of different individuals. This big data can feed other pre-determined emission models as inputs to make the emission estimation feasible. In the literature, this approach has widely been utilized to estimate exhaust emissions, such as emission models associated with agents' speed profiles [153], and feed other emission-analysis software like Environmental Protection Agency's MOVES (Motor Vehicle Emission Simulator) emission model [154]–[156], Passenger car and Heavy-duty Emission Mode (PHEM) [157], [158] , and Comprehensive Modal Emission Model (CMEM) [148], [159]. However, besides all these attempts, no evidence can be found in the literature in which the outputs of traffic microsimulation modeling are used to estimate the non-exhaust emission. The complexity of dealing with the emissions generated by the braking system can be the main reason for this gap in the literature. Brake emission estimation needs the investigation of various vehicle-related characteristics at different levels, including subsystem, system, and suprasystem levels. The emission released by the braking system can be assessed at the subsystem level, whereas the movements of vehicles and agents' real activities in a transportation network need to be evaluated at the suprasystem level, considering the impacts of vehicle dynamics at the system level. The synchronization between all these investigation levels imposes numerous challenges on emission estimation, which can solely be answered by an interdisciplinary approach. The present dissertation aims to estimate the number of brake emissions generated in the field using an interdisciplinary approach among subsystem, system, suprasystem investigation levels.

3.2.4. VISSIM Simulation Parameters

The present dissertation considers two main approaches for traffic microsimulation in VISSIM. First, 18 separate traffic models are simulated in VISSIM based on the 18 scenarios' configurations to predict the amount of exhaust emission and the fuel consumption rate in the case study (See Chapter 4) using the embedded exhaust emission and fuel consumption model in VISSIM. Second, the real traffic condition in the case study is simulated in VISSIM for the brake emission estimations of targeted vehicles considering subsystem, system, and suprasystem levels and using vehicle activity records. For both these approaches, numerous traffic network information, including traffic input volumes, pedestrian volume, modal splits, pedestrians, road geometry, signal configurations, timings, parking lots, and other related parameters, must be inserted in VISSIM as input variables to shape the simulation models. However, based on the project needs, other parameters may also be provided.

The default vehicle composition defined in VISSIM is based on the dominant vehicles resorting in the United States. Although this default composition can be acceptable in most cases, the dominant vehicle types obtained by the vehicle type analysis during the field survey in the case study (See Chapter 4) are considered as the baseline vehicle composition for both approaches (exhaust and non-exhaust), i.e., the vehicle type distributions are identified based on the proportion of dominant cars in the case study, and VISSIM default setups and 2D/3D model distributions are customized accordingly. This selection makes the results of the research to be much closer to reality. The pedestrian ground-truth data obtained in the data collection process is applied to the models regardless of gender. Based on the observations in the field, all the sidewalks and pedestrian-signalized crosswalks are designed exclusively in the simulation models to avoid interfering with vehicle movements. The signal timings for pedestrians are also considered protected due to the field observations.

To ensure the reliability of the embedded exhaust emission and fuel consumption models in VISSIM, all simulation models (18 scenarios) are repeated 30 times in a 3-hour (10800 seconds) simulation running time. However, the simulation models designed for monitoring vehicle movements in order to estimate the brake emissions are repeated ten times in a one-

hour simulation run (3600 seconds) regarding the millions of captured data at each simulation run and the accuracy of the ANN brake emission model. On average, more than 26 million records are extracted from the VISSIM simulation model at each simulation run. For both approaches, the simulation resolution is considered as 20 time-steps per simulation second (a record at each 0.05 Sec) with 42 random seeds. To calculate the final exhaust and non-exhaust emissions and fuel consumption, the average results among all simulation iterations are calculated, and finally, the results are reported and concluded.

Throughout capturing the vehicle activities at each 0.05 second, all the information needed for feeding the vehicle dynamics and ANN brake emission models are recorded at each timestamp. This information includes the vehicle's front and rear x, y, z coordination, speed, acceleration, type, manufacturer brand, length, height, width, lane state, driving state, and position in the network.

3.3. Exhaust Emissions Estimation

3.3.1. Proposed Method

For the part of exhaust emission estimation, the following steps were defined. First, the rate of traffic congestion in the case study and different aspects of field specifications are investigated. Then, a field survey was conducted (See Chapter 4) in a case study to collect every necessary traffic and non-traffic data needed for the exhaust emission prediction. Third, 18 separate scenarios are defined based on the various speeds of light-duty and heavy-duty vehicles considering the HV percentage changes (modal splits). Taking speed and HV% changes into account, the expected traffic volumes in all roads and intersection legs are determined in each adopted scenario. In the fourth step, traffic microsimulation software is employed to model all identified scenarios to gain the individuals' rate of emission generation and fuel consumption. To make the simulation models more accurate, every single traffic element is modeled throughout the scenarios' configurations. In order to model all 18 scenarios, the fifth step is subsequently updated after each scenario analysis according to the various configurations of vehicles' speed and HV percentage determined in the scenarios. After estimating the exhaust emissions and fuel consumption results, a set of

verification tests are conducted on the models to evaluate their reliability. The obtained air pollution volume and fuel consumption rate near the proposed sensitive location are two main factors to consider in analyzing and prioritizing different scenarios. The results obtained by the proposed method are beneficial for the decision-makers to get acquainted with the interaction between speed and HV percentage to manage the amount of exhaust emission, vehicle speed, and fuel consumption rate in congested areas. Figure 3-1 summarizes the steps of the proposed method.

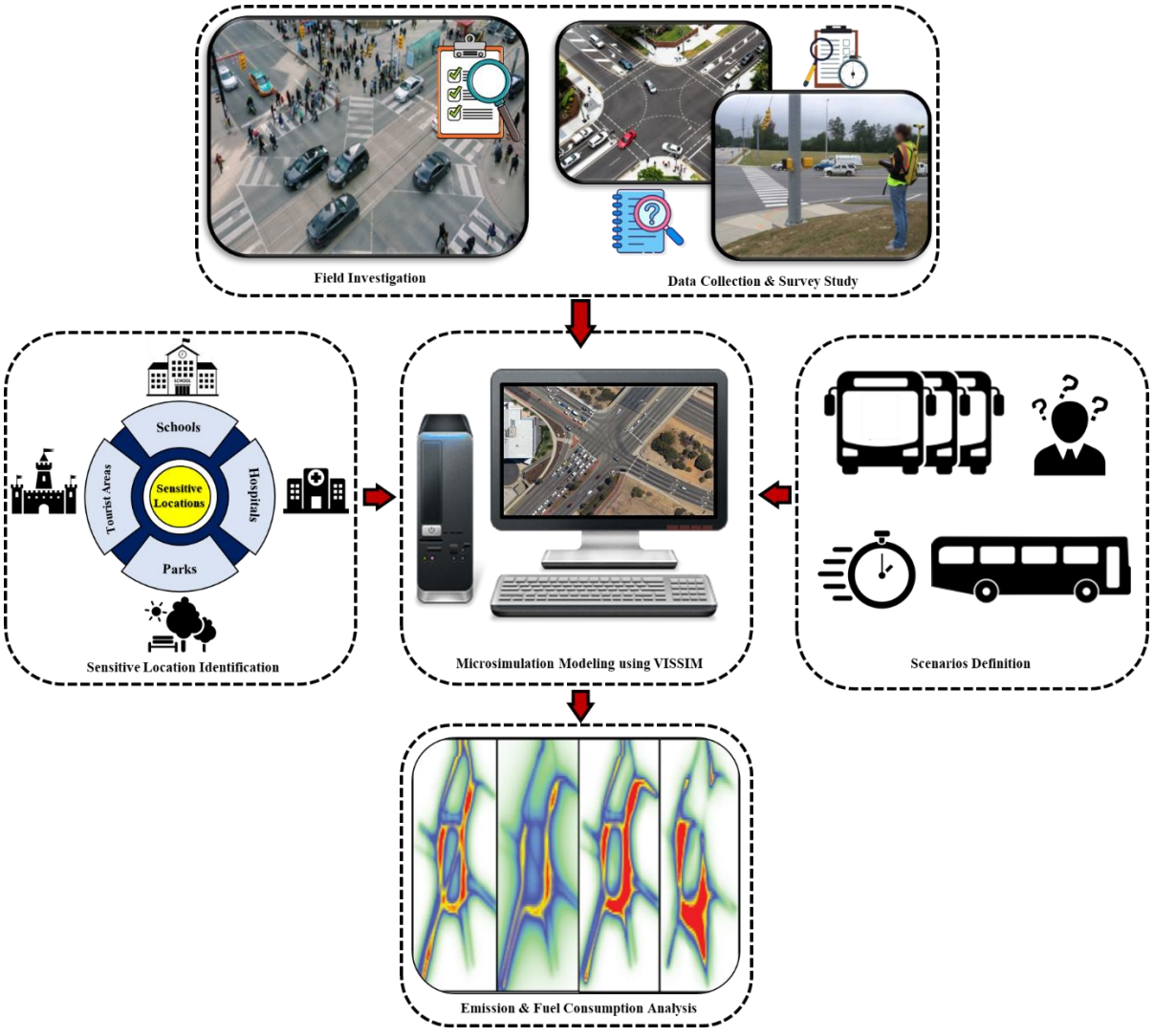

Figure 3-1. Proposed method for exhaust emission estimation

3.3.2. Available Scenarios

In the present dissertation, vehicle speed and modal split (contribution of different vehicle types in the vehicle composition) are considered as the main factors influencing mobility, vehicle movements, and, consequently, the rate of exhaust emission generation in a congested area. The entangled interaction between these factors and their undeniable effect on each other is crystal clear. Thus, 18 separate scenarios are defined to ensure covering all the contingent interactions between speed and HV%. These 18 scenarios are defined based on the three baseline speed series presented as follows:

1. Light Vehicles (60km/h) - Heavy Vehicles (50km/h)
2. Light Vehicles (50km/h) - Heavy Vehicles (40km/h)
3. Light Vehicles (40km/h) - Heavy Vehicles (30km/h)

The intuition behind considering these speeds is retrieved from the speed limitation standards regulated by the European Union for urban areas. According to this matter, the reasonable speeds in urban areas throughout almost all European countries are 40-60 km/h and 30-50 km/h for light and heavy-duty vehicles, respectively. To build the scenarios, the HV contribution percentage in the network is increased by 0, 20, 40, 60, 80, and 100 percent for each of the above speed series. A 0% increase in HV percentage is representative of the baseline scenario (ground-truth data). This means that the first three scenarios, which depict three-speed variations, are the representatives of real consideration of heavy vehicle percentage in the case study. Considering these baseline scenarios, as they have been built based on the actual number of HVs, makes the comparison between different scenarios accessible. The details of scenarios' considerations are summarized in Table 3-1:

Table 3-1. Configurations of available scenarios

		Scenario																	
		1	2	3	4	5	6	7	8	9	10	11	12	13	14	15	16	17	18
LV Speed	60 km/h	✓	✓	✓	✓	✓	✓												
	50 km/h							✓	✓	✓	✓	✓	✓						
	40 km/h													✓	✓	✓	✓	✓	✓
HV Speed	50 km/h	✓	✓	✓	✓	✓	✓												
	40 km/h							✓	✓	✓	✓	✓	✓						
	30 km/h													✓	✓	✓	✓	✓	✓
HV Contribution Increase	0%	✓						✓						✓					
	20%		✓						✓						✓				
	40%			✓						✓						✓			
	60%				✓						✓						✓		
	80%					✓						✓						✓	
	100%						✓						✓						✓

The strategy for increasing the percentage of heavy vehicles in scenarios is based on freezing the total vehicle inputs, i.e., for each HV% increase, accordingly, a similar percentage is decreased in light vehicle contribution (the percentage of motorcycles remained constant), which, in turn, makes the total vehicle inputs be unchanged. Table 3-2 demonstrates the whole vehicle compositions in various roads simulated in VISSIM to build the determined scenarios based on the HV percentage increases.

Table 3-2. Vehicle composition in available scenarios regarding HV% increase

Roads	Vehicle type	Heavy vehicle increase					
		0%	20%	40%	60%	80%	100%
East ↔ West	Light-vehicle	0.857	0.8422	0.8274	0.8126	0.7978	0.783
	Heavy-vehicle	0.074	0.0888	0.1036	0.1184	0.1332	0.148
	Motorcycle	0.069	0.069	0.069	0.069	0.069	0.069
North ↔ South	Light-vehicle	0.888	0.8796	0.8712	0.8628	0.8544	0.846
	Heavy-vehicle	0.042	0.0504	0.0588	0.0672	0.0756	0.084
	Motorcycle	0.07	0.07	0.07	0.07	0.07	0.07

3.4. Brake Emissions Estimation

3.4.1. Proposed Method

Three phases of brake emission investigation are proposed in the current research: suprasystem, system, and subsystem levels [160]. In the first step, a minidynamometer machine is used at the subsystem level to conduct more than one thousand tribological tests with different configurations of brake torques, disc and pad temperatures, rotor speeds, and other functional parameters to evaluate the amount of airborne brake wear particles generated for every brake operation. Then, the minidyno output data is used to build an artificial neural network brake emission model considering selected variables (initial speeds, final speeds, and brake torques) as independent variables. At the suprasystem level, the input volumes, route choices, pedestrian volumes, modal splits, number of parking lots, and traffic light green and red timings data collected in the field survey (real case study) are fed into traffic microsimulation software for monitoring the vehicles' trajectories and finding the route choice decisions. Similar to the traffic microsimulation for the exhaust emissions, every single traffic element is modeled based on the actual captured data. In the simulation configuration, all the individuals in the transportation network are monitored; their movements are recorded every 0.05 seconds. Next, to perform vehicle dynamics considerations and estimate brake wear emissions, the records of dominant sport utility

vehicle (SUV) family cars, including speed, acceleration, vehicle coordination, number, length, height, mass, width, and positions in the networks, are accurately extracted from the microsimulation model outputs.

At the system level, a custom vehicle longitudinal dynamics model is developed to convert the vehicle's kinematic behavior into brake emission-relevant quantities (inverse dynamic). For this purpose, real vehicle design information, like the height of the center of mass, coefficient of friction, drag coefficient, wheel radius, and other related parameters, is collected through brochures and materials provided by the vehicle manufacturer. The vehicle's front and rear wheels' brake torques and angular velocities starting from the vehicle simulation-based speed time series, were calculated using the developed vehicle inverse dynamics model. The resulting data obtained by the traffic microsimulation and vehicle system dynamic, including brake torques, and initial and final speeds for every braking event, are inserted into the subsystem level ANN-based model to predict the real brake emission at each braking event. In the final step, the number of brake particles the targeted vehicle generates at each route decision and in the whole transportation system is estimated and comprehensively analyzed. This proposed method opens a state-of-the-art way for traffic engineers and environmental scientists to monitor the rate of real brake emissions generation in congested areas regarding different traffic conditions. Also, controlling the number of brake particles released by either motor vehicles or electric cars can be more accessible for decision-makers to improve air quality. Figure 3-2 summarizes the steps of the proposed method.

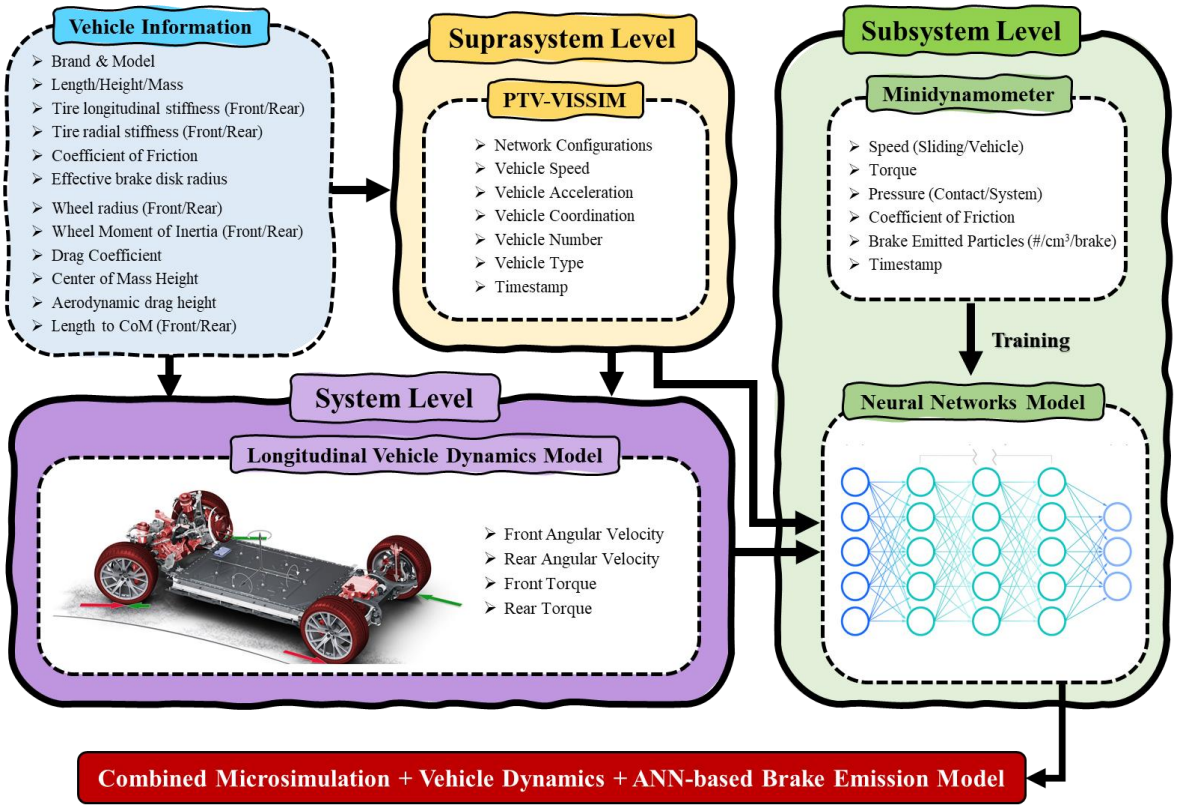

Figure 3-2. Proposed method for brake emission estimation

3.4.2. Materials and models specifications

3.4.2.1. Targeted Vehicle

Vehicle design characteristics are known as one of the influential factors which remarkably affect the generation rate of non-exhaust emissions. In the present dissertation, the number of brake emissions produced by dominant family SUV vehicles (hereafter "targeted vehicles") in the case study is estimated. The design information of the targeted vehicle is one of the fundamental inputs for the microsimulation software and longitudinal vehicle dynamics model. This information is collected from the manufacturer's brochure, and necessary material is obtained from the official providers. Table 3-3 demonstrates all the targeted vehicle information used in this study.

Table 3-3. Targeted vehicle information

Parameter	Value	Parameter	Value
Drag coefficient	0.36	Vehicle Mass	2060 Kg
Nominal radius of the front wheel	0.37 m	Height of the center of mass	0.712 m
Radial stiffness of the front tire	218000 N/m	Height of the direction of application of the aerodynamic drag	1.2 m
Nominal radius of the rear wheel	0.37 m	Distance between front axle and center of mass	1.5219 m
Radial stiffness of the rear tire	218000 N/m	Distance between rear axle and center of mass	1.3381 m
Front tire longitudinal stiffness	30.6217	Front wheel moment of inertia	1.65 $Kg.m^2$
Rear tire longitudinal stiffness	30.6217	Rear wheel moment of inertia	1.65 $Kg.m^2$
Front tire coefficient of rolling resistance	0.0124	Braking torque front/rear axles distribution	52%
Rear tire coefficient of rolling resistance	0.0124	Friction coefficient between brake pads	0.35
Average fuel mass	70 kg	Average payload mass	366 kg

3.4.2.2. Subsystem Level

3.4.2.2.1. Minidyno

As comprehensively represented in Chapter 2, the minidyno (reduced-scale dynamometer) is a well-known reliable machine for brake wear estimations. In the present study, more than one thousand tests with different speeds, deceleration, disc temperature, brake duration, cycle length, and brake torque were conducted using the LINK minidyno machine model 1200. This brand has been regarded well in the literature regarding its effective capabilities in reality-based simulating vehicle braking systems [159]–[161]. Besides the main brake pads and rotor embedded inside the machine, other subsidiary devices should be attached to the machine to collect and measure the emission generations. In this research, one of the well-thought-of emission analyzer devices worldwide, called TSI Optical Particle Sizer (OPS), is installed in the way of the outlet pipe of the main chamber to collect and measure the emissions. OPS device can count particle sizes from 0.3 to 10 μm (in 16 in-

size channels), which is applicable to capture most of the particles contributing to the PM10 and $PM_{2.5}$, but no nano-sized particles. Figure 3-3 shows the minidyno machine and OPS device used in this research.

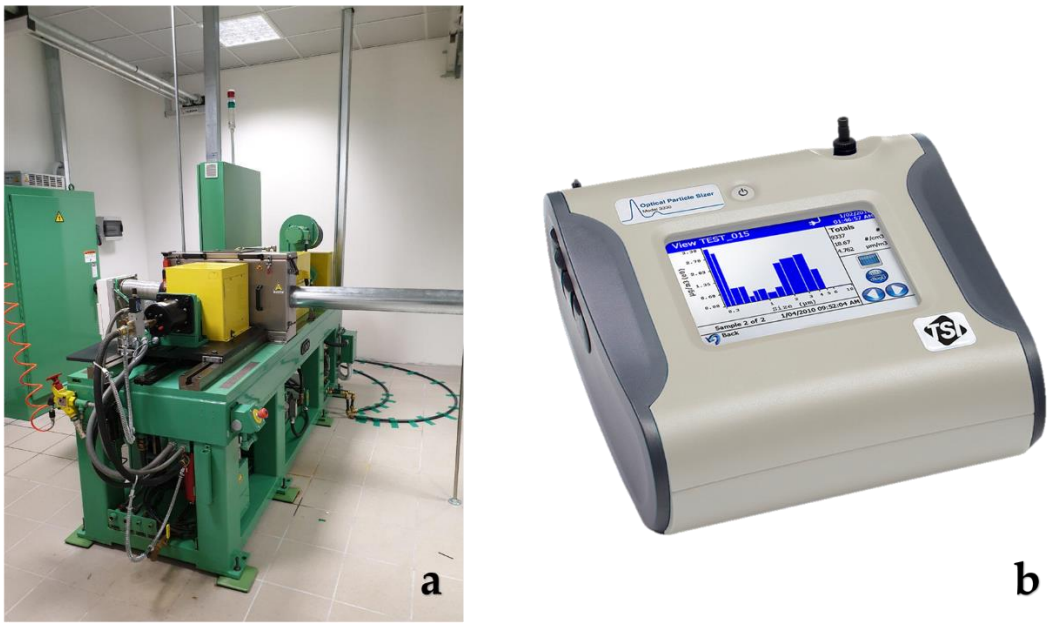

Figure 3-3. a) Minidyno machine, b) OPS device

The airflow going throughout the system is provided by a fan with an rate of 0.74m^3/min installed at the left side of the minidyno. A high-efficiency particulate air filter (HEPA) filters the generated airflow, installed just after the fan. Figure 3-4 shows the scheme of the system with all its components.

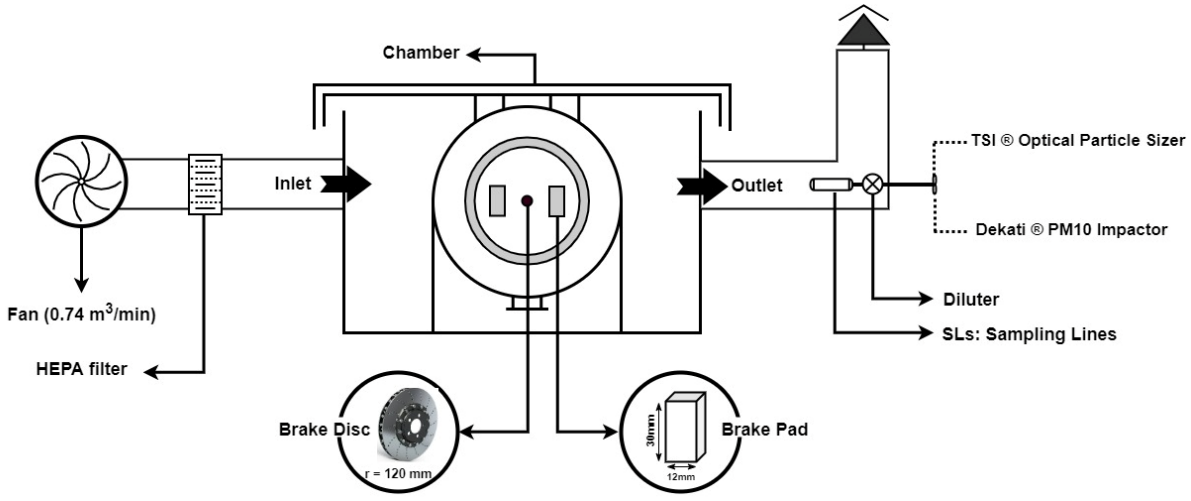

Figure 3-4. Scheme of the minidyno experimental setup

For the tribological tests, a confining sealed chamber is installed ahead of the main reduced-scale braking system to avoid leaking air flow and brake debris outside the control volume. Throughout this system, the generated airborne particles are carried by the airflow crossing through the chamber, conveying to the outlet pipe. The outlet large-diameter pipe is equipped with a diluter and sampling probe to help OPS collect the emissions' particles.

Low-metallic brake pads, which are the most common pads in the market, are considered for the experiments. For installing brake pads inside the machine, pads' size adjustments is needed. To achieve this end, the pads are cut into rectangular-shaped samples with a geometry size of 12 mm × 30 mm. To simulate the motions of the vehicle's brake rotor, a conventional pearlitic cast-iron brake disc with the diameter, thickness, effective radius, and hardness of 120 mm, 6 mm, 50 mm, and 235 HV10, respectively, is considered. Figure 3-5 presents the brake pads and disc used for the experiments performed by the minidyno machine.

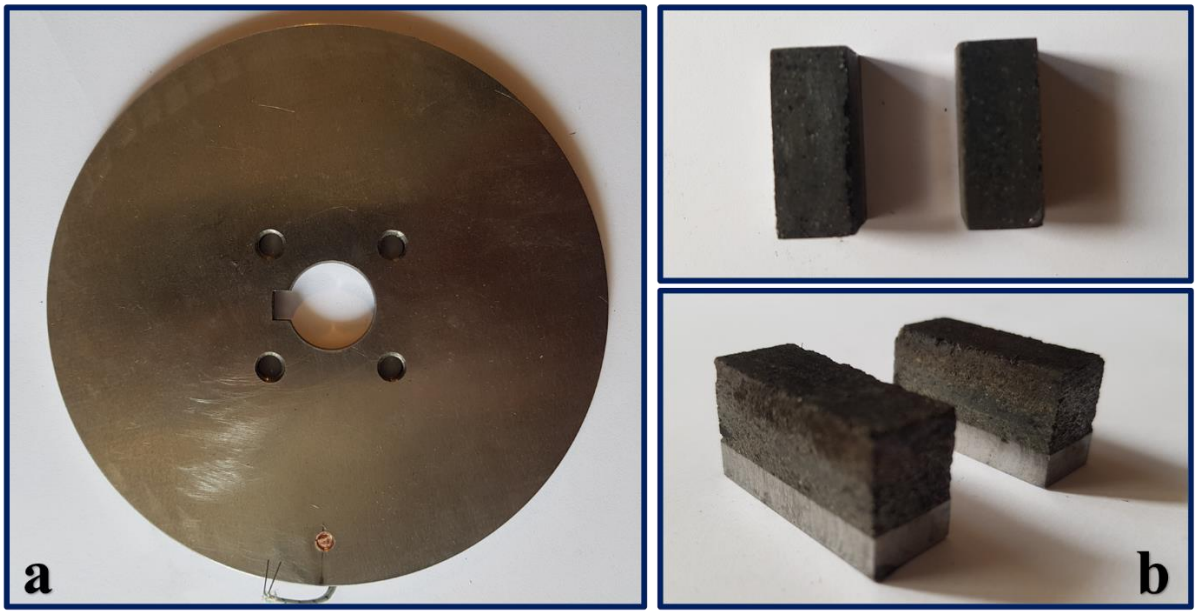

Figure 3-5. Minidyno main components; a: Brake disc, b: Brake pads

To expand the variables' domain for boosting the data training in the ANN brake emission model and reducing the time of cost function minimization, various configurations for the tribological tests are considered, including the changes in the rotor speed, contact

temperature, contact pressure, and deceleration. Taking these changes in tribological parameters into accounts, more than one thousand separate configurations are made and defined as practical scenarios for the minidyno machine. An example of a brake event measured by OPS device is presented in Figure 3-6, demonstrating the total particle numbers per brake operation in the cycle length.

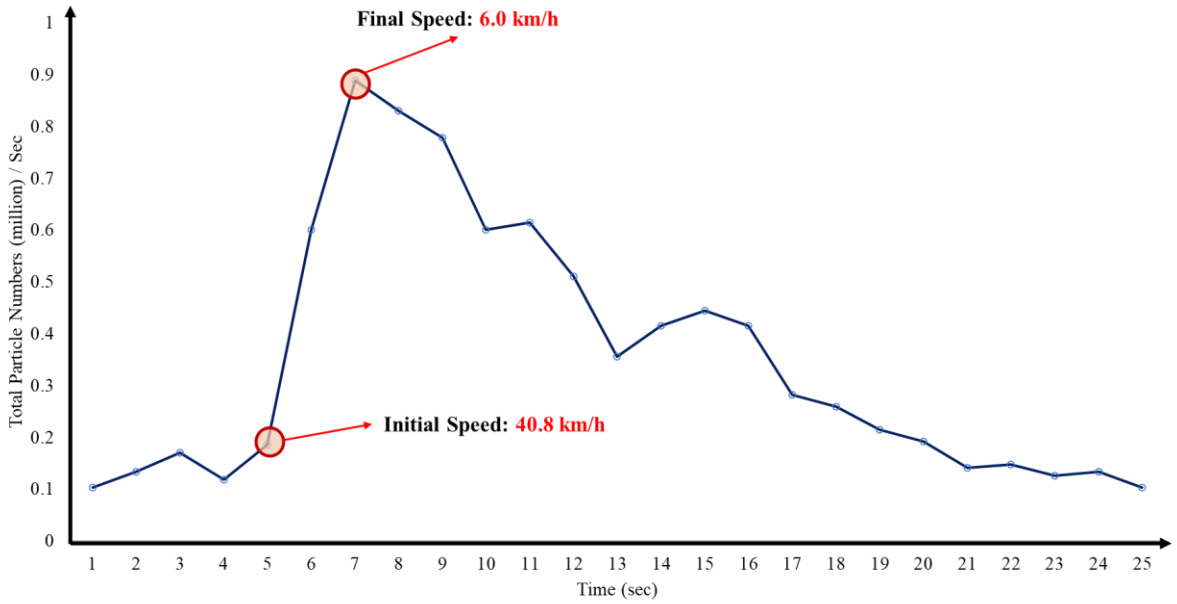

Figure 3-6. An example of the emission generation in a brake event collected by OPS device in minidyno tests

By default, OPS reports the total concentration ($\frac{\#}{cm^3}$) of brake emissions. To convert the total concentration to the total particle numbers ($\frac{\#}{sec}$), the below equation were used:

$$Total\ Particle\ Numbers\left(\frac{\#}{sec}\right) = Total\ Concentration\left(\frac{\#}{cm^3}\right) \times 0.74\left(\frac{m^3}{min}\right) \times 10^6 \times 10 \div 60$$

Volume Conversion
Airflow
Dilution Factor
Time Conversion

3.4.2.2.2. Data Preparation

Throughout the observations during the experimental test in minidyno, it was found that the braking system continued generating airborne particles even after the brake event

termination. Many reasons can cause this eccentric phenomenon. For instance, a residual high temperature on pads and discs is recorded after the end of the brake event. Also, an inherent feature of pad components and airflow impacts can be counted as other influential factors. In response to the challenges of particle collection during a brake event imposed by this phenomenon, the brake particles are collected for remarkably higher periods than the brake durations. However, the periods of particle collections are chosen based on the fact that they do not exceed the cycle length defined for the brake operations.

By visualizing the data, it was found that a greater number of scenarios are performed with a brake duration of fewer than 8 seconds. However, the rest was found in less than 10 seconds. To collect the whole brake emitted particles, a novel synchronization approach was implemented among minidyno and OPS outputs. By plotting the whole cycle length of different brake events, some noises were observed before and after the brake duration. These noises may be related to the machines' calibrations or the time needed for the transmission of particles from the minidyno chamber to the OPS recognition probe. To collect a more realistic number of brake particles, a threshold encompassing the noise particles (before and after the brake duration) was defined based on the starting point plus the standard deviation among some points with a minimum number of brake particles in the whole cycle length. Then, all the emission particles above the threshold were collected and reported.

3.4.2.2.3. Artificial Neural Network (ANN) brake emission modeling

ANNs are computational models inspired by an animal's central nervous systems. Artificial neural networks are composed by various layers of interconnected artificial neurons powered by activation functions. They can learn and model the relationships between input and output data that are nonlinear and complex. Regarding their compatibility to model time-series data, they can depict excellent functions on emission models [161], [162]. In an ANN model, determined data is passed through specified layers to predict the outputs and compare them with the target observations. In terms of concept, this process is called "training" or "data training", including two techniques: Forward-propagation and Back-propagation. Generally, an artificial neural network consists of three

components: an Input layer, Hidden (computational) layers, and an Output layer. This multi-layered structure increases the change of successfully modeling unknown phenomena [161].

Numerous studies can be found in the literature focused on the implementation of AI-based models for brake emission estimations [163]–[167]. In 2016, Hassan & Mohammad developed an artificial neural network model to predict the rate of wear generation and temperature based on the tribological data obtained by pin-on-disc machine [167]. The proposed model has been successfully performed on data and presented sensible results, the same as the results shown in [168]. Furthermore, Aleksendric found the ANN-based method as an effective way for brake wear estimation considering friction materials, sliding speed, temperature, and applied load [169]. Recently, the ANN brake emission models have been improved significantly in terms of accuracy and efficiency. Argatov and Chai used an Archard–Kragelsky model to develop an ANN-supported regression model, which could predict the rate of brake wear with high accuracy [170]. The unique feature of their model was to reduce the number of degrees of freedom compared to standard ANN brake wear models. In addition, a simple model of linear regression (single variable) was performed by Gailis et al. considered the mileage of the vehicle as the only variable in the model to predict the brake wear out [171]. In 2006, Durmuş et al. investigated the rate of wear loss and surface roughness of the aluminum alloy by accomplishing a model based on the artificial neural network [172], as well as similar investigations performed by [173]–[175].

In the present dissertation, minidyno brake wear data is used for developing a brake emission neural network model. For this purpose, first, the prepared minidyno data is analyzed, and the correlations between the number of emitted particles and tribological parameters at each timestamp are evaluated. Among all tribological parameters, initial speed, final speed, and brake torques are found to be the most correlated parameters with brake wear emissions. For considering the impacts of vehicle dynamics on emission generation, brake torque is also selected as it showed high correlation results with brake emission production. In summary, initial speed, final speed, and brake torque are chosen as the main independent variables to apply for developing the brake emission ANN model.

3.4.2.2.3.1. Neighboring points selection approach

One of the effective approaches to improve the training of time-series data in ANN models is to use the neighboring points selection. According to this approach, the dependent variable in the model is predicted based on a "cloud" of neighboring points characterized experimentally, i.e., neighboring points surrounding the reference point are used rather than a single point for the estimation of the dependent variable. In the present research, the triplet initial speed, final speed, and brake torque are trained on the neighboring points and, finally, evaluated on the given triplet. In the phase-space, a total of 10 neighboring points are selected, which have the closest distance to the reference point. Considering the neighboring point selections approach, using the "local" ANN approach instead of the "global" ANN approach, remarkably increased the accuracy of brake emission predictions due to the average R-Squared results equaled more than 0.9 in most cases. Figure 3-7 shows the architecture of the proposed ANN model and the scheme of the neighboring points selection approach.

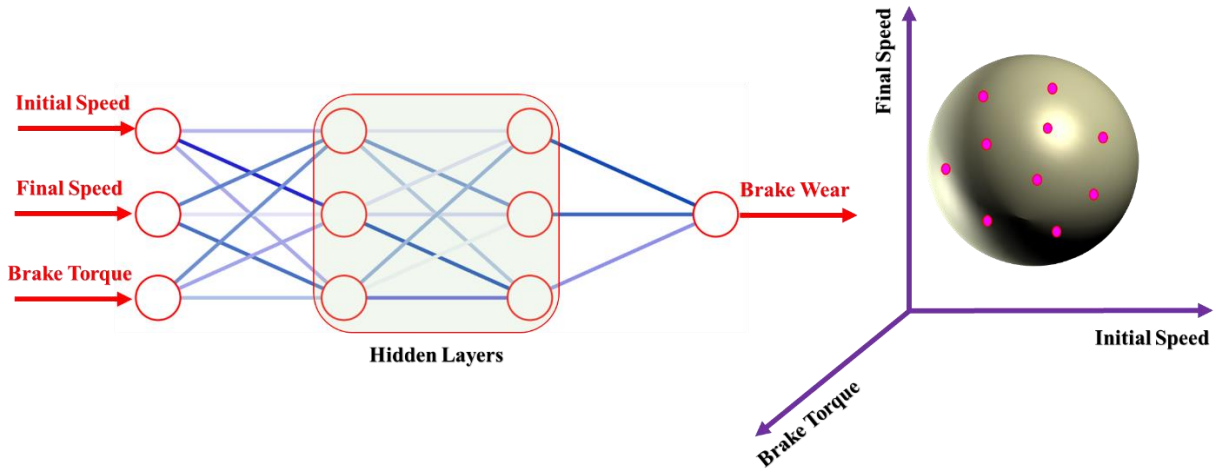

Figure 3-7. Proposed ANN model architecture and scheme of neighboring points

3.4.2.3. System Level

3.4.2.3.1. Vehicle System Dynamics Model

Vehicle dynamics is a complicated experimental and analytical technique used to study the responses of a vehicle in various in-motion situations by which the vehicle's actual

behavior can be modeled at the system level [176]. The dynamics of a vehicle can be influenced by many factors, such as the type of pads, vehicle mass, ground coefficient of friction, road slope, radial and longitudinal stiffnesses of tires. To gain real emission results, considering these factors is essential as they may directly impact the emission production rate. For example, the heterogeneous distribution of the vehicle mass between the front and rear axle can affect the generation rate of emitted front and rear particles. Therefore, considering vehicle dynamics plays a crucial role in realistic emission prediction.

Although the simulation models has increased the insight for the brake wear estimation, the effects of vehicle dynamics on emissions were less regarded. Torque, speed and acceleration, which are the main vehicle dynamic attributes, were widely used in previous studies to predict exhaust emissions such as CO_2, NOx, and THC and vehicles' fuel consumption using vehicle dynamic-based simulation models [177]–[180].

Traffic microsimulation can be integrated with the concept of vehicle dynamics to shape a new approach to the simulation of vehicle mobility. However, this perspective has not been regarded widely in previous studies. The Handbook Emission Factors for Road Transport (HBEFA) offers reliable exhaust emission factors for different vehicle types considering PHEM (Passenger car and Heavy duty Emission Model), a simulation-based vehicle emission model developed by the TU Graz since 1999, in which the emissions were estimated based on the vehicle longitudinal dynamics and on engine emission maps [181]. Expectedly, the integration of traffic microsimulation and vehicle dynamics guided the exhaust emission factors to be more accurate and reliable compared to the sole use of traffic microsimulation models. In 2018, in a research conducted by So et al., the tailpipe emission estimation was conducted based on the integration of microscopic traffic simulation and vehicle dynamics model [182]. Integrating the vehicle trajectories obtained by the VISSIM simulation models with a vehicle dynamic model shaped the main elements of their exhaust emission estimation methodology and resulted in more reliable results compared to the similar-approach studies.

In this dissertation, a mathematical longitudinal vehicle dynamics model is developed in Wolfram Mathematica programming language as traffic microsimulation models in VISSIM

are crippled to present such dynamic considerations. As shown in Figure 3-8, the model was developed by writing the symbolic equations of motion of the longitudinal dynamics of the vehicle including the wheels, subjected to the traction and resistance forces. The vehicle longitudinal dynamic model here described assumes that no limit conditions are reached by the tires, making it possible to adopt linear models for the tires' forces and torques. The assumptions of main involvement of the longitudinal dynamics (i.e. negligible impact of the vehicle lateral dynamics) and of linear response of the tires are both quite reasonable in the frame of a low-speed urban scenario.

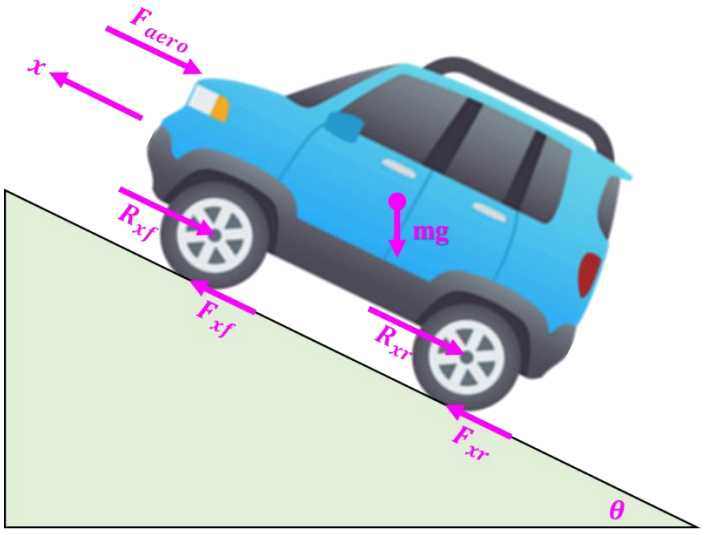

Figure 3-8. Sketch of longitudinal dynamics forces on a vehicle

As shown in Figure 3-8, we write the Newton's equation of the vehicle projected along the longitudinal direction of the vehicle (x):

$$m\,\ddot{x} = F_{xf} + F_{xr} - R_{xf} - R_{xr} - F_{aero} - mgsin(\vartheta) \qquad \text{(Eq. 3-1)}$$

where:

$m \rightarrow$ vehicle mass

$\ddot{x} \rightarrow$ vehicle acceleration

$F_{aero} \rightarrow$ aerodynamic drag force

$F_{xf} \rightarrow$ longitudinal force of front tire

$F_{xr} \rightarrow$ longitudinal force of rear tire

R_{xf} → front tires rolling resistance force

R_{xr} → rear tires rolling resistance force

g → gravity acceleration

ϑ → road slope

The resistances are estimated as follows:

$$R_{xf} = f\ F_{zf} \quad \text{(Eq. 3-2)}$$

$$R_{xr} = f\ F_{zr} \quad \text{(Eq. 3-3)}$$

$$F_{aero} = \frac{1}{2}\rho\ C_w A\ \dot{x}^2 \quad \text{(Eq. 3-4)}$$

where:

f → rolling resistance coefficient

F_{zf} → normal force on front tire

F_{zr} → normal force on rear tire

ρ → air mass density

C_w → aerodynamic drag coefficient

A → vehicle frontal area

$\dot{x}$ → vehicle speed

Projecting the Euler's equation in the moving frame, we can calculate the normal forces on the front and rear tires assuming that the vehicle pitch acceleration is negligible:

$$F_{zf} = \frac{1}{l_f + l_r}(-F_{aero}h_{aero} - m\ \ddot{x}\ h - mghsin(\vartheta) + mgl_r cos(\vartheta)) \quad \text{(Eq. 3-5)}$$

$$F_{zr} = \frac{1}{l_f + l_r}(F_{aero}h_{aero} + m\ \ddot{x}\ h + mghsin(\vartheta) + mgl_f cos(\vartheta)) \quad \text{(Eq. 3-6)}$$

where:

l_f → longitudinal distance between front axle and center of mass

l_r → longitudinal distance between rear axle and center of mass

h_{aero} → height of aerodynamic drag force

h → center of mass height

The tire longitudinal forces are assumed to be proportional to the longitudinal slip and the normal forces:

$$F_{xf} = k_f F_{zf} \sigma_f \quad \text{(Eq. 3-7)}$$

$$F_{xr} = k_r F_{zr} \sigma_r \quad \text{(Eq. 3-8)}$$

where:

$k_f \rightarrow$ front tire longitudinal stiffness

$k_r \rightarrow$ rear tire longitudinal stiffness

$\sigma_f \rightarrow$ Front longitudinal slip ratio

$\sigma_r \rightarrow$ Rear longitudinal slip ratio

Where the front and rear slip ratios are defined as follows:

$$\sigma_f = \frac{r_{ef}\omega_f - \dot{x}}{\dot{x}} \quad \text{(Eq. 3-9)}$$

$$\sigma_r = \frac{r_{er}\omega_r - \dot{x}}{\dot{x}} \quad \text{(Eq. 3-10)}$$

where:

$\omega_f \rightarrow$ front wheel angular velocity

$\omega_r \rightarrow$ rear wheel angular velocity

$r_{ef} \rightarrow$ Front wheel effective radius

$r_{er} \rightarrow$ Rear wheel effective radius

The effective radius are:

$$r_{ef} = r_0 - \frac{F_{zf}}{k_t} \quad \text{(Eq. 3-11)}$$

$$r_{er} = r_0 - \frac{F_{zr}}{k_t} \quad \text{(Eq. 3-12)}$$

where:

$r_0 \rightarrow$ undeformed tire radius

$k_t \rightarrow$ vertical tire stiffness

The wheels' dynamics is described by the two Euler equations:

$$J_f \dot{\omega}_f = -F_{xf} r_{ef} - T_f - T_{rf} \quad \text{(Eq. 3-13)}$$

$$J_r\dot{\omega}_r = -F_{xr}r_{er} - T_r - T_{rr} \quad \text{(Eq. 3-14)}$$

where:

$\omega_f \rightarrow$ front wheel angular acceleration

$\dot{\omega}_r \rightarrow$ rear wheel angular acceleration

$J_f \rightarrow$ front wheel inertia

$J_r \rightarrow$ rear wheel inertia

$T_f \rightarrow$ front braking torque

$T_r \rightarrow$ rear braking torque

$T_{rf} \rightarrow$ front wheel resistance torque

$T_{rr} \rightarrow$ rear wheel resistance torque

We assume hereinafter that the braking system is tuned to provide a pre-defined front/rear braking torque partition:

$$T_f = k_b T \quad \text{(Eq. 3-15)}$$

$$T_r = (1 - k_b)T \quad \text{(Eq. 3-16)}$$

where:

$k_b \rightarrow$ brake distribution coefficient

The resistance torques are given by:

$$T_{rf} = fr_{ef}F_{zf} \quad \text{(Eq. 3-17)}$$

$$T_{rr} = fr_{er}F_{zr} \quad \text{(Eq. 3-18)}$$

The inverse dynamics model is found by means of the following steps. The tires' slip equations 3-9 and 3-10 are solved for the angular velocities, which are substituted into the wheels' Euler equations together with the tires' normal and longitudinal forces. The two equations are then solved for the tires' slip, which result functions of the vehicle acceleration. The calculated forces are substituted into the Newton's equation, which is solved for the total braking torque T, yielding T_f and T_r as functions of the vehicle acceleration. The wheels' angular velocities are calculated by means of the tires' slip and vehicle velocity, according to

equations 3-9 and 3-10. The final set of four equations (two torques and two angular velocities) constitute and inverse dynamics algebraic model: given the vehicle motion (acceleration time history) it provides the relevant quantities.

In this study, the vehicles' trajectory information (vehicles' movement records) obtained by VISSIM is used as the input for the customized longitudinal vehicle dynamics model presented above. In addition to VISSIM data, applying the design information of the targeted vehicle is also essential for the aforementioned vehicle dynamics model. The expected outputs of this model are the vehicle's front and rear brake torques and angular velocities based on the given inputs. The obtained outputs, together with the traffic microsimulation outputs, are then applied to the ANN model, previously obtained by the minidyno data, to estimate the brake emission in the case study.

3.4.2.4. Suprasystem Level

Until now, the subsystem and system investigation levels and their considerations throughout the proposed method are comprehensively described. All the traffic microsimulation models are mainly described at the suprasystem level as it makes the investigation of various systems (individuals) in a network feasible. To keep the integration of this thesis, all the details of considerations in this level has been comprehensively discussed in the section "3.2. Traffic microsimulation". For scrutinizing the details, please refer to this section.

3.4.2.4.1. Data Preparation

By simulating the ground-truth scenario in VISSIM, a total of 26 million records is obtained at each simulation run. After extracting the data related to the targeted vehicles from the database, on average, approximately 650,000 records are obtained for each simulation repetition. With ten iterations of the simulation model, more than 7 million data is obtained. To estimate the number of brake particles route-by-route, six separate routes are determined for the vehicles resorting in the network, covering all the roads of the case study map. Figure 3-9 presents the defined routes in detail.

Point	Direction
1	Two-way
2	One-way
3	Two-way
4	One-way

Trip	Route
1 → 2	A
1 → 3	B
3 → 1	C
4 → 1	D
4 → 2	E
4 → 3	F

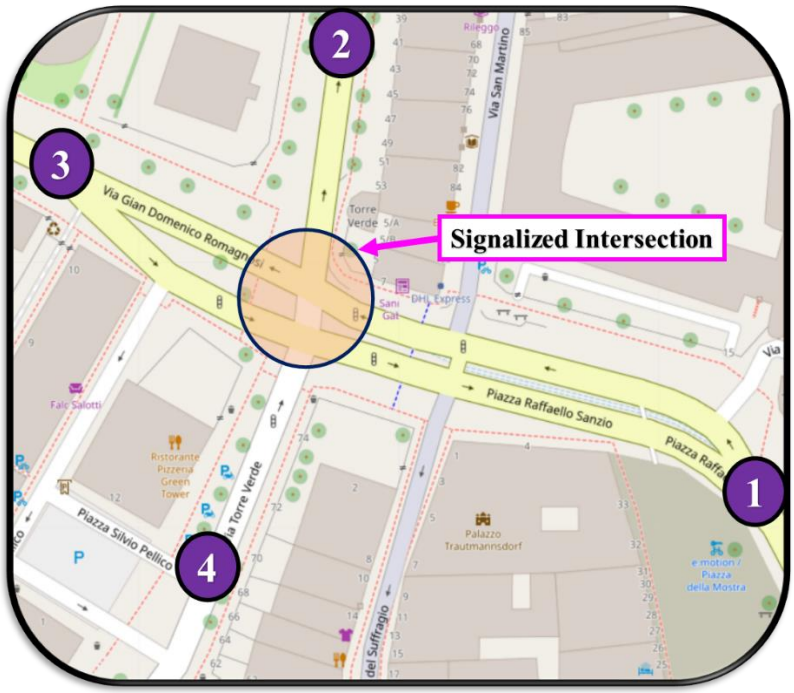

Figure 3-9. Route definitions

The vehicle trajectories obtained by VISSIM simulation consist of the speed, acceleration, deceleration, brake event, the intensity of the brake events, and brake duration collected from the vehicles' activities in the network. To calculate the brake torque and angular velocities for each targeted vehicles, this obtained data is then inserted into the vehicle dynamics model (See the section "3.4.2.3.1"). As mentioned in the section "3.4.2.2.3", initial speed, final speed, and brake torque are selected as the leading independent variables for the ANN brake emission model. To feed the ANN model, a new data frame is built by considering the brake torque results obtained from the vehicle dynamics model and extracting the initial and final speeds from the VISSIM output database. After feeding the ANN model, the total emissions generated by each vehicle in a specific route are calculated by summating the obtained number of particles for all brake events per vehicle.

Chapter 4

Case Study

4. Chapter 4: Case study

4.1. Air pollution in Italy

Similar to many European countries, Italy is suffering from high level of air pollution not only in urban but also in suburban or rural areas. The rate of pollutants in some northern cities, including Cremona, Vicenza, Brescia, and Pavia, is the highest among all European cities, as reported by European Economic Area (EEA) [183], [184]. In Italy, dominant emissions are different depending on the regions' topographical location. For instance, NO_2, CO, VOC, and $PM_{2.5}$ (particulate matter with a diameter of 2.5μm or less) are the dominant emissions in the northern part of the country [185]. However, the rate of O_3 is more dominant in the south and central provinces [185]. These high emission levels are more critical and important in Italy compared to other European countries as it is not only the third populated country in the European Union (more than 60 million citizens), but also the destination of more than 61 million international tourists every year [186].

Featuring some 119,760 inhabitants, Trento is the capital of the autonomous province of Trento located on the Adige River in Trentino-Alto Adige, north of Italy. In the coldest month (January), the average low temperature can reach about −2.1°C, and in the warmest months (July), the average high temperature can reach 29.4°C. Having the area of 158 km^2, Trento is witness of thousands of national and international tourists every year due to its unique features. Graceful weather condition and humidity level, together with many ancient tourist attractions like Buonconsiglio Castle (13th century), Church of San Pietro (12th century), and Palazzo delle Albere (16th century) convince a huge numbers of tourists using the main railway connection between Italy and Germany for their journey to visit the city. Statista reported that more than 836,000 international tourists visited Trento in 2016 [187]. Moreover, annually, Trento is the host of many international sport events like Alpine and European Road Cycling Championships as it has been surrounded by wide sport-friendly mountains. All these features have made this city as one of the congested cities in the north of Italy regardless of its limited area.

In November 2021, emission measuring devices in Trento recorded a rate of $PM_{2.5}$, 2.2 times above the WHO annual air quality guideline [188]. Besides the Particulate Matters problem, the air quality in Trento has been significantly affected by other harmful emissions such as nitrogen dioxide, volatile organic compounds, and carbon monoxide. In Trentino, in 2021, there was an average annual level of 34 micrograms per cubic meter ($\mu g/m^3$) of nitrogen dioxide compared to a maximum value recommended by the World Health Organization (WHO) of 10 $\mu g/m^3$: an overrun of over three times the limit [189]. The Trentino area is characterized by vast numbers of motor vehicles, which can be associated with non-negligible emissions of volatile organic compounds (VOCs). Also, due to the massive spread of CO in urban areas, the Legislative Decree of 13 August 2010, n. 155 was established to limit the concentration of carbon monoxide in the ambient air produced daily to 10 $\mu g/m^3$ to protect citizens' health [190]. As a result, air pollution is known as one of the dominant issues in this city threatening the lives of residences and commuters.

4.2. Case specifications

Buonconsiglio Castle, firstly built in the 13th century, is one of the well-known and eye-catching tourist sights in Trento attracting thousands of international tourists and visitors annually. Located roughly close to the city center of Trento and very near to the Trento central railway station (to Munich, Germany suburban train line), Buonconsiglio Castle possesses one of the best location of the city. The main route to reach the castle entrance is using the main street named “Via Bernardo Clesio”, which ends at the Trento central railway station (500m distance). In response to the volume of visitors in/outside the castle, many minimarkets, restaurants, ice-cream stores (Gelateria), and a busy and popular store (Tabacchi shop) were established around the castle. Figure 4-1 presents the case location on the map.

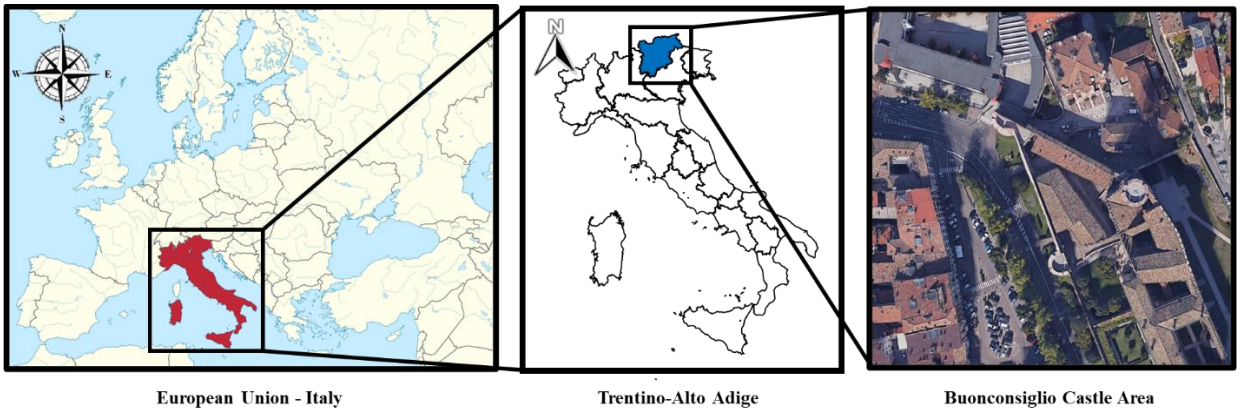

Figure 4-1. Location of the studied case

Trentino trasporti S.p.A has established a set of urban passenger buses throughout 23 exclusive lines to connect different part of the city and the surrounding villages to each other. Compared to the other parts of the city, Buonconsiglio Castle area is more congested as all the routes determined for these public fleets end to the central railway station to provide urban and suburban mobilities. Daily, thousands of commuters use the public transport or private cars to reach the central station by crossing the castle surrounding roads, especially in rush hours. Moreover, the number of intake passengers traveling Trento from other cities like Revereto, Verona, Bolzano, and even Munich should not be underestimated. Besides railway transportation fleets, many suburban buses are also resorting Trento every day to transfer dozens of passengers from/to other part of Italy or Europe to/from Trento, including Flixbus and Itabus. All these commutes make to area around the castle become more congested and in some cases (weekends), traffic oversaturation can be observed.

4.3. Signalized intersection in front of the castle

The mobility around the castle is being controlled by a highly-congested four-legged signalized intersection roughly close to the main entrance, which has been developed by the cross of two high-demanded roads named Piazza Raffaello Sanzio and via Alessandro Manzoni (Via Torre Verde). To facilitate the pedestrians resorts throughout the intersection, beside the pre-determined crosswalks in the four-leg intersection, the municipality considered a big pedestrian crosswalk areas on the Bernardo Clesio street, where the majority of pedestrians and cycling resorts were happening. All these commutes were performed in

an exclusive sidewalk without interfering vehicle movements. Protected signal timings were observed for all signalized crosswalks in the field survey. Also, the right turn movement of Via Torre Verde was found protected with different green and red timings. However, all the other turning signals were configured to be a permitted moving allowance. Moreover, all signal timings was set as pretimed timings, not actuated or semi-actuated as expected. Figure 4-2 represents the sketch of the aforementioned signalized intersection in front of the Buonconsiglio Castle.

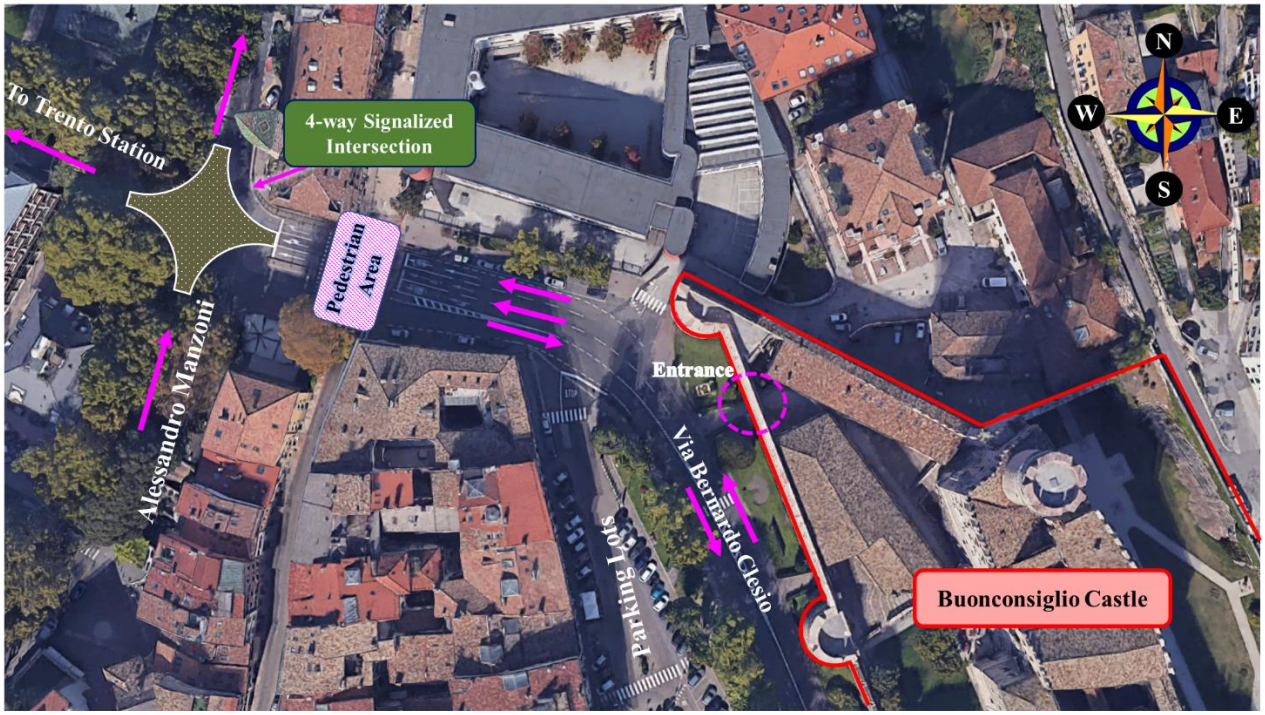

Figure 4-2. Sketch of signalized intersection in front of the Buonconsiglio Castle

4.4. Data Collection

The evening rush hour in a sunny day was considered as the critical time for the data collection when the maximum number of vehicles can be observed in the transportation network and the traffic rate was found uniformly distributed. For this purpose, full-HD cameras were directly employed by the research team for capturing the vehicle inputs, number of pedestrians, parking lots, traffic flow rate, signal timings, number of lanes at each leg, and distribution of different types of vehicles (modal splits). All the recordings were then accurately analyzed by the research team to determine the traffic parameters like the route

choices and non-traffic parameters like roads geometry, intersection characteristics, and agents conflict areas. Expectedly, the percentage of heavy vehicles (passenger buses) was found significantly high compared to the other part of the city regarding the vicinity to the central bus terminal in the Trento railway station. The contribution of heavy vehicles in the network model split was found different at each intersection legs because of the bus pre-determined stations and the according route choices. Figure 4-3 summarizes the collected traffic data. All units in the figure are "per hour" except the traffic lights which has the "second" unit.

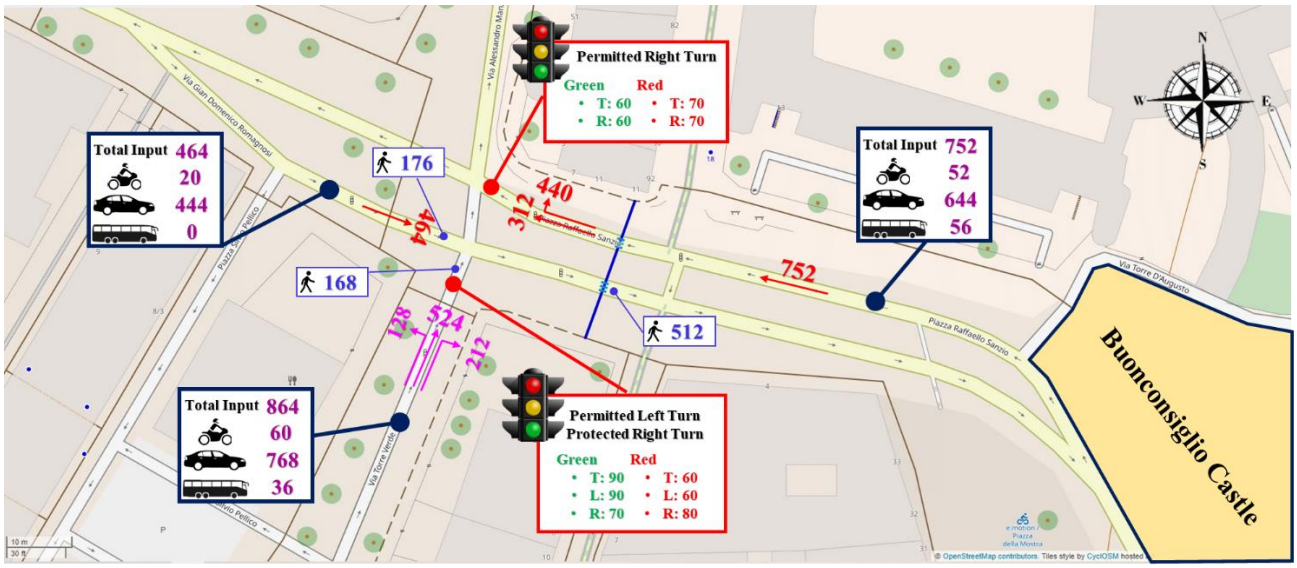

Figure 4-3. Collected traffic data

Chapter 5

Results

5. Chapter 5: Results

5.1. Exhaust Emissions

The models simulated in VISSIM were first tested through a series of verification tests as explained in the following paragraph [191].

5.1.1. Model Verification Tests

To verify the reliability of the proposed model, a set of verification tests was conducted considering the verification steps suggested by Sterman [192] and Banks et al. [193]. In the beginning, the sensitivity of the model to vehicle input fluctuations was tested [192]. To reach this end, vehicle inputs for all traffic inlets were decreased by 50%, increased by 50%, and 100%. Considering different vehicle inputs provides essential information about the direction of changes in emission generations. Figure 5-1 presents the results obtained in the sensitivity analysis.

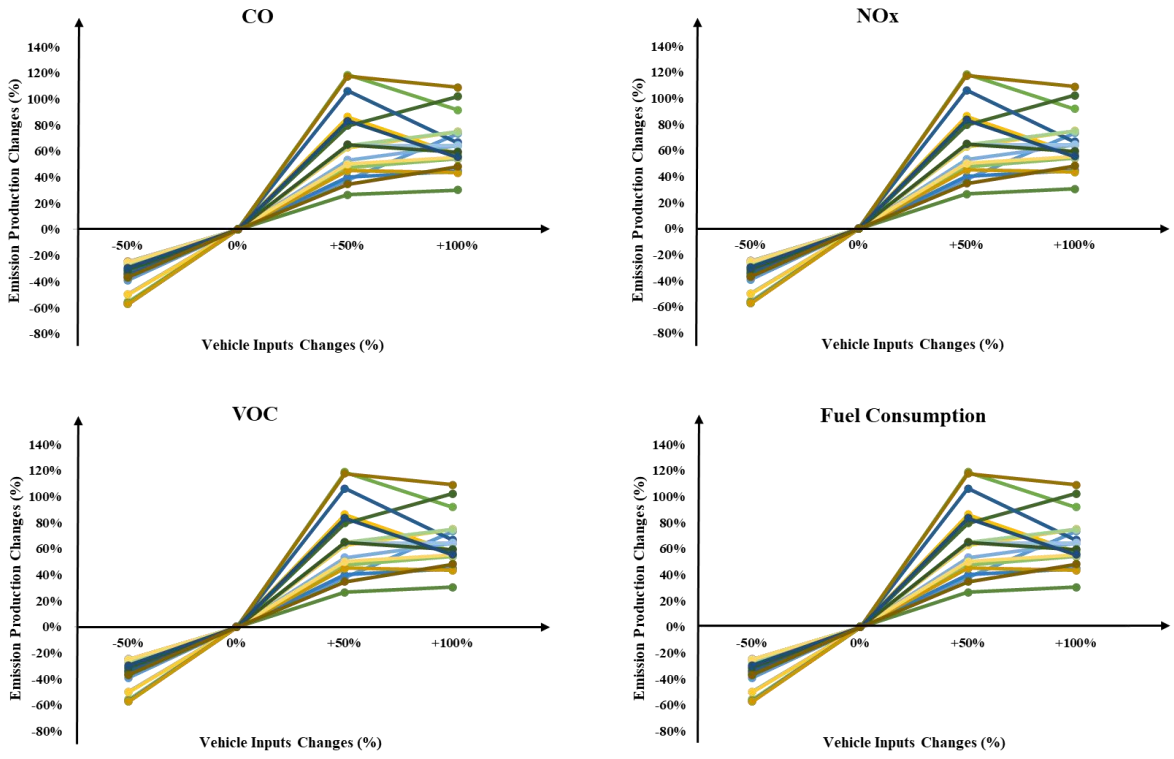

Figure 5-1. The emissions sensitivity to the input vehicles deviations in 18 scenarios

As shown in Figure 5-1, expectedly, the direction of changes in emission generation and vehicle input variations conformed to the traffic modeling logic in all scenarios. Based on the

observations during the simulation runs, increasing the vehicle inputs by 50% completely blocked the individuals' movements in the network. This blockage resulted in preventing the remained traffic inputs from entering the transportation network, which caused a trivial reduction in exhaust emissions production within the network by a 100% increase in vehicle inputs.

Sterman also recommended another verification test named the "Extreme Condition Test" to assess the simulation models' response to the extreme conditions in the system [192]. Based on the definition, the individuals in the system will experience a full-blockage traffic condition during the extreme conditions, which significantly increases the congestion during the simulation run. These conditions were also applied to all traffic microsimulation models designed in VISSIM. For this purpose, one of the main roads, heading to the Trento Central Train Station, was chosen as the primary road for the full-blockage. After blocking the main vehicle output, traffic oversaturation was observed in all upstream roads after some minutes passed the simulation's beginning time. Figure 5-2 demonstrates the total emission deviations in the extreme condition tests. The trend shown in Figure 5-2 was also repeated for the fuel consumption deviations.

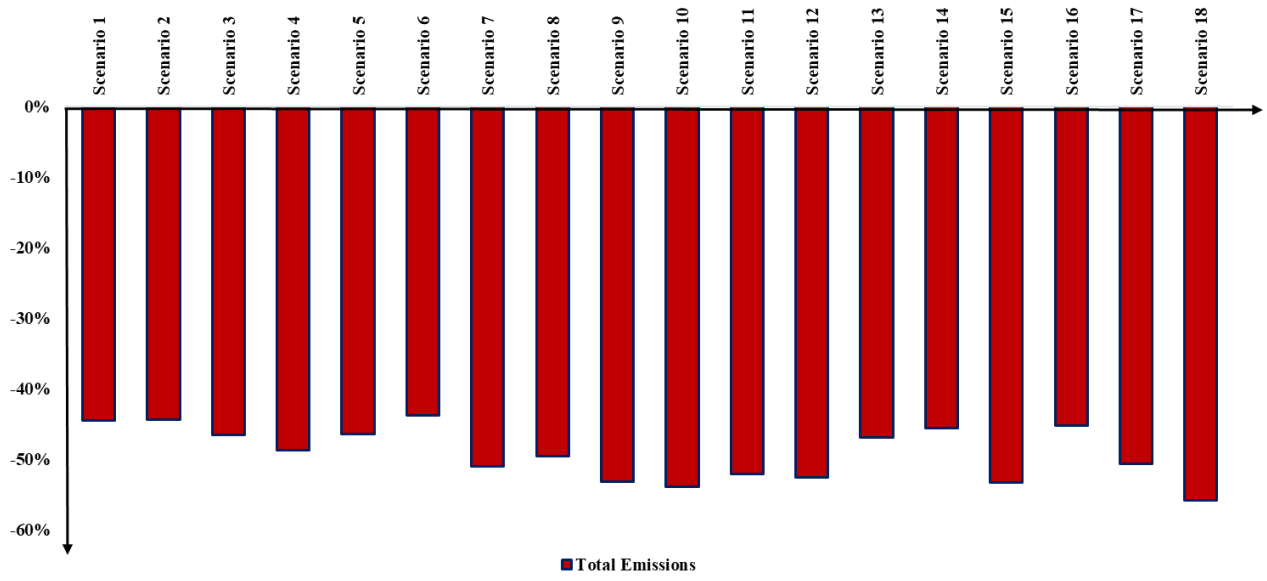

Figure 5-2. Total emission deviations in the blockage test

Same as in the previous verification test, after the complete oversaturation through the network, many vehicles could not find a vacancy to begin their journey during the simulation

run, which, in turn, caused a remarkable reduction in the total exhaust emission generation and fuel consumption. As shown in Figure 5-2, conducting the extreme conditions in all scenarios resulted in a more than 40% reduction in exhaust emission production compared to normal conditions.

Moreover, as recommended by Banks et al. [193], the obtained results in all scenarios were verified by the experts familiar with the system conditions for verification of simulation reasonability.

5.1.2. Emissions and Fuel Consumption Results

In this section of the present dissertation, the amount of dominant exhaust emission, including CO, NOx, and VOC, and fuel consumption rates in the whole network were estimated using 18 simulation models in VISSIM. Table 5-1 shows the average vehicle emission of these three exhaust emissions achieved in the 18 adopted scenarios during the peak hours, together with their corresponding standard deviations. Based on the observations in Table 5-1, vehicles produced a high level of CO emissions compared to the other exhaust emissions. However, the amount of generated NOx and VOC is relatively similar. Moreover, the least amount of emission generation in Scenario 13 (LV40-HV30, No HV increase) resulted in minimal CO, NOx, and VOC emissions with approximately 9931, 1887, and 2248 grams, respectively. In contrast, Scenario 3 (LV60-HV50, 40% HV increase) creates maximal CO, NOx, and VOC emissions with approximately 14974, 2914, and 3470 grams, respectively. It can be concluded that considering the simultaneous impacts of speed and HV contribution can increase almost 50% the emission generation in the congested areas.

Table 5-1. Estimated average vehicle emissions and fuel consumption and their corresponding standard deviations in the 18 adopted scenarios

	CO (gram)	STD	NOx (gram)	STD	VOC (gram)	STD	FC (liter)	STD
Scenario 1	14355.76	2009.27	2793.11	390.93	3327.09	465.67	777.43	108.81
Scenario 2	14666.26	2204.17	2853.52	428.85	3399.05	510.84	794.25	119.37
Scenario 3	14973.90	2470.59	2913.38	480.69	3470.35	572.58	810.91	133.80
Scenario 4	14908.02	2631.15	2900.56	511.93	3455.08	609.79	807.34	142.49
Scenario 5	14842.19	2903.49	2887.75	564.91	3439.82	672.91	803.78	157.24
Scenario 6	14765.82	2508.22	2872.89	488.01	3422.12	581.30	799.64	135.83
Scenario 7	12068.38	1933.47	2348.07	376.18	2796.96	448.10	653.56	104.71
Scenario 8	12250.38	1611.69	2383.48	313.58	2839.14	373.52	663.42	87.28
Scenario 9	12311.78	1562.98	2395.43	304.10	2853.37	362.24	666.74	84.64
Scenario 10	12356.71	1637.18	2404.17	318.54	2863.79	379.43	669.17	88.66
Scenario 11	12552.45	1611.19	2442.25	313.48	2909.15	373.41	679.77	87.25
Scenario 12	12376.85	1250.50	2408.09	243.30	2868.46	289.81	670.26	67.72
Scenario 13	9698.86	992.14	1887.05	193.03	2247.81	229.94	525.24	53.73
Scenario 14	9930.59	1090.36	1932.13	212.14	2301.51	252.70	537.79	59.05
Scenario 15	10135.67	1333.67	1972.03	259.48	2349.04	309.09	548.89	72.23
Scenario 16	10212.32	1389.47	1986.95	270.34	2366.80	322.02	553.04	75.25
Scenario 17	10122.60	1003.53	1969.49	195.25	2346.01	232.58	548.18	54.35
Scenario 18	10328.28	1067.53	2009.51	207.70	2393.68	247.41	559.32	57.81

5.1.3. Vehicles' speed and HV effects

To better understand the effects of simultaneously considering vehicle speed and HV percentage on NOx and VOC emission generations, bar charts were implemented on all results obtained by the 18 scenarios, as represented in Figure 5-3. Expectedly, the main contributor to the changes in emission generation is the vehicle speed imposing significant emission changes while increasing. In the first view, the VOC emission showed higher generation rates than NOx emission in all scenarios. Based on the results presented in Figure

5-3, the generation of NOx and VOC emissions can be increased up to approximately 20% by a 10 km/h augmentation in the LV ad HV speed limits. In contrast, the increase of the HV percentage at the same speed does not seem to produce a significant change in the NOx and VOC emissions. In order to understand the impact of the HV percentage on the NOx and VOC emissions, the compatibility tests (t-test) were conducted on all scenario sets presented in Figure 5-3. The null hypothesis in the t-tests was considered as the mean of the sets, whereas the alternative hypothesis was associated with the different mean of the high HV rate sets. Based on these assumptions, no rejection of the null hypothesis was observed among all the scenario pairs due to the significant p-values (p-values >> 0.05). These tests confirmed that the HV% does not influence the NOx and VOC emissions remarkably.

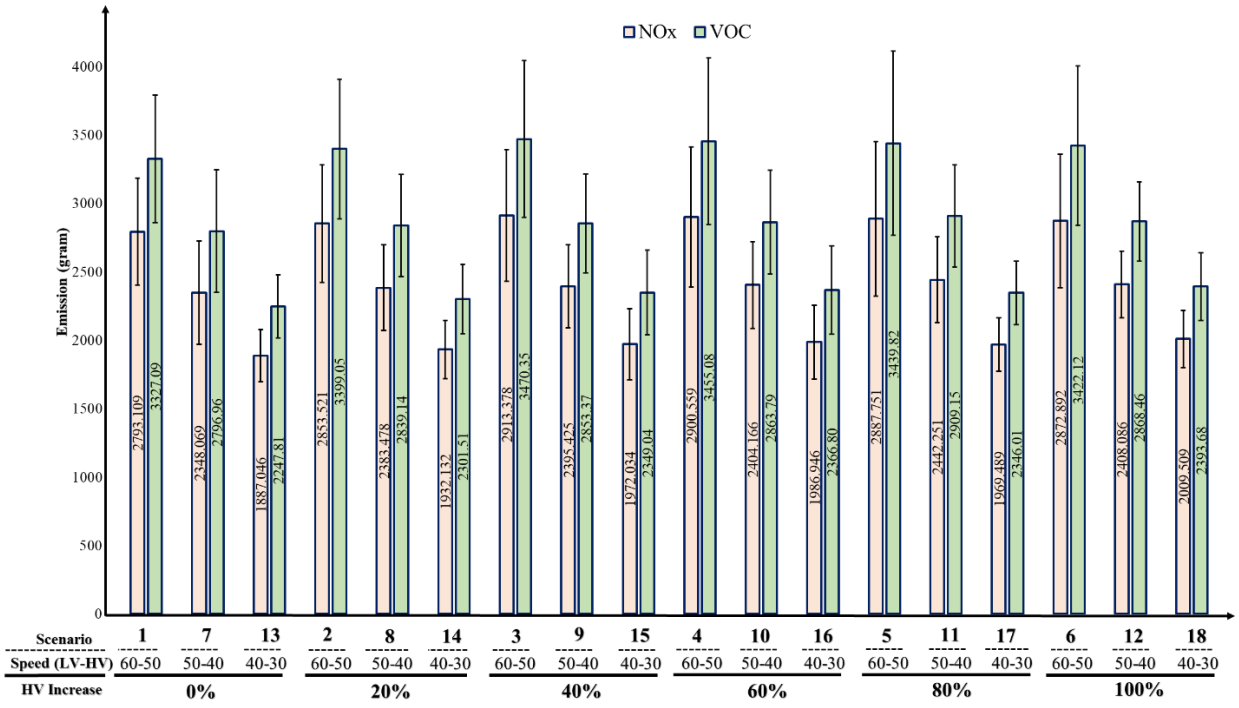

Figure 5-3. NOx and VOC emission results in various scenarios regarding HV contribution

5.1.4. CO Emission and Fuel consumption

Regarding the detrimental effects of fuel consumption on the economy and environment, the rate of fuel consumption in the case study was also estimated in this dissertation, besides the emission predictions using the VISSIM simulation package. The results of the CO

emission prediction and fuel consumption estimation in all 18 scenarios are presented in Figure 5-4.

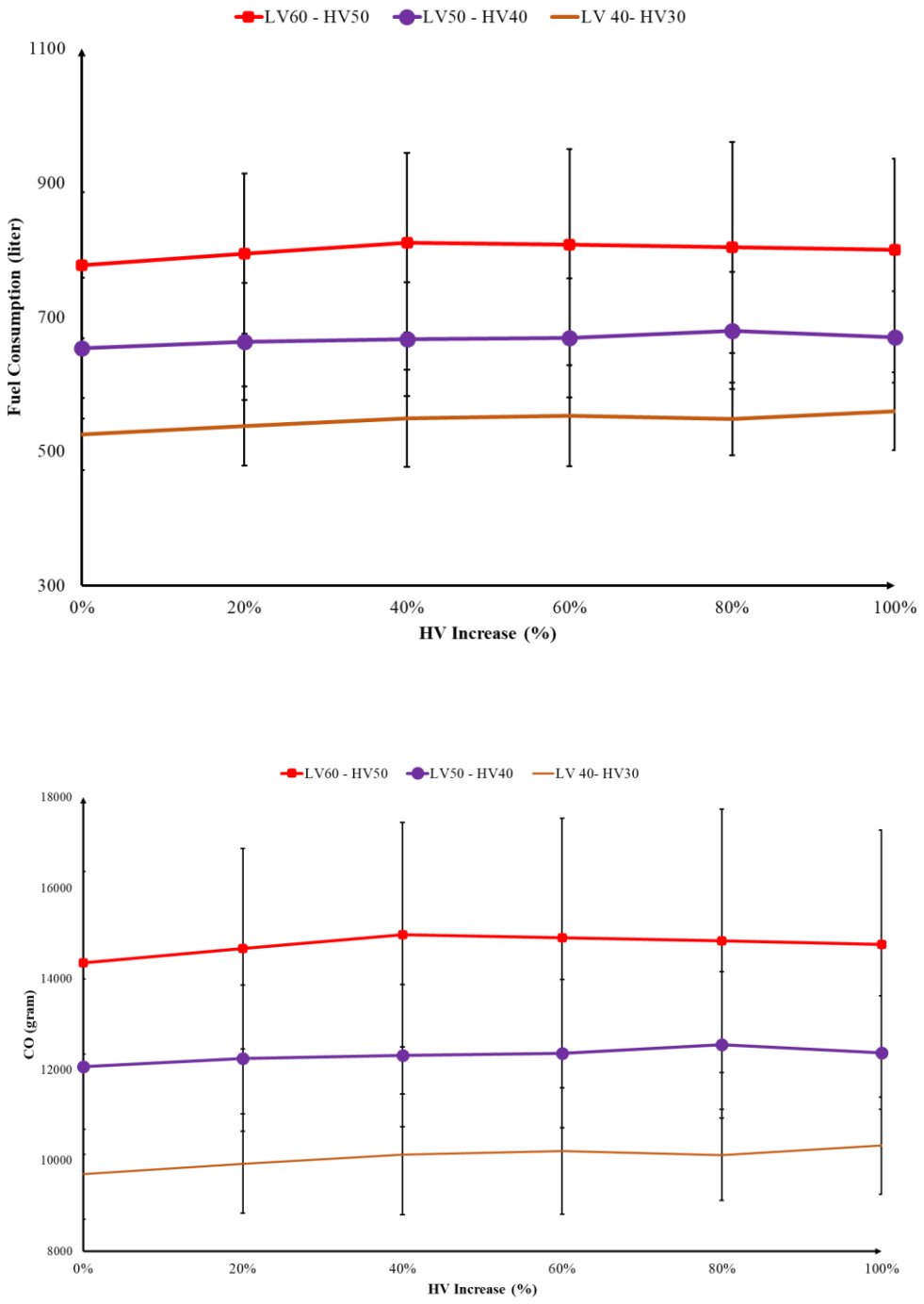

Figure 5-4. CO and fuel consumption fluctuations in various scenarios regarding HV contribution

A reasonably linear dependence of fuel consumption and CO emission on the vehicle speed can be seen in Figure 5-4. Based on the findings, a 20 km/h increase in HV speed (30

km/h to 50 km/h) can increase the emitted amount of CO emission and the fuel consumption rate up to approximately 33%. The sensitivity of CO emission generation to HV% changes was assessed using the compatibility tests (t-test) conducted on all scenario sets. Similar to section "5.1.3", no rejection of the null hypothesis was observed among all the scenario pairs, except one pair which tested scenario 13 (HV increase = 0%, LV–HV speed = 40-30 km/h) with scenario 18 (HV increase = 100%, LV–HV speed = 40-30 km/h) with a p-value equal to 0.021. As all pairs of the comparison showed large p-values (more than 0.05), making them compatible with each other, this "violation of the rule" is not a strong alert. Thus, this violation can be negligible. To sum up, based on the observations on traffic microsimulation results, the HV percentage fluctuations cannot affect considerable changes in the fuel consumption and overall emissions released by urban vehicles in congested areas.

5.1.5. Amount of emission per seat

The effects of heavy vehicles on emission generation can also be evaluated based on the index "Emission per seat". This index is also beneficial to a better understanding of emission detrimental effects on the network users. The number of seats in a transportation network is specified according to the fleets' capacity to transfer users. In the case study chosen in this dissertation, five, thirty, and two available seats were considered as the seating capacity of LVs, HVs, and motorcycles, respectively. Every seat is representative of a single user of the network. Regarding the different configurations of HV percentage for each scenario, the number of seats may vary scenario-by-scenario. Table 5-2 represents the results of emission per seat calculations in detail.

Table 5-2. Emission results per seat

	Number of Seats	CO (gram)	CO per seat	NOx (gram)	NOx per seat	VOC (gram)	VOC per seat
Scenario 1	36921	14355.76	0.3888	2793.11	0.0757	3327.09	0.0901
Scenario 2	38326	14666.26	0.3827	2853.52	0.0745	3399.05	0.0887
Scenario 3	39701	14973.90	0.3772	2913.38	0.0734	3470.35	0.0874
Scenario 4	41106	14908.02	0.3627	2900.56	0.0706	3455.08	0.0841
Scenario 5	42446	14842.19	0.3497	2887.75	0.0680	3439.82	0.0810
Scenario 6	43821	14765.82	0.3370	2872.89	0.0656	3422.12	0.0781
Scenario 7	36921	12068.38	0.3269	2348.07	0.0636	2796.96	0.0758
Scenario 8	38326	12250.38	0.3196	2383.48	0.0622	2839.14	0.0741
Scenario 9	39701	12311.78	0.3101	2395.43	0.0603	2853.37	0.0719
Scenario 10	41106	12356.71	0.3006	2404.17	0.0585	2863.79	0.0697
Scenario 11	42446	12552.45	0.2957	2442.25	0.0575	2909.15	0.0685
Scenario 12	43821	12376.85	0.2824	2408.09	0.0550	2868.46	0.0655
Scenario 13	36921	9698.86	0.2627	1887.05	0.0511	2247.81	0.0609
Scenario 14	38326	9930.59	0.2591	1932.13	0.0504	2301.51	0.0601
Scenario 15	39701	10135.67	0.2553	1972.03	0.0497	2349.04	0.0592
Scenario 16	41106	10212.32	0.2484	1986.95	0.0483	2366.80	0.0576
Scenario 17	42446	10122.60	0.2385	1969.49	0.0464	2346.01	0.0553
Scenario 18	43821	10328.28	0.2357	2009.51	0.0459	2393.68	0.0546

As shown in Table 5-2, the total number of seats increases by HV% augmentation in the case of similar speed limitations. By increasing the number of seats, the "emission per seat" index will be reduced as the seat is placed in the denominator. Consequently, increasing the number of heavy vehicles in congested areas reduces the emissions inhaled by potential passengers. According to the findings presented in Table 5-2, a 20 km/h reduction in speed limits, together with a 100% increase in HV%, can reduce the emission per seat by up to 40%, meaning the passengers inhale much less pollution in the network. In the case of a 10 km/h reduction in vehicle speeds, while HV% is doubled, the emission per seat index can reduce up to 27% (compare Scenarios 1 and 12). In conclusion, the vehicle speed limit holds a higher

contribution in exhaust emission production and fuel consumption compared to the HV percentage.

5.1.6. Average Vehicle Speed

Analyzing the condition of traffic congestion and its effects on average vehicle speed is also another indispensable indicator for comparing different traffic models. Enviver, directly derived from the TNO vehicle emission model VERSIT+, is a well-known emission modeler available in the market. Enviver can use the VISSIM outputs (sync with VISSIM as an adds-in) to analyze the emission and speed conditions in the networks based on the user attributes. In the present dissertation, this software was used for analyzing the average vehicle's speed during peak hours. Figure 5-5 represents the estimated average speed of vehicles in different parts of Buonconsiglio Castle in the 18 scenarios. As shown in Figure 5-5, increasing HV percentage in the network didn't show significant differences in the average speed of vehicles during the peak hour.

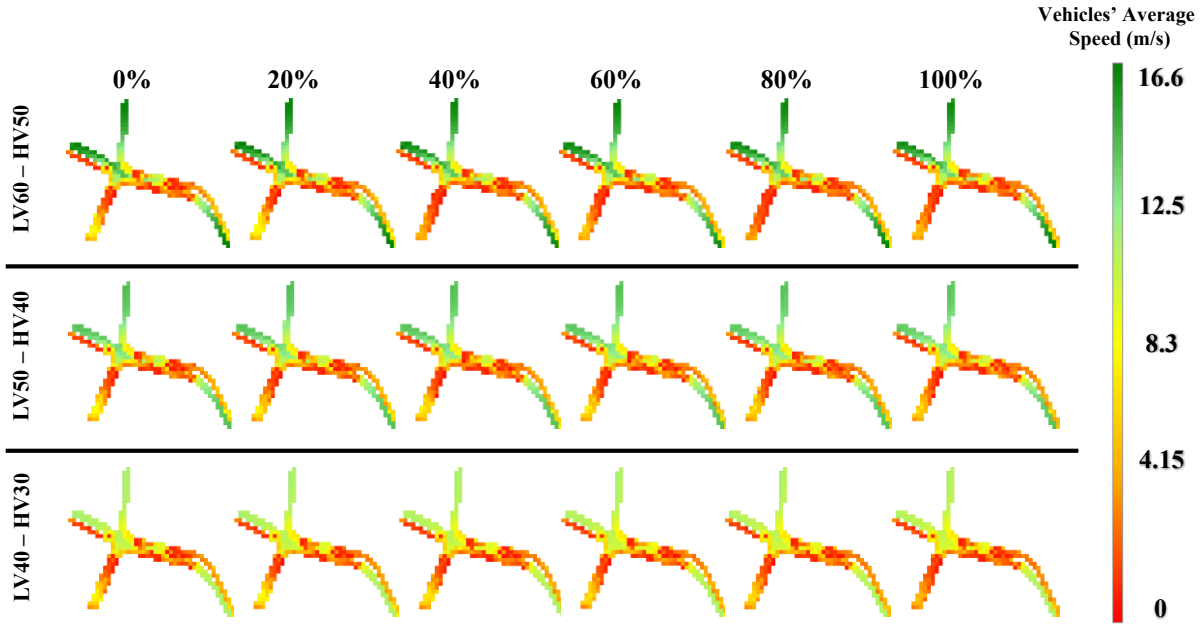

Figure 5-5. Average vehicle speed around Buonconsiglio Castle during the peak hour for different scenarios

Table 5-3 and Table 5-4 present the average speeds of LVs and HVs, respectively, based on their route decision in every scenario configuration, which was obtained by repeating

each scenario in VISSIM 10 times. All the speed values in both Table 5-3 and Table 5-4 have the unit of (km/hr).

Table 5-3. Average speeds of LVs in km/h for every scenario at each route in 10 iterations

	Route A		Route B		Route C		Route D		Route E		Route F	
	Speed	STD	Speed	STD	Speed	STD	Speed	STD	Speed	STD	Speed	STD
Scenario 1	45.31*	4.33	56.26	8.48	35.60	13.80	16.73	2.71	49.85	14.08	31.17	13.90
Scenario 2	44.98	4.45	56.10	8.48	36.27	6.56	17.18	5.45	48.92	16.06	31.03	13.94
Scenario 3	45.03	4.39	56.16	8.55	35.33	6.87	17.33	5.41	48.81	16.27	31.47	13.32
Scenario 4	44.83	4.50	55.71	9.10	37.51	10.44	16.22	6.43	51.66	12.85	30.46	14.49
Scenario 5	44.18	4.42	55.02	9.14	34.39	11.82	15.83	6.71	51.54	13.05	30.77	14.00
Scenario 6	44.29	4.40	55.66	8.82	36.41	11.69	15.67	6.71	51.52	13.04	31.72	12.77
Scenario 7	41.77	3.37	47.73	9.47	40.09	9.51	15.69	2.31	47.25	4.17	29.83	11.53
Scenario 8	41.73	3.34	47.19	9.67	37.78	9.74	16.02	2.93	46.32	5.30	30.33	10.71
Scenario 9	41.37	3.49	47.06	9.73	36.04	9.61	16.91	3.67	43.94	11.24	29.45	12.39
Scenario 10	41.37	3.49	46.95	9.76	36.91	7.87	15.71	4.69	43.87	11.57	29.87	12.13
Scenario 11	41.10	3.33	47.63	9.57	37.04	8.17	16.25	4.21	43.96	11.22	29.67	12.48
Scenario 12	41.21	3.35	47.52	9.51	36.06	9.60	16.10	4.13	43.83	11.16	29.61	12.59
Scenario 13	35.26	3.39	38.77	6.64	35.63	3.93	15.66	4.53	39.77	2.60	28.47	8.67
Scenario 14	34.94	3.97	36.77	8.63	34.52	4.71	15.91	4.16	39.70	2.61	28.14	9.54
Scenario 15	35.09	3.87	38.22	7.31	35.14	4.72	15.98	4.12	37.04	8.93	27.43	11.02
Scenario 16	35.15	3.82	38.42	7.28	33.25	5.79	14.80	5.33	37.06	7.36	27.29	10.02
Scenario 17	34.87	3.72	35.19	11.35	33.44	5.99	14.96	4.71	37.10	7.38	27.44	10.00
Scenario 18	34.89	3.64	38.04	7.12	33.27	6.25	15.10	4.65	38.90	3.28	28.53	9.28

* Approximately 3.5 million vehicle records at each iteration

Table 5-4. Average speeds of HVs in km/h for every scenario at each route in 10 iterations

	Route A		Route B		Route C		Route D		Route E		Route F	
	Speed	STD	Speed	STD	Speed	STD	Speed	STD	Speed	STD	Speed	STD
Scenario 1	23.58	14.40	23.31	16.41	25.64	16.54	8.64	3.94	28.89	16.79	22.84	16.98
Scenario 2	23.42	13.90	21.17	14.56	25.58	16.90	7.91	3.35	27.04	17.23	21.82	15.66
Scenario 3	27.49	14.85	22.92	14.97	26.99	15.84	7.57	3.41	27.67	18.62	27.69	16.38
Scenario 4	27.33	14.93	22.86	15.01	27.23	15.67	8.55	3.87	34.28	19.44	28.81	15.45
Scenario 5	29.22	14.80	25.84	13.86	25.91	13.86	8.04	2.82	33.96	21.52	28.21	15.38
Scenario 6	28.86	14.52	26.36	15.02	26.79	14.67	8.52	2.88	35.34	21.06	24.67	15.82
Scenario 7	19.97	11.29	21.31	13.70	29.35	9.37	8.60	4.46	25.52	13.77	21.21	14.72
Scenario 8	23.97	12.22	19.59	12.08	25.90	11.19	8.85	4.75	26.29	14.26	18.97	15.02
Scenario 9	24.42	11.53	21.15	12.65	26.37	11.05	8.57	4.28	26.74	14.89	24.87	13.62
Scenario 10	24.44	11.51	21.07	12.70	25.74	11.09	9.70	5.25	28.04	14.66	22.80	12.23
Scenario 11	25.45	12.32	21.52	12.56	24.97	11.84	10.18	5.09	28.35	15.69	23.12	12.64
Scenario 12	22.38	12.22	24.39	13.17	25.65	12.65	10.40	4.94	29.37	15.01	21.86	12.12
Scenario 13	18.87	8.30	15.65	8.56	24.31	8.04	8.48	4.14	20.27	9.97	15.09	10.97
Scenario 14	20.62	8.74	15.68	6.75	22.62	9.34	7.37	1.85	20.24	10.49	15.40	11.29
Scenario 15	21.09	8.10	17.04	7.97	23.19	9.22	7.13	1.89	20.36	11.27	21.72	10.37
Scenario 16	19.89	8.51	16.88	7.99	21.78	8.22	7.37	2.47	23.25	11.07	21.75	10.52
Scenario 17	21.70	8.01	17.43	7.78	23.50	7.56	7.36	2.53	23.22	11.70	21.58	10.35
Scenario 18	21.68	8.09	21.98	8.85	23.06	7.28	7.57	2.48	24.81	9.96	21.03	10.10

5.2. Brake Emissions

5.2.1. Total number of unique targeted vehicles

The number of brake wears, and their intensity unconditionally depends on the driving conditions every targeted vehicle experiences in the system. Vehicles may confront the red light signal timing, forcing them to start braking either continuously or intermittently to stop the vehicle behind the crosswalk. The intensity of their brake operation can be related to their initial speed, acceleration, road conditions, and the distance to the previously-stopped vehicle. The total number of released brake emissions during brake operations can be varied

on the vehicles' route decisions. For this purpose, assessing the total number of unique targeted vehicles in the transportation network is essential, which is presented in Table 5-5.

Table 5-5. Total number of unique targeted vehicles at each route per iteration

	Route A	Route B	Route C	Route D	Route E	Route F
Iteration 1	90	36	68	21	19	9
Iteration 2	80	31	38	21	25	7
Iteration 3	79	35	56	12	23	12
Iteration 4	71	37	67	25	19	9
Iteration 5	80	39	58	23	32	6
Iteration 6	85	39	55	18	22	10
Iteration 7	66	29	51	22	18	4
Iteration 8	78	44	68	19	24	7
Iteration 9	86	29	55	20	20	6
Iteration 10	81	33	65	22	17	9
Average	79.6	35.2	58.1	20.3	21.9	7.9
STD	7.01	4.83	9.43	3.53	4.43	2.33

5.2.2. Total number of brake events

VISSIM microsimulation output dataset was used as the source of activity information of targeted vehicles. Regarding the presence of a saturated signalized intersection in the case study, most targeted vehicles in the network recorded various brake operations following their route. The recorded brake events differed in duration, initial speed, final speed, and deceleration. To collect the real brake particles, all the regenerative brakes, in which vehicles used the engine as an alternative tool to brake cooperatively, were dropped from the total number of brakes. To avoid calculating negligible emission particles, all the brake events with the velocity drop less than 5 km/h ($\Delta V < 5\, km/h$) were dropped from the dataset. Finally, the total number of acceptable brake events at each route were acquired as presented in Table 5-6.

Table 5-6. Total number of brake events at each route per iteration

	Route A	Route B	Route C	Route D	Route E	Route F
Iteration 1	117	37	83	27	19	9
Iteration 2	99	32	52	26	25	7
Iteration 3	101	37	67	17	23	12
Iteration 4	92	37	85	33	19	9
Iteration 5	99	42	65	34	32	6
Iteration 6	109	39	70	22	22	10
Iteration 7	83	29	62	36	18	4
Iteration 8	96	45	76	26	25	7
Iteration 9	104	29	66	29	20	6
Iteration 10	97	33	84	29	17	9
Average	99.7	36	71	27.9	22	7.9
STD	9.23	5.29	10.82	5.70	4.50	2.33

To earn a better insight about the velocity fluctuation during a real vehicle trajectory, an example of the velocity time history of a targeted vehicle in the simulation model is presented in Figure 5-6. This example shows a vehicle stuck behind the signalized intersection during its journey. As shown in Figure 5-6, the main factor imposing significant impacts on emission generation during the brake operation is the initial speed.

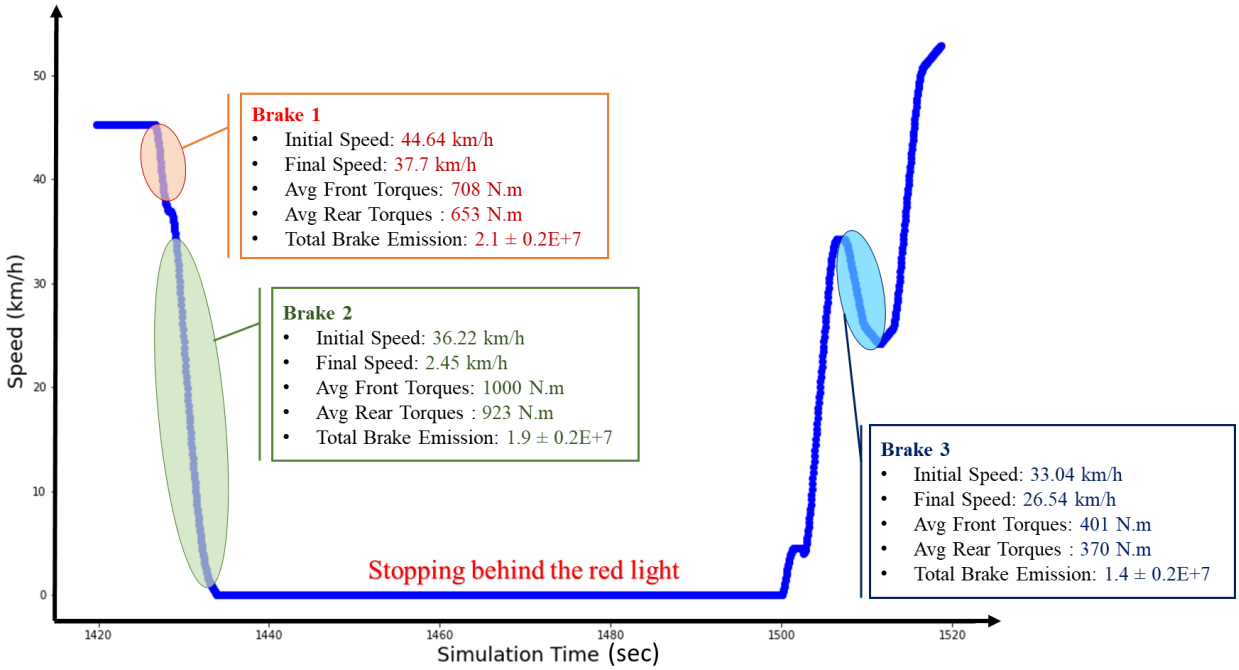

Figure 5-6. An example of a vehicle trajectory with the number of brakes, initial and final speeds, and emitted emissions

In the present dissertation, the emission measurement uncertainty was used to determine the uncertainties of the artificial neural network model's predictions. The iterations of the traffic microsimulation models were considered as the main source of dispersion of the emission estimations as they showed significantly higher values of standard deviations of the overall emission (on the order of 10^8 particles) compared to the prediction uncertainty of brake emissions obtained by minidyno (on the order of 10^6 particles).

5.2.3. Distribution of key quantities in measured and simulated data

In order to improve the accuracy and reliability of the ANN emission model, the distribution of key quantities (for the Route A as an example), i.e., initial speed, final speed, front and rear braking torques, obtained by the experimental minidyno tests and the VISSIM simulation models, were compared in Figure 5-7.

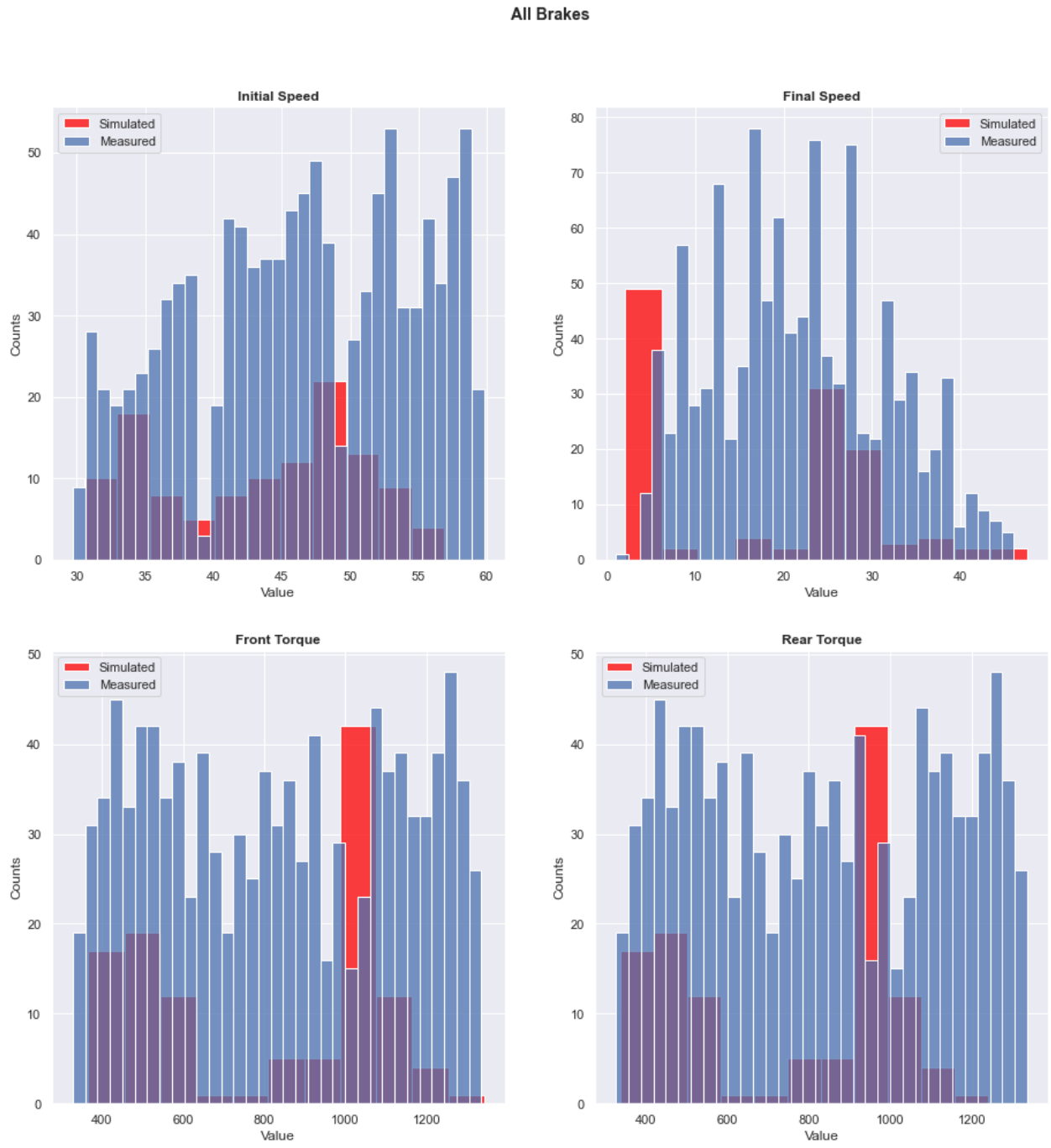

Figure 5-7. Distribution of key quantities in measured and simulated data

The observations showed that the measured and simulated data of the key quantities for the Route A overlapped to a great extent, which remarkably increased the training scores.

5.2.4. Total number of generated brake wear particles at each route

The total number of brake emissions generated by the targeted vehicles at each route was calculated in 10 iterations and presented in Table 5-7. The statistical analyses of results for

each route, including average, standard deviation, skewness, kurtosis, minimum, maximum, and all quartile intervals, were also presented in Table 5-7.

Table 5-7. Total number of brake wear emissions at each route for every iteration

	Route A	Route B	Route C	Route D	Route E	Route F
Iteration 1	2.52E+09	9.97E+08	1.80E+09	4.90E+08	3.38E+08	2.45E+08
Iteration 2	2.26E+09	9.01E+08	1.11E+09	5.16E+08	4.26E+08	1.50E+08
Iteration 3	2.17E+09	1.05E+09	1.45E+09	2.37E+08	4.63E+08	2.95E+08
Iteration 4	1.93E+09	9.28E+08	1.79E+09	4.54E+08	5.34E+08	2.05E+08
Iteration 5	2.24E+09	1.07E+09	1.44E+09	5.45E+08	5.85E+08	1.45E+08
Iteration 6	2.24E+09	1.09E+09	1.43E+09	3.15E+08	4.20E+08	2.70E+08
Iteration 7	1.90E+09	8.25E+08	1.33E+09	5.74E+08	3.64E+08	8.20E+07
Iteration 8	2.06E+09	1.28E+09	1.67E+09	4.66E+08	8.81E+08	1.50E+08
Iteration 9	2.36E+09	6.75E+08	1.40E+09	4.85E+08	5.04E+08	1.44E+08
Iteration 10	2.12E+09	8.78E+08	1.69E+09	3.93E+08	2.89E+08	2.20E+08
Average	2.18E+09	9.69E+08	1.51E+09	4.48E+08	4.80E+08	1.90E+08
STD	1.90E+08	1.66E+08	2.22E+08	1.05E+08	1.67E+08	6.71E+07
Skewness	0.124	0.071	-0.184	-1.018	1.594	0.099
Kurtosis	-0.076	0.578	-0.579	0.490	3.406	-0.893
Min	1.90E+09	6.75E+08	1.11E+09	2.37E+08	2.89E+08	8.20E+07
25%	2.08E+09	8.84E+08	1.40E+09	4.09E+08	3.78E+08	1.46E+08
50%	2.20E+09	9.62E+08	1.44E+09	4.76E+08	4.44E+08	1.77E+08
75%	2.26E+09	1.07E+09	1.68E+09	5.10E+08	5.26E+08	2.39E+08
Max	2.52E+09	1.28E+09	1.80E+09	5.74E+08	8.81E+08	2.95E+08

As presented in Table 5-7, Route A accounts for the highest generation of brake emissions with an average of 2.18E+09 (±1.9E+08) particles in the peak hour. The maximum number of generated particles was also observed in Route A with 2.52E+09 particles. As the least number of brake events happened in Route F, it showed the least number of generated brake particles with an average of 1.9E+08 (±6.71E+07) particles in the peak hour.

To illustrate the density distribution based on the vehicles route decision, the Kernel Density Estimator (KDE) was also implemented in this dissertation. Figure 5-8 demonstrates

the KD estimation of brake wear emissions considering route decisions over histograms of results to determine the distribution shape better and have a continuous distribution view.

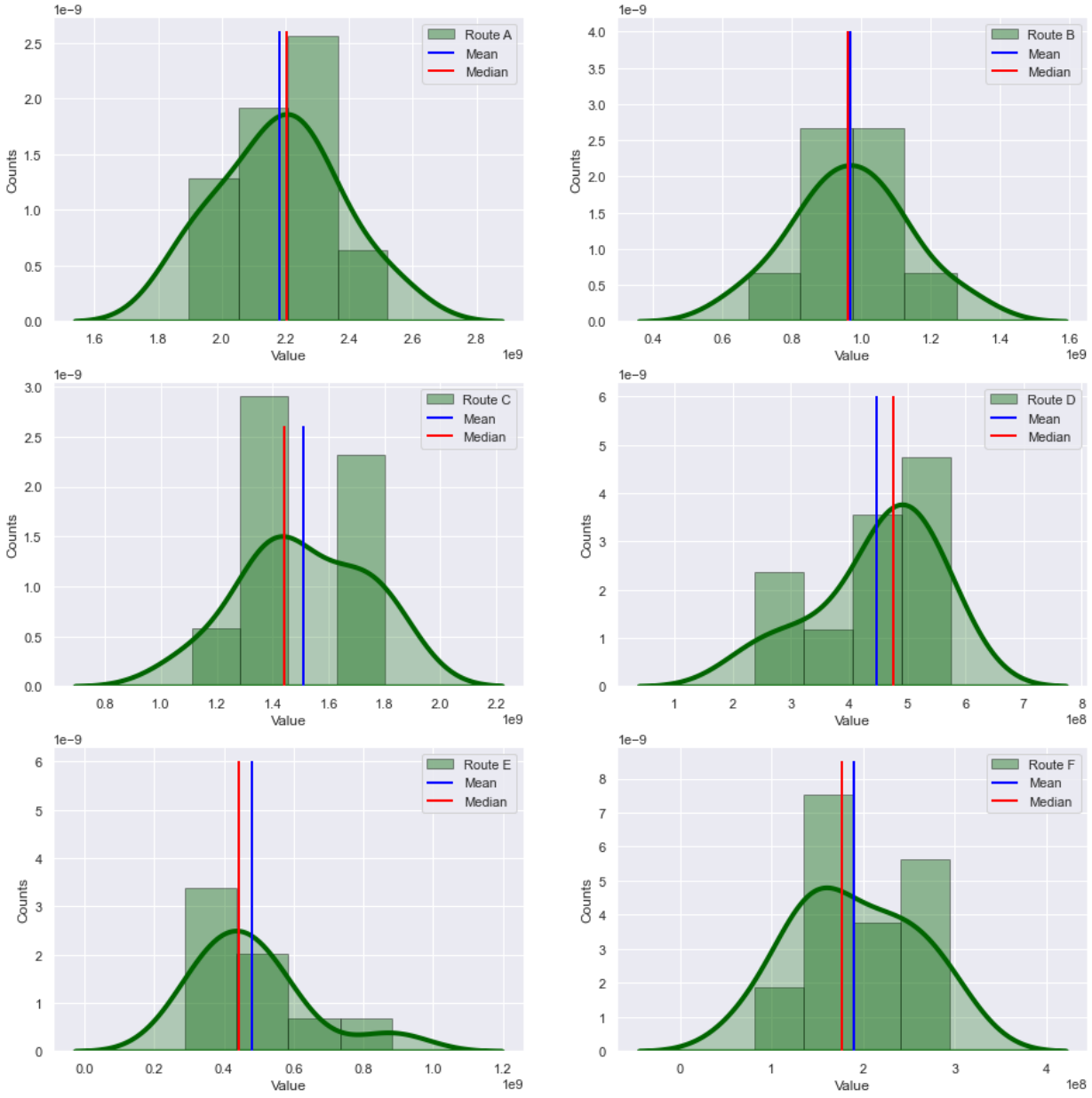

Figure 5-8. Kernel Density estimation of brake wear emissions for each route

The fair equality of means and medians over the route-oriented results can be deducted from Figure 5-8 as in plots, the concentration of brake emission results can be observed in the middle of intervals (in almost all routes). However, the Route D results showed a median value more significant than the mean value due to the right-skewed density curve. To better understand the medians and distributional characteristics of each route, box plots were represented in Figure 5-9.

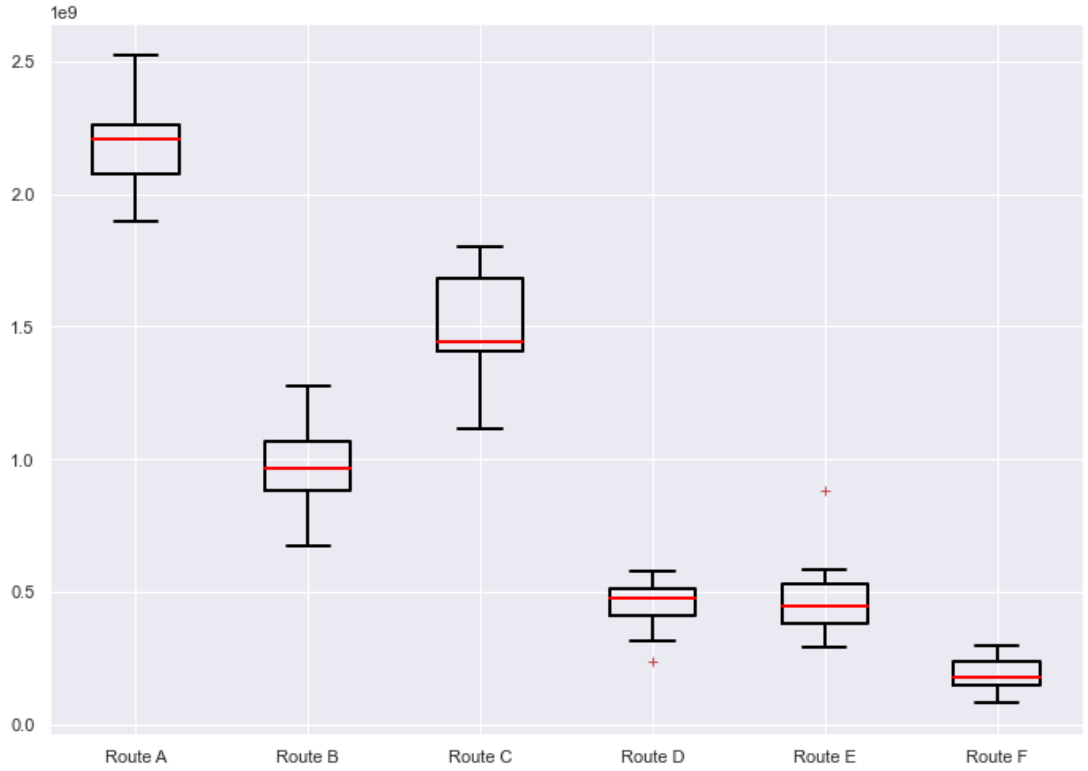

Figure 5-9. Box plot of the total brake wear emissions per route

In the first view, in Figure 5-9, relatively condensed box plots can be observed in all routes except Route C, meaning that the results in these routes are more consistent (vary less). Nevertheless, Route C presents a much greater width of the box plot making the median to be off by quite a bit. Therefore, Route A, B, D, E, and F, with a more consistent total number of brake wear particles, should make predictions more dependable (the box plot is significantly condensed) than the more variable Route C results. Close medians in the Routes D and E results represent a relatively equal number of emitted brake emissions.

5.2.5. Total number of generated brake wear particles in the whole network

The total number of generated brake wear particles in the whole network is one of the essential information for policy-makers, helping them to have better surveillance on brake emission generation in the congested areas. The airborne brake particles released by the targeted vehicles resorting at each route are aggregated and cumulated in the air shaping a big emission bulk above the whole transportation network. Figure 5-10 illustrates the total number of particles emitted by all the targeted vehicles existing in the network in 10 simulation runs.

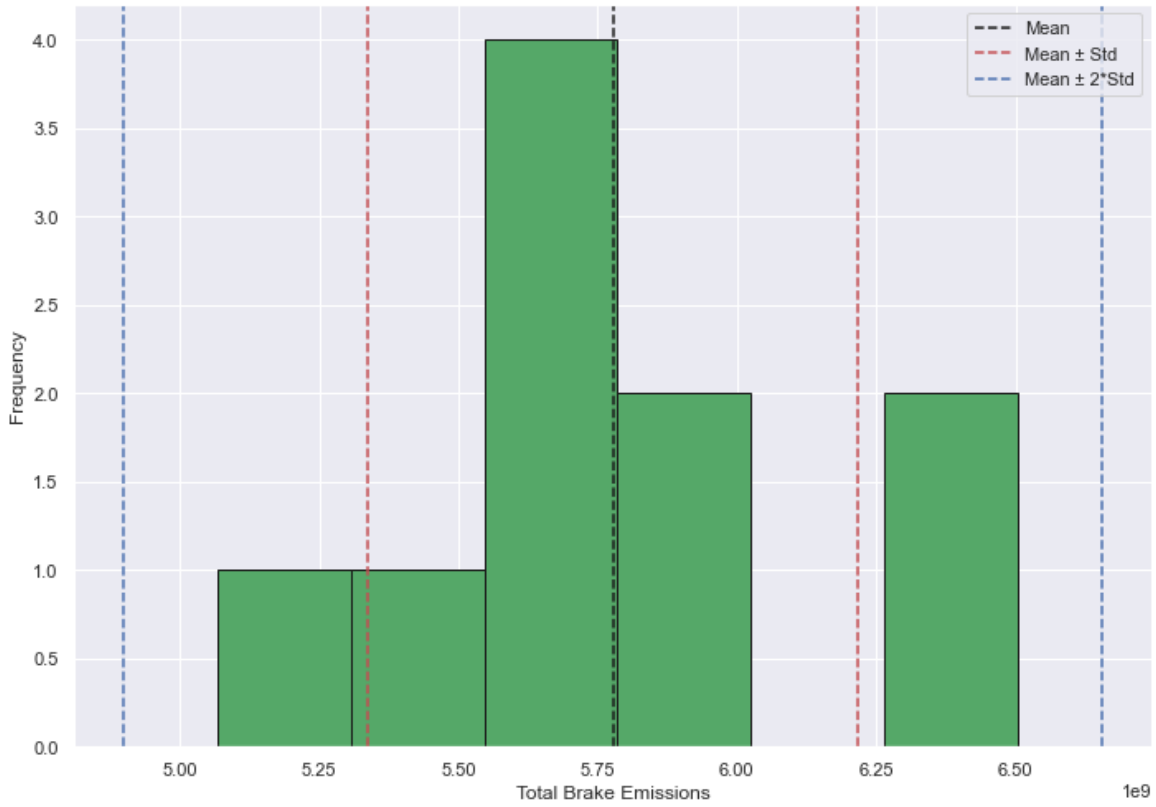

Figure 5-10. Total number of brake wear emissions in the whole transportation network in terms of simulation run

As shown in Figure 5-10, the total number of brake emissions for the 5.75E+09 interval occurs four times out of 10 iterations. Therefore, it has a relative frequency of 40% in the whole emission results. While the total emissions for the 5.06E+09 and 5.36E+09 intervals demonstrated the minimum frequency among all repetitions.

Chapter 6

Conclusions and Future Research

6. Chapter 6: Conclusions and Future Research

6.1. Conclusions

This dissertation presented novel ideas for estimating exhaust and non-exhaust emissions in urban areas. The proposed method was successfully applied to a real case study, Buonconsiglio Castle region and surrounding areas (Trento, Italy) as a congested and sensitive location. For this purpose, at the first step, traffic and non-traffic data collection was implemented in the case study during the peak hours, and the obtained data were filtered and prepared. In order to predict the exhaust and non-exhaust emissions, various levels of investigations were introduced, including the Subsystem Level, System Level, Environmental Level, and Suprasystem Level. Based on the proposed methods considered for each of these approaches, the investigations were implemented at the corresponding investigation level.

In terms of emission prediction, in the first approach, traffic microsimulation models were conducted at the suprasystem level to estimate the generation rate of exhaust emissions and fuel consumption in the case study considering the vehicles' speeds and HV% fluctuations. Considering three different vehicle speeds and increasing the heavy vehicle percentage by 0%, 20%, 40%, 60%, 80%, and 100% shaped 18 different scenarios with various configurations for exhaust emission estimations. Also, a set of verification tests, including extreme conditions and full-blockage tests, were conducted on all scenarios to assess the reliability of the traffic simulation-based models in estimating emission generation in the case study.

The findings of the first approach showed that the effects of vehicle speed and HV% could not be negligible by demonstrating the existing deviations in traffic congestion, emission production, and fuel consumption rate in various configured scenarios. In other words, considering the simultaneous impacts of speed and HV contribution can increase almost 50% of the emission generation in congested areas. Based on the findings, the generation of NOx and VOC emissions can be increased up to approximately 20% by a 10 km/h increase in the vehicles' speed limits. In contrast, the increase of the HV percentage at the same speed did not seem to produce a significant change in the NOx and VOC emissions. Moreover, a 20

km/h increase in vehicles' speed (30 km/h to 50 km/h) can increase the emitted amount of CO emission and fuel consumption rate by up to approximately 33%. Conversely, the HV percentage changes cannot remarkably influence the fuel consumption and overall emissions released by urban vehicles in congested areas, assuming the total vehicle inputs as constant. This trend can happen in other congested areas as well.

Also, in the first approach, the emission per seat index was calculated based on the determined scenarios' configurations. According to the obtained results, the number of potential passengers inhaling detrimental exhaust-origin particles in congested areas is reduced when the HV percentage increases. The emission per seat analysis showed that considering a 100% increase in HV percentage and a 20 km/h decrease in speed limits can reduce this index by up to 40%. In the case of doubling the heavy vehicle percentage and a 10 km/h reduction in vehicle speeds, the emission per seat index can decrease to 27%.

The second approach of this dissertation discussed the brake emission estimation in the case study regarding its momentous role in air pollution generation. Although many previous efforts have been done to estimate the rate of brake emission production using lab-based and on-road experiments, no research in the literature has regarded the implementation of traffic simulation models in non-exhaust emission estimation. Filling this gap was considered the main goal of the present research by proposing an innovative simulation-based approach using traffic models, vehicle dynamics models, and machine learning algorithms. All predictions of brake emissions (in total/route) were implemented on a targeted vehicle, a dominant SUV family car in the case study, in real driving conditions. To achieve this aim, a downstream approach, starting from the traffic microsimulation model (suprasystem level), vehicle dynamic model (system level), and ANN brake emission model trained by more than 1000 experimental tribological tests on a minidyno (subsystem level), was proposed.

Deviations in the production of total brake wear particles in terms of route decisions and simulation repetitions were observed in the findings of the second approach. Moreover, the total number of brake particles in the whole transportation network represented fairly

smooth variations through all repetitions. Also, immense numbers of brake particles (in the order of billion particles) were observed in the case study, which can significantly affect the air quality in the region and existing congested areas. This trend can happen in other congested places as well, where the number of brake events is relatively tangible. In total brake emission estimation, four repetitions out of 10 iterations occurred in the 5.75E+09 interval accounting for 40% of the whole emission results. Also, the maximum number of particles generated by the targeted vehicles in terms of routes was obtained at 2.52E+09, which is a high quantity amount of emission in urban areas.

6.2. Findings Benefits

Providing supplementary information, the findings of this research can be remarkably beneficial for decision-makers to understand the acute adverse effects of emissions on the health of commuters, visitors, tourists, and citizens resorting to congested areas. Indeed, they can tackle the spread of unpredictable diseases caused by motor vehicles using this information and establish more restrictive speed behavior rules in such vulnerable areas. By following the proposed method for such congested areas, traffic engineers and planners will earn better insight into the details of emission estimations in urban areas, which can be helpful for their future considerations and approaches in transport planning.

This dissertation recommends policy-makers establish more restrictions on vehicle speeds around congested areas to control the volume of emission generation, both exhaust, and non-exhaust. Regarding the findings of this research, even a 10 km/h reduction in vehicle speed limitation can significantly decrease the amount of emitted emission, which, in turn, provides a better healthy life for visitors, citizens, and commuters. However, this skimp reduction does not remarkably influence vehicle movements in congested areas.

6.3. Study Limitations and Future Research

The traffic microscopic simulation, vehicle dynamics, and machine learning modeling conducted on minidyno results was a first step towards promoting the real estimation of brake emission in urban areas. By taking the proposed method instead of traditional lab- or on-road experiments for building the emission models and predicting the related emissions,

the process of ground-truth emission estimation with data collected from various urban vehicles would be straightforward and simple. Utilizing different investigation levels enables researchers to build up more realistic emission models by considering all aspects affecting the rate of emission generation. Moreover, the proposed approach is compatible and adaptable not only with vehicle data obtained by simulation models, but also with measured signals of vehicle activities.

The present dissertation opens avenues to use of machine learning techniques for rapid development of simulation-based microscale brake emission models. However, it lacks in a few aspects which could be addressed in future works. The field surveys and traffic data collection was implemented in a sunny day under no extreme weather conditions. Thus, a question worth answering through further research is whether the proposed method is capable of estimating correct emission rates, both exhaust and non-exhaust, or not. Although considering peak hours for traffic investigation is an excellent strategy, the estimation of emission in off-peak hours or day-and-night is recommended to complete the results of this research.

Expanding the size of the minidyno experiments used as the training dataset for building up the ANN model can definitely improve the modeling scores. In addition, it is recommended to build ANN brake emission models based on brake particle diameters (16 channels of the OPS instrument) to create a diameter-based brake emission spectrum. Also, the number of repetitions for the traffic microsimulation models was limited to ten iterations because of time, data volume, and computational constraints. Relaxing some of these limitations could improve the accuracy of the emission estimations.

A possible extension to the current proposed method is to select other vehicles as the targeted vehicle rather than an SUV family car. Such an approach would make new brake emission models, which can be combined with the emission predictions obtained by this research to build a comprehensive brake emissions prediction model.

A touristic congested area in Trento, Italy, was chosen as the case study to investigate the emission quantities. Having a populated region for earning tangible number of brake events

plays an important role in predicting emission generation patterns. Thus, implementing the proposed framework in other congested areas such as hospitals, schools, stop-sign intersections, semi-actuated and actuated signalized intersections, bus terminals, and train stations can supplement the results of this study. In this viewpoint, exploring the results of our proposed method in other cases with totally different traffic behaviors and various geometries (different curvature and inclination) is highly recommended.

7. References

[1] A. Amin, B. Altinoz, and E. Dogan, "Analyzing the determinants of carbon emissions from transportation in European countries: the role of renewable energy and urbanization," *Clean Technol Environ Policy*, vol. 22, no. 8, 2020, doi: 10.1007/s10098-020-01910-2.

[2] D. Eißel and C. P. Chu, "The future of sustainable transport system for Europe," *AI Soc*, vol. 29, no. 3, 2014, doi: 10.1007/s00146-013-0461-3.

[3] T. Mesimeris, N. Kythreotou, G. Partasides, and K. Piripitsi, "Cyprus' draft integrated national energy and climate plan for the period 2021-2030," *Republic of Cyprus*, 2019.

[4] M. J. Sajid, Q. Cao, and W. Kang, "Transport sector carbon linkages of EU's top seven emitters," *Transp Policy (Oxf)*, vol. 80, 2019, doi: 10.1016/j.tranpol.2019.05.002.

[5] R. M. González, G. A. Marrero, J. Rodríguez-López, and Á. S. Marrero, "Analyzing CO2 emissions from passenger cars in Europe: A dynamic panel data approach," *Energy Policy*, vol. 129, 2019, doi: 10.1016/j.enpol.2019.03.031.

[6] W. Yang, W. Wang, and S. Ouyang, "The influencing factors and spatial spillover effects of CO2 emissions from transportation in China," *Science of the Total Environment*, vol. 696, 2019, doi: 10.1016/j.scitotenv.2019.133900.

[7] A. Ghorani-Azam, B. Riahi-Zanjani, and M. Balali-Mood, "Effects of air pollution on human health and practical measures for prevention in Iran," *Journal of Research in Medical Sciences*, vol. 21, no. 5. 2016. doi: 10.4103/1735-1995.189646.

[8] E. O. Ogur and S. M. Kariuki, "Effect of car emissions on human health and the environment," *International Journal of Applied Engineering Research*, vol. 9, no. 21, 2014.

[9] P. G. Kumar, P. Lekhana, M. Tejaswi, and S. Chandrakala, "Effects of vehicular emissions on the urban environment- a state of the art," in *Materials Today: Proceedings*, 2020, vol. 45. doi: 10.1016/j.matpr.2020.10.739.

[10] S. Ali, "New study reveals thousands of deaths prevented thanks to lower vehicle emissions," *The Hill*, 2021. https://thehill.com/changing-america/well-being/longevity/585630-new-study-reveals-thousands-of-deaths-prevented-thanks/#:~:text=Researchers estimated that roughly 17%2C000,year from transportation air pollution.

[11] E. Commission, *Roadmap to a Single European Transport Area: Towards a Competitive and Resource Efficient Transport System: White Paper*. Publications Office of the European Union, 2011.

[12] G. Filer, "Brake Particulate Measuring System for Non-exhaust Emissions in the Context of Euro 7," *ATZ worldwide*, vol. 124, no. 11, pp. 16–19, 2022.

[13] S. Anenberg, J. Miller, D. Henze, and R. Minjares, "A global snapshot of the air pollution-related health impacts of transportation sector emissions in 2010 and 2015," *International Council on Clean Transportation*, 2019.

[14] M. Rahimi, D. Bortoluzzi, and J. Wahlström, "Input parameters for airborne brake wear emission simulations: A comprehensive review," *Atmosphere (Basel)*, vol. 12, no. 7, 2021, doi: 10.3390/atmos12070871.

[15] T. Grigoratos and G. Martini, "Brake wear particle emissions: a review," *Environmental Science and Pollution Research*, vol. 22, no. 4. pp. 2491–2504, 2015. doi: 10.1007/s11356-014-3696-8.

[16] H. Denier van der Gon, J. Hulskotte, M. Jozwicka, R. Kranenburg, J. Kuenen, and A. Visschedijk, "European emission inventories and projections for road transport non-exhaust emissions: analysis of consistency and gaps in emission inventories from EU member states," in *Non-Exhaust Emissions*, 2018. doi: 10.1016/B978-0-12-811770-5.00005-4.

[17] C. Asbach, A. M. Todea, M. Zessinger, and H. Kaminski, "Generation of Fine and Ultrafine Particles During Braking and Possibilities for Their Measurement," 2019. doi: 10.1007/978-3-662-58024-0_10.

[18] P. G. Sanders, N. Xu, T. M. Dalka, and M. M. Maricq, "Airborne brake wear debris: Size distributions, composition, and a comparison of dynamometer and vehicle tests," *Environ Sci Technol*, vol. 37, no. 18, pp. 4060–4069, 2003, doi: 10.1021/es034145s.

[19] B. D. Garg, S. H. Cadle, P. A. Mulawa, P. J. Groblicki, C. Laroo, and G. A. Parr, "Brake wear particulate matter emissions," *Environ Sci Technol*, 2000, doi: 10.1021/es001108h.

[20] M. Fiala and H. M. Hwang, "Development of a Static Model to Identify Best Management Practices for Trace Metals from Non-Exhaust Traffic Emissions," *Environmental Processes*, 2019, doi: 10.1007/s40710-019-00367-w.

[21] J. Wahlström, "Towards a cellular automaton to simulate friction, wear, and particle emission of disc brakes," *Wear*, 2014, doi: 10.1016/j.wear.2014.02.014.

[22] A. Sinha, G. Ischia, C. Menapace, and S. Gialanella, "Experimental characterization protocols for wear products from disc brake materials," *Atmosphere*, vol. 11, no. 10. 2020. doi: 10.3390/atmos11101102.

[23] G. Perricone, V. Matějka, M. Alemani, J. Wahlström, and U. Olofsson, "A test stand study on the volatile emissions of a passenger car brake assembly," *Atmosphere (Basel)*, 2019, doi: 10.3390/atmos10050263.

[24] J. Wahlström, V. Matějka, Y. Lyu, and A. Söderberg, "Contact pressure and sliding velocity maps of the friction, wear and emission from a low-metallic/cast-iron disc brake contact pair," *Tribology in Industry*, 2017, doi: 10.24874/ti.2017.39.04.05.

[25] J. Kukutschová *et al.*, "On airborne nano/micro-sized wear particles released from low-metallic automotive brakes," *Environmental Pollution*, 2011, doi: 10.1016/j.envpol.2010.11.036.

[26] O. Nosko, J. Vanhanen, and U. Olofsson, "Emission of 1.3–10 nm airborne particles from brake materials," *Aerosol Science and Technology*, 2017, doi: 10.1080/02786826.2016.1255713.

[27] M. Alemani, J. Wahlström, and U. Olofsson, "On the influence of car brake system parameters on particulate matter emissions," *Wear*, 2018, doi: 10.1016/j.wear.2017.11.011.

[28] J. Ma, U. Olofsson, Y. Lyu, J. Wahlström, A. H. Åström, and M. Tu, "A Comparison of Airborne Particles Generated from Disk Brake Contacts: Induction Versus Frictional Heating," *Tribology Letters*, vol. 68, no. 1. 2020. doi: 10.1007/s11249-020-1279-z.

[29] S. Lawrence, R. Sokhi, K. Ravindra, H. Mao, H. D. Prain, and I. D. Bull, "Source apportionment of traffic emissions of particulate matter using tunnel measurements," *Atmospheric Environment*, vol. 77. pp. 548–557, 2013. doi: 10.1016/j.atmosenv.2013.03.040.

[30] A. Liati, D. Schreiber, D. Lugovyy, S. Gramstat, and P. Dimopoulos Eggenschwiler, "Airborne particulate matter emissions from vehicle brakes in micro- and nano-scales: Morphology and chemistry by electron microscopy," *Atmospheric Environment*, vol. 212. pp. 281–289, 2019. doi: 10.1016/j.atmosenv.2019.05.037.

[31] A. Paulus, "Investigation of Brake Emissions of Different Brake Pad Materials with Regard to Particle Mass (PM) and Particle Number (PN)." pp. 81–94, 2019. doi: 10.1007/978-3-662-59825-2_11.

[32] J. Wahlström, A. Söderberg, and U. Olofsson, "A cellular automaton approach to numerically simulate the contact situation in disc brakes," *Tribol Lett*, 2011, doi: 10.1007/s11249-011-9772-z.

[33] J. Wahlström, "Towards a simulation methodology for prediction of airborne wear particles from disc brakes." 2009.

[34] J. Kukutschová *et al.*, "Wear mechanism in automotive brake materials, wear debris and its potential environmental impact," *Wear*, vol. 267, no. 5–8. pp. 807–817, 2009. doi: 10.1016/j.wear.2009.01.034.

[35] M. A. S. Mohamed, "Brake features enhancing the wear debris bimodal distribution," *Wear*, vol. 267, no. 9–10. pp. 1525–1533, 2009. doi: 10.1016/j.wear.2009.05.004.

[36] F. H. Farwick zum Hagen *et al.*, "On-road vehicle measurements of brake wear particle emissions," *Atmospheric Environment*, vol. 217. 2019. doi: 10.1016/j.atmosenv.2019.116943.

[37] J. H. Kwak, H. Kim, J. Lee, and S. Lee, "Characterization of non-exhaust coarse and fine particles from on-road driving and laboratory measurements," *Science of the Total Environment*, vol. 458–460. pp. 273–282, 2013. doi: 10.1016/j.scitotenv.2013.04.040.

[38] D. Wakeling, T. Murrells, D. Carslaw, J. Norris, and L. Jones, "The contribution of brake wear emissions to particulate matter in ambient air," *FAT-Schriftenreihe*, no. 301. 2017.

[39] G. Riva, "A methodology to simulate automotive disc brake tribology and emissions." KTH Royal Institute of Technology, 2020.

[40] B. C. Goo, "A study on the contact pressure and thermo-elastic behavior of a brake disc-pad by infrared images and finite element analysis," *Applied Sciences (Switzerland)*, 2018, doi: 10.3390/app8091639.

[41] M. Müller and G. P. Ostermeyer, "A Cellular Automaton model to describe the three-dimensional friction and wear mechanism of brake systems," *Wear*, 2007, doi: 10.1016/j.wear.2006.12.022.

[42] H. Niemann, H. Winner, C. Asbach, H. Kaminski, and M. Zessinger, "Map Based Simulation of Brake Wear Particle Emissions," 2020. doi: 10.46720/eb2020-stp-022.

[43] V. Ricciardi, K. Augsburg, S. Gramstat, V. Schreiber, and V. Ivanov, "Survey on modelling and techniques for friction estimation in automotive brakes," *Applied Sciences (Switzerland)*, 2017, doi: 10.3390/app7090873.

[44] G. P. Ostermeyer, "On the dynamics of the friction coefficient," *Wear*, 2003, doi: 10.1016/S0043-1648(03)00235-7.

[45] F. Philippe *et al.*, "Relevance of pin-on-disc and inertia dynamometer bench experiments for braking emission studies," *Journal of Physics: Conference Series*, vol. 1323, no. 1. 2019. doi: 10.1088/1742-6596/1323/1/012025.

[46] C. Agudelo, R. T. Vedula, and T. Odom, "Estimation of Transport Efficiency for Brake Emissions Using Inertia Dynamometer Testing," in *SAE Technical Papers*, 2018. doi: 10.4271/2018-01-1886.

[47] M. Alemani *et al.*, "Scaling effects of measuring disc brake airborne particulate matter emissions – A comparison of a pin-on-disc tribometer and an inertia dynamometer bench under dragging conditions," *Proceedings of the Institution of Mechanical Engineers, Part J: Journal of Engineering Tribology*, vol. 232, no. 12. pp. 1538–1547, 2018. doi: 10.1177/1350650118756687.

[48] B. S. Joo, Y. H. Chang, H. J. Seo, and H. Jang, "Effects of binder resin on tribological properties and particle emission of brake linings," *Wear*, vol. 434–435. 2019. doi: 10.1016/j.wear.2019.202995.

[49] Y. Lyu, M. Leonardi, J. Wahlström, S. Gialanella, and U. Olofsson, "Friction, wear and airborne particle emission from Cu-free brake materials," *Tribology International*, vol. 141. 2020. doi: 10.1016/j.triboint.2019.105959.

[50] G. Riva, G. Valota, G. Perricone, and J. Wahlström, "An FEA approach to simulate disc brake wear and airborne particle emissions," *Tribology International*, vol. 138. pp. 90–98, 2019. doi: 10.1016/j.triboint.2019.05.035.

[51] L. Wei, Y. S. Choy, C. S. Cheung, and D. Jin, "Tribology performance, airborne particle emissions and brake squeal noise of copper-free friction materials," *Wear*, vol. 448–449. 2020. doi: 10.1016/j.wear.2020.203215.

[52] M. Leonardi, M. Alemani, G. Straffelini, and S. Gialanella, "A pin-on-disc study on the dry sliding behavior of a Cu-free friction material containing different types of natural graphite," *Wear*, vol. 442–443. 2020. doi: 10.1016/j.wear.2019.203157.

[53] H. Yanar, G. Purcek, and H. H. Ayar, "Effect of steel fiber addition on the mechanical and tribological behavior of the composite brake pad materials," *IOP Conference Series: Materials Science and Engineering*, vol. 724, no. 1. 2020. doi: 10.1088/1757-899X/724/1/012018.

[54] C. R. Raghavendra, S. Basavarajappa, and I. Sogalad, "Analysis of temperature field in dry sliding wear test on pin-on-disc," *Heat and Mass Transfer/Waerme- und Stoffuebertragung*, vol. 55, no. 5. pp. 1545–1552, 2019. doi: 10.1007/s00231-018-2524-y.

[55] A. Mohammadnejad, A. Bahrami, M. Goli, H. D. Nia, and P. Taheri, "Wear induced failure of automotive disc brakes-A case study," *Materials*, vol. 12, no. 24. 2019. doi: 10.3390/ma1224214.

[56] Y. Lyu, J. Wahlström, M. Tu, and U. Olofsson, "A friction, wear and emission tribometer study of non-asbestos organic pins sliding against alsic mmc discs," *Tribology in Industry*, 2018, doi: 10.24874/ti.2018.40.02.11.

[57] J. Wahlström, A. Söderberg, L. Olander, U. Olofsson, and A. Jansson, "Airborne wear particles from passenger car disc brakes: A comparison of measurements from field tests, a disc brake assembly test stand, and a pin-on-disc machine," *Proceedings of the Institution of Mechanical Engineers, Part J: Journal of Engineering Tribology*, 2010, doi: 10.1243/13506501JET633.

[58] M. Federici, M. Alemani, C. Menapace, S. Gialanella, G. Perricone, and G. Straffelini, "A critical comparison of dynamometer data with pin-on-disc data for the same two friction material pairs – A case study," *Wear*, 2019, doi: 10.1016/j.wear.2019.02.009.

[59] J. Wahlström, "A study of airborne wear particles from automotive disc brakes," *Engineering*. 2011.

[60] L. Wei, Y. S. Choy, and C. S. Cheung, "A study of brake contact pairs under different friction conditions with respect to characteristics of brake pad surfaces," *Tribol Int*, 2019, doi: 10.1016/j.triboint.2019.05.016.

[61] G. Straffelini, *Friction and Wear: Methodologies for Design and Control*. 2015. doi: 10.1007/978-3-319-05894-8.

[62] J. Wahlström, A. Söderberg, L. Olander, A. Jansson, and U. Olofsson, "A pin-on-disc simulation of airborne wear particles from disc brakes," *Wear*, 2010, doi: 10.1016/j.wear.2009.11.014.

[63] A. P. Gomes Nogueira, D. Carlevaris, C. Menapace, and G. Straffelini, "Tribological and Emission Behavior of Novel Friction Materials," *Atmosphere (Basel)*, vol. 11, no. 10, p. 1050, 2020.

[64] P. Chandra Verma, L. Menapace, A. Bonfanti, R. Ciudin, S. Gialanella, and G. Straffelini, "Braking pad-disc system: Wear mechanisms and formation of wear fragments," *Wear*, 2015, doi: 10.1016/j.wear.2014.11.019.

[65] V. Matějka, I. Metinöz, J. Wahlström, M. Alemani, and G. Perricone, "On the running-in of brake pads and discs for dyno bench tests," *Tribol Int*, 2017, doi: 10.1016/j.triboint.2017.06.008.

[66] D. Plachá *et al.*, "Release of volatile organic compounds by oxidative wear of automotive friction materials," *Wear*, 2017, doi: 10.1016/j.wear.2016.12.016.

[67] H. Barosova *et al.*, "Biological response of an in vitro human 3D lung cell model exposed to brake wear debris varies based on brake pad formulation," *Arch Toxicol*, 2018, doi: 10.1007/s00204-018-2218-8.

[68] G. Riva, G. Perricone, and J. Wahlström, "A multi-scale simulation approach to investigate local contact temperatures for commercial Cu-full and Cu-free brake pads," *Lubricants*, 2019, doi: 10.3390/lubricants7090080.

[69] S. Gramstat, D. Lugovyy, R. Waninger, and M. Schroeder, "Investigations of the Measurement Layout for Brake Particle Emissions," in *SAE Technical Papers*, 2018. doi: 10.4271/2018-01-1885.

[70] C. Menapace, A. Mancini, M. Federici, G. Straffelini, and S. Gialanella, "Characterization of airborne wear debris produced by brake pads pressed against HVOF-coated discs," *Friction*, 2019, doi: 10.1007/s40544-019-0284-4.

[71] J. Wahlström, A. Söderberg, L. Olander, and U. Olofsson, "A disc brake test stand for measurement of airborne wear particles," *Lubrication Science*, 2009, doi: 10.1002/ls.87.

[72] H. Hagino, M. Oyama, and S. Sasaki, "Airborne brake wear particle emission due to braking and accelerating," *Wear*, vol. 334–335. pp. 44–48, 2015. doi: 10.1016/j.wear.2015.04.012.

[73] J. Kukutschová and P. Filip, "Review of Brake Wear Emissions: A Review of Brake Emission Measurement Studies: Identification of Gaps and Future Needs," *Non-Exhaust Emissions*. pp. 123–146, 2018. doi: 10.1016/B978-0-12-811770-5.00006-6.

[74] M. Alemani, O. Nosko, I. Metinoz, and U. Olofsson, "A study on emission of airborne wear particles from car brake friction pairs," *SAE International Journal of Materials and Manufacturing*, 2016, doi: 10.4271/2015-01-2665.

[75] O. Nosko and U. Olofsson, "Quantification of ultrafine airborne particulate matter generated by the wear of car brake materials," *Wear*, 2017, doi: 10.1016/j.wear.2017.01.003.

[76] P. H. S. Tsang, M. G. Jacko, and S. K. Rhee, "Comparison of Chase and inertial brake Dynamometer testing of automotive friction materials," *Wear*, 1985, doi: 10.1016/0043-1648(85)90012-2.

[77] M. G. Jacko and R. T. Ducharme, "Simulation and characterization of used brake friction materials and rotors," in *SAE Technical Papers*, 1973. doi: 10.4271/730191.

[78] M. Kumar and J. Bijwe, "NAO friction materials with various metal powders: Tribological evaluation on full-scale inertia dynamometer," *Wear*, 2010, doi: 10.1016/j.wear.2010.08.011.

[79] F. H. F. zum Hagen *et al.*, "Study of Brake Wear Particle Emissions: Impact of Braking and Cruising Conditions," *Environ Sci Technol*, 2019, doi: 10.1021/acs.est.8b07142.

[80] A. Mamakos, M. Arndt, D. Hesse, and K. Augsburg, "Physical characterization of brake-wear particles in a PM10 dilution tunnel," *Atmosphere (Basel)*, 2019, doi: 10.3390/atmos10110639.

[81] V. Matějka, G. Perricone, J. Vlček, U. Olofsson, and J. Wahlström, "Airborne wear particle emissions produced during the dyno bench tests with a slag containing semi-metallic brake pads," *Atmosphere (Basel)*, vol. 11, no. 11, 2020, doi: 10.3390/atmos11111220.

[82] P. G. Sanders, T. M. Dalka, and R. H. Basch, "A reduced-scale brake dynamometer for friction characterization," *Tribol Int*, 2001, doi: 10.1016/S0301-679X(01)00053-6.

[83] A. E. Anderson, S. Gratch, and H. P. Hayes, "A new laboratory friction and wear test for the characterization of brake linings," in *SAE Technical Papers*, 1967. doi: 10.4271/670079.

[84] M. Kermc, M. Kalin, J. Vižintin, and Z. Stadler, "A reduced-scale testing machine for tribological evaluation of brake materials," *Tribology and Interface Engineering Series*, 2005, doi: 10.1016/s0167-8922(05)80081-1.

[85] A. A. Alnaqi, D. C. Barton, and P. C. Brooks, "Reduced scale thermal characterization of automotive disc brake," *Appl Therm Eng*, 2015, doi: 10.1016/j.applthermaleng.2014.10.001.

[86] M. Kumar and J. Bijwe, "Studies on reduced scale tribometer to investigate the effects of metal additives on friction coefficient - Temperature sensitivity in brake materials," *Wear*, 2010, doi: 10.1016/j.wear.2010.08.012.

[87] Y. Desplanques, O. Roussette, G. Degallaix, R. Copin, and Y. Berthier, "Analysis of tribological behaviour of pad-disc contact in railway braking. Part 1. Laboratory test development, compromises between actual and simulated tribological triplets," *Wear*, 2007, doi: 10.1016/j.wear.2006.07.004.

[88] T. Liu, S. K. Rhee, and K. L. Lawson, "A study of wear rates and transfer films of friction materials," *Wear*, 1980, doi: 10.1016/0043-1648(80)90246-X.

[89] A. J. Burkman and F. H. Hishley, "Laboratory evaluation of brake lining materials," SAE Technical Paper, 1967.

[90] J. Wahlström, A. Söderberg, and U. Olofsson, "Simulation of airborne wear particles from disc brakes," SAE Technical Paper, 2009.

[91] M. J. Han, C. H. Lee, T. W. Park, J. M. Park, and S. M. Son, "Coupled thermo-mechanical analysis and shape optimization for reducing uneven wear of brake pads," *International Journal of Automotive Technology*, 2017, doi: 10.1007/s12239-017-0100-y.

[92] D. P. Vertenten, "Method and apparatus for determining a brake overheating condition." Google Patents, Mar. 07, 2006.

[93] A. Beji *et al.*, "Non-exhaust particle emissions under various driving conditions: Implications for sustainable mobility," *Transp Res D Transp Environ*, 2020, doi: 10.1016/j.trd.2020.102290.

[94] V. Franco, M. Kousoulidou, M. Muntean, L. Ntziachristos, S. Hausberger, and P. Dilara, "Road vehicle emission factors development: A review," *Atmospheric Environment*. 2013. doi: 10.1016/j.atmosenv.2013.01.006.

[95] N. P. Cheremisinoff, "Pollution Management and Responsible Care," in *Waste*, 2011. doi: 10.1016/B978-0-12-381475-3.10031-2.

[96] T. Grigoratos and M. Giorgio, *Non-exhaust traffic related emissions. Brake and tyre wear PM*. 2014. doi: 10.2790/21481.

[97] S. Kim *et al.*, "A comparative study of non-asbestos organics vs. low steel lomets for humidity sensitivity," in *SAE Technical Papers*, 2012. doi: 10.4271/2012-01-1788.

[98] S. W. Kim, S. J. Lee, B. K. Park, and S. K. Rhee, "A comprehensive study of humidity effects on friction, pad wear, disc wear, DTV, brake noise and physical properties of pads," in *SAE Technical Papers*, 2011. doi: 10.4271/2011-01-2371.

[99] L. Chasapidis, T. Grigoratos, A. Zygogianni, A. Tsakis, and A. G. Konstandopoulos, "Study of Brake Wear Particle Emissions of a Minivan on a Chassis Dynamometer," *Emission Control Science and Technology*, 2018, doi: 10.1007/s40825-018-0105-7.

[100] M. Mathissen, T. Grigoratos, T. Lahde, and R. Vogt, "Brake Wear Particle Emissions of a Passenger Car Measured on a Chassis Dynamometer," *Atmosphere (Basel)*, 2019, doi: 10.3390/atmos10090556.

[101] S. Cha, P. Carter, and R. L. Bradow, "Simulation of automobile brake wear dynamics and estimation of emissions," in *SAE Technical Papers*, 1983. doi: 10.4271/831036.

[102] J. Kwak, S. Lee, and S. Lee, "On-road and laboratory investigations on non-exhaust ultrafine particles from the interaction between the tire and road pavement under braking conditions," *Atmos Environ*, 2014, doi: 10.1016/j.atmosenv.2014.08.014.

[103] M. Mathissen, V. Scheer, U. Kirchner, R. Vogt, and T. Benter, "Non-exhaust PM emission measurements of a light duty vehicle with a mobile trailer," *Atmos Environ*, 2012, doi: 10.1016/j.atmosenv.2012.05.020.

[104] D. R. Fitz and C. Bufalino, "Measurement of PM10 emission factors from paved roads using on-board particle sensors," in *US EPA 11th International Emission Inventory Conference*, 2002, vol. 15, no. 18.4, p. 2002.

[105] J. Wahlström and U. Olofsson, "A field study of airborne particle emissions from automotive disc brakes," in *Proceedings of the Institution of Mechanical Engineers, Part D: Journal of Automobile Engineering*, 2015. doi: 10.1177/0954407014550053.

[106] G. Perricone, M. Alemani, J. Wahlström, and U. Olofsson, "A proposed driving cycle for brake emissions investigation for test stand," *Proceedings of the Institution of Mechanical Engineers, Part D: Journal of Automobile Engineering*, 2020, doi: 10.1177/0954407019841222.

[107] C. Puisney *et al.*, "Brake wear (nano)particle characterization and toxicity on airway epithelial cells: In vitro," *Environ Sci Nano*, 2018, doi: 10.1039/c7en00825b.

[108] D. Varrica, F. Bardelli, G. Dongarrà, and E. Tamburo, "Speciation of Sb in airborne particulate matter, vehicle brake linings, and brake pad wear residues," *Atmos Environ*, 2013, doi: 10.1016/j.atmosenv.2012.08.067.

[109] E. Adamiec, E. Jarosz-Krzemińska, and R. Wieszała, "Heavy metals from non-exhaust vehicle emissions in urban and motorway road dusts," *Environmental Monitoring and Assessment*, vol. 188, no. 6. 2016. doi: 10.1007/s10661-016-5377-1.

[110] X. Wang *et al.*, "Real-World Vehicle Emissions Characterization for the Shing Mun Tunnel in Hong Kong and Fort McHenry Tunnel in the United States.," *Res Rep Health Eff Inst*, no. 199, 2019.

[111] M. Abu-Allaban *et al.*, "Exhaust particle size distribution measurements at the Tuscarora Mountain tunnel," *Aerosol Science and Technology*, vol. 36, no. 6, 2002, doi: 10.1080/02786820290038401.

[112] S. Lawrence, R. Sokhi, and K. Ravindra, "Quantification of vehicle fleet PM10 particulate matter emission factors from exhaust and non-exhaust sources using tunnel measurement techniques," *Environmental Pollution*, vol. 210. pp. 419–428, 2016. doi: 10.1016/j.envpol.2016.01.011.

[113] R. M. Harrison, A. M. Jones, J. Gietl, J. Yin, and D. C. Green, "Estimation of the contributions of brake dust, tire wear, and resuspension to nonexhaust traffic particles derived from atmospheric measurements," *Environmental Science and Technology*, vol. 46, no. 12. pp. 6523–6529, 2012. doi: 10.1021/es300894r.

[114] F. Amato *et al.*, "Size and time-resolved roadside enrichment of atmospheric particulate pollutants," *Atmos Chem Phys*, 2011, doi: 10.5194/acp-11-2917-2011.

[115] M. C. Minguillón *et al.*, "Spatial variability of trace elements and sources for improved exposure assessment in Barcelona," *Atmos Environ*, 2014, doi: 10.1016/j.atmosenv.2014.02.047.

[116] G. Omstedt, S. Andersson, L. Gidhagen, and L. Robertson, "Evaluation of new model tools for meeting the targets of the EU Air Quality Directive: A case study on the studded tyre use in Sweden," *Int J Environ Pollut*, 2011, doi: 10.1504/IJEP.2011.047328.

[117] B. R. Denby *et al.*, "A coupled road dust and surface moisture model to predict non-exhaust road traffic induced particle emissions (NORTRIP). Part 2: Surface moisture and salt impact modelling," *Atmos Environ*, 2013, doi: 10.1016/j.atmosenv.2013.09.003.

[118] M. Gustafsson, G. Blomqvist, A. Gudmundsson, A. Dahl, P. Jonsson, and E. Swietlicki, "Factors influencing PM10 emissions from road pavement wear," *Atmos Environ*, 2009, doi: 10.1016/j.atmosenv.2008.04.028.

[119] J. J. Schauer *et al.*, "Characterization of metals emitted from motor vehicles.," *Res Rep Health Eff Inst*, 2006.

[120] D. S. T. Hjortenkrans, B. G. Bergbäck, and A. v. Häggerud, "Metal emissions from brake linings and tires: Case studies of Stockholm, Sweden 1995/1998 and 2005," *Environ Sci Technol*, 2007, doi: 10.1021/es070198o.

[121] A. Wik and G. Dave, "Occurrence and effects of tire wear particles in the environment - A critical review and an initial risk assessment," *Environmental Pollution*. 2009. doi: 10.1016/j.envpol.2008.09.028.

[122] T. Hussein, C. Johansson, H. Karlsson, and H. C. Hansson, "Factors affecting non-tailpipe aerosol particle emissions from paved roads: On-road measurements in Stockholm, Sweden," *Atmos Environ*, 2008, doi: 10.1016/j.atmosenv.2007.09.064.

[123] H. Kuhns, V. Etyemezian, D. Landwehr, C. MacDougall, M. Pitchford, and M. Green, "Testing Re-entrained Aerosol Kinetic Emissions from Roads : A new approach to infer silt loading on roadways," *Atmos Environ*, 2001, doi: 10.1016/S1352-2310(01)00079-6.

[124] V. Etyemezian, H. Kuhns, J. Gillies, M. Green, M. Pitchford, and J. Watson, "Vehicle-based road dust emission measurement: I - Methods and calibration," *Atmos Environ*, 2003, doi: 10.1016/S1352-2310(03)00528-4.

[125] L. Pirjola, K. J. Kupiainen, P. Perhoniemi, H. Tervahattu, and H. Vesala, "Non-exhaust emission measurement system of the mobile laboratory SNIFFER," *Atmos Environ*, 2009, doi: 10.1016/j.atmosenv.2008.08.024.

[126] C. Gunawardana, A. Goonetilleke, P. Egodawatta, L. Dawes, and S. Kokot, "Source characterisation of road dust based on chemical and mineralogical composition," *Chemosphere*, 2012, doi: 10.1016/j.chemosphere.2011.12.012.

[127] R. O. Gonzalez, S. Strekopytov, F. Amato, X. Querol, C. Reche, and D. Weiss, "New Insights from Zinc and Copper Isotopic Compositions into the Sources of Atmospheric Particulate Matter from Two Major European Cities," *Environ Sci Technol*, 2016, doi: 10.1021/acs.est.6b00863.

[128] M. Gustafsson *et al.*, "Inhalable particles from the interaction between tyres, road pavement and friction materials. Final report from the WearTox project," *VTI Rapport*, no. 520, 2005.

[129] K. J. Kupiainen, H. Tervahattu, M. Räisänen, T. Mäkelä, M. Aurela, and R. Hillamo, "Size and composition of airborne particles from pavement wear, tires, and traction sanding," *Environ Sci Technol*, 2005, doi: 10.1021/es035419e.

[130] G. Omstedt, B. Bringfelt, and C. Johansson, "A model for vehicle-induced non-tailpipe emissions of particles along Swedish roads," *Atmos Environ*, 2005, doi: 10.1016/j.atmosenv.2005.06.037.

[131] I. Düring, W. Bächlin, R. Bösinger, W. J. Müller, and A. Lohmeyer, "Experiences when modelling roadside PM10 concentrations," in *Proceedings 9th Int. Conf. on Harmonisation within Atmospheric Dispersion Modelling for Regulatory Purposes, Garmisch-Partenkirchen, Germany*, 2004, pp. 1–4.

[132] I. Düring, J. Jacob, A. Lohmeyer, M. Lutz, and W. Reichenbächer, "Estimation of the 'non exhaust pipe' PM10 emissions of streets for practical traffic air pollution modelling," in *Proceedings of the 11th International Symposium: Transport and Air Pollution*, 2002.

[133] M. Ketzel *et al.*, "Estimation and validation of PM2.5/PM10 exhaust and non-exhaust emission factors for practical street pollution modelling," *Atmos Environ*, 2007, doi: 10.1016/j.atmosenv.2007.09.005.

[134] M. Abu-Allaban, J. A. Gillies, A. W. Gertler, R. Clayton, and D. Proffitt, "Tailpipe, resuspended road dust, and brake-wear emission factors from on-road vehicles," in *Atmospheric Environment*, 2003. doi: 10.1016/j.atmosenv.2003.05.005.

[135] J. Kukkonen, J. Härkönen, A. Karppinen, M. Pohjola, H. Pietarila, and T. Koskentalo, "A semi-empirical model for urban PM10 concentrations, and its evaluation against data from an urban measurement network," *Atmos Environ*, 2001, doi: 10.1016/S1352-2310(01)00254-0.

[136] J. Berger and B. Denby, "A generalised model for traffic induced road dust emissions. Model description and evaluation," *Atmos Environ*, 2011, doi: 10.1016/j.atmosenv.2011.04.021.

[137] M. Norman *et al.*, "Modelling road dust emission abatement measures using the NORTRIP model: Vehicle speed and studded tyre reduction," *Atmos Environ*, 2016, doi: 10.1016/j.atmosenv.2016.03.035.

[138] I. Mawdsley, M. Jerksjö, S. Andersson, J. Arvelius, and G. Omstedt, "New method of calculating emissions from tyre and brake wear and road abrasion." 2015.

[139] L. Gidhagen, H. Johansson, and G. Omstedt, "SIMAIR-Evaluation tool for meeting the EU directive on air pollution limits," *Atmos Environ*, 2009, doi: 10.1016/j.atmosenv.2008.01.056.

[140] A. S. Nagpure, B. R. Gurjar, V. Kumar, and P. Kumar, "Estimation of exhaust and non-exhaust gaseous, particulate matter and air toxics emissions from on-road vehicles in Delhi," *Atmospheric Environment*, vol. 127. pp. 118–124, 2016. doi: 10.1016/j.atmosenv.2015.12.026.

[141] S. Singh, "The demand for road-based passenger mobility in India: 1950-2030 and relevance for developing and developed countries," *EUROPEAN JOURNAL OF TRANSPORT AND INFRASTRUCTURE RESEARCH*, 2006, doi: 10.18757/ejtir.2006.6.3.3448.

[142] Wikipedia, "PTV VISSIM," *Wikipedia*, 2022. https://en.wikipedia.org/wiki/PTV_VISSIM

[143] PTV Group, "PTV Vissim is the tool of choice for top-notch microscopic traffic simulation," *PTV-Group*, 2022. https://your.vissim.ptvgroup.com/comparison-software-for-traffic-simulation

[144] A. Alvanchi, M. Rahimi, and H. Alikhani, "Air pollution concentration near sensitive urban locations: A missing factor to consider in the grade separation projects," *J Clean Prod*, vol. 228, 2019, doi: 10.1016/j.jclepro.2019.04.300.

[145] A. Alvanchi, M. Rahimi, M. Mousavi, and H. Alikhani, "Construction schedule, an influential factor on air pollution in urban infrastructure projects," *J Clean Prod*, vol. 255, p. 120222, May 2020, doi: 10.1016/j.jclepro.2020.120222.

[146] M. Ziemska, "Exhaust emissions and fuel consumption analysis on the example of an increasing number of hgvs in the port city," *Sustainability (Switzerland)*, vol. 13, no. 13, 2021, doi: 10.3390/su13137428.

[147] A. Kocić, N. Čelar, J. Kajalić, and S. Stanković, "Signal timing optimization to minimize fuel consumption," *Put i saobraćaj*, vol. 65, no. 3, 2019, doi: 10.31075/pis.65.03.03.

[148] A. Stevanovic, J. Stevanovic, K. Zhang, and S. Batterman, "Optimizing traffic control to reduce fuel consumption and vehicular emissions: Integrated approach with VISSIM, CMEM, and VISGAOST," *Transp Res Rec*, no. 2128, 2009, doi: 10.3141/2128-11.

[149] PTV Group, "PTV Vissim 2022 User Manual," *Ptv Ag*, 2022.

[150] P. Li, P. Mirchandani, and X. Zhou, "Simulation-based traffic signal optimization to minimize fuel consumption and emission: A Lagrangian relaxation approach," 2015.

[151] W. Li, X. J. Ban, and J. Wang, "Traffic signal timing optimization incorporating individual vehicle fuel consumption characteristics under connected vehicles environment," in *2016 International Conference on Connected Vehicles and Expo, ICCVE 2016 - Proceedings*, 2016. doi: 10.1109/ICCVE.2016.3.

[152] K. CHEN and L. YU, "Microscopic Traffic-Emission Simulation and Case Study for Evaluation of Traffic Control Strategies," *Journal of Transportation Systems Engineering and Information Technology*, vol. 7, no. 1, 2007, doi: 10.1016/S1570-6672(07)60011-7.

[153] K. Salamati, N. M. Rouphail, H. C. Frey, B. Liu, and B. J. Schroeder, "Simplified method for comparing emissions in roundabouts and at signalized intersections," *Transp Res Rec*, vol. 2517, 2015, doi: 10.3141/2517-06.

[154] H. H. Karabag *et al.*, "Estimating the impact of green light optimized speed advisory (Glosa) on exhaust emissions through the integration ofvissim and moves," *Advances in Transportation Studies*, vol. 52, 2020, doi: 10.4399/97888255370311.

[155] H. Abou-Senna and E. Radwan, "VISSIM/MOVES integration to investigate the effect of major key parameters on CO2 emissions," *Transp Res D Transp Environ*, vol. 21, 2013, doi: 10.1016/j.trd.2013.02.003.

[156] H. Abou-Senna, E. Radwan, K. Westerlund, and C. D. Cooper, "Using a traffic simulation model (VISSIM) with an emissions model (MOVES) to predict emissions from vehicles on a limited-access highway," *J Air Waste Manage Assoc*, vol. 63, no. 7, 2013, doi: 10.1080/10962247.2013.795918.

[157] K. Hirschmann, M. Zallinger, M. Fellendorf, and S. Hausberger, "A new method to calculate emissions with simulated traffic conditions," in *IEEE Conference on Intelligent Transportation Systems, Proceedings, ITSC*, 2010. doi: 10.1109/ITSC.2010.5625030.

[158] K. Kraschl-Hirschmann, M. Zallinger, R. Luz, M. Fellendorf, and S. Hausberger, "A method for emission estimation for microscopic traffic flow simulation," in *2011 IEEE Forum on Integrated and Sustainable Transportation Systems, FISTS 2011*, 2011. doi: 10.1109/FISTS.2011.5973625.

[159] R. B. Noland and M. A. Quddus, "Flow improvements and vehicle emissions: Effects of trip generation and emission control technology," *Transp Res D Transp Environ*, vol. 11, no. 1, 2006, doi: 10.1016/j.trd.2005.06.003.

[160] M. Rahimi, D. Bortoluzzi, S. Candeo, F. Biral, and J. Wahlström, "A Novel Approach for Brake Emission Estimation based on Traffic Microsimulation, Vehicle System Dynamics, and Machine Learning Modeling," 2022.

[161] E. Moradi, *A Machine Learning Methodology for Developing Microscopic Vehicular Fuel Consumption and Emission Models for Local Conditions Using Real-World Measures*. McGill University (Canada), 2021.

[162] E. Moradi and L. Miranda-Moreno, "Vehicular fuel consumption estimation using real-world measures through cascaded machine learning modeling," *Transp Res D Transp Environ*, vol. 88, 2020, doi: 10.1016/j.trd.2020.102576.

[163] T. Nasir, B. F. Yousif, S. McWilliam, N. D. Salih, and L. T. Hui, "An artificial neural network for prediction of the friction coefficient of multi-layer polymeric composites in

three different orientations," *Proc Inst Mech Eng C J Mech Eng Sci*, 2010, doi: 10.1243/09544062JMES1677.

[164] L. A. Gyurova, P. Miniño-Justel, and A. K. Schlarb, "Modeling the sliding wear and friction properties of polyphenylene sulfide composites using artificial neural networks," *Wear*, 2010, doi: 10.1016/j.wear.2009.11.008.

[165] A. Nagaraj, D. Shivalingappa, and H. Koti, "Channankaiah," Modelling and predicting adhesive wear behaviour of Aluminium-Silicon Alloy using neural network," *Int J Recent Sci Res*, vol. 3, pp. 378–381, 2012.

[166] C. Ramesh and R. Kumar, "Mathematical and neural network models for prediction of wear of mild steel coated with inconel 718—A comparative study," *International Journal of Scientific and Research Publications*, vol. 2, no. 7, pp. 1–8, 2012.

[167] A. K. F. Hassan and S. Mohammed, "Artificial Neural Network Model for Estimation of Wear and Temperature in Pin-disc Contact," *Universal Journal of Mechanical Engineering*, 2016, doi: 10.13189/ujme.2016.040204.

[168] J. Bao, M. Tong, Z. Zhu, and Y. Yin, "Intelligent tribological forecasting model and system for disc brake," in *Proceedings of the 2012 24th Chinese Control and Decision Conference, CCDC 2012*, 2012. doi: 10.1109/CCDC.2012.6243100.

[169] D. Aleksendrić, "Neural network prediction of brake friction materials wear," *Wear*, 2010, doi: 10.1016/j.wear.2009.07.006.

[170] I. I. Argatov and Y. S. Chai, "An artificial neural network supported regression model for wear rate," *Tribol Int*, vol. 138, 2019, doi: 10.1016/j.triboint.2019.05.040.

[171] M. Gailis and D. Berjoza, "On prediction of motor vehicle brake pad wearout," in *Engineering for Rural Development*, 2012.

[172] H. K. Durmuş, E. Özkaya, and C. Meriç, "The use of neural networks for the prediction of wear loss and surface roughness of AA 6351 aluminium alloy," *Mater Des*, 2006, doi: 10.1016/j.matdes.2004.09.011.

[173] R. G. Song, Q. Z. Zhang, M. K. Tseng, and B. J. Zhang, "The application of artificial neural networks to the investigation of aging dynamics in 7175 aluminium alloys," *Materials Science and Engineering C*, 1995, doi: 10.1016/0928-4931(95)00068-2.

[174] E. AtiK, C. Meriç, and B. Karlik, "Determination Of Yield Strenght of 2014 Aluminium Alloy under Aging Conditions by Means of Artifical Neural Networks Method," *Mathematical and Computational Applications*, 1996, doi: 10.3390/mca1020016.

[175] T. Hariprasad, D. Shivalingappa, A. Nagaraj, and G. Manivasagam, "The use of artificial neural network for the prediction of wear loss of aluminium-magnesium alloys,"

International Journal of Computer Aided Engineering and Technology, 2015, doi: 10.1504/IJCAET.2015.066174.

[176] R. Rajamani, *Vehicle dynamics and control*. Springer Science & Business Media, 2011.

[177] S. Tsiakmakis *et al.*, "From lab-to-road & vice-versa: Using a simulation-based approach for predicting real-world CO2 emissions," *Energy*, vol. 169, 2019, doi: 10.1016/j.energy.2018.12.063.

[178] P. Srinivasan and K. U. M, "Performance fuel economy and CO2 prediction of a vehicle using AVL cruise simulation techniques," in *SAE Technical Papers*, 2009. doi: 10.4271/2009-01-1862.

[179] M. Ehsani, A. Ahmadi, and D. Fadai, "Modeling of vehicle fuel consumption and carbon dioxide emission in road transport," *Renewable and Sustainable Energy Reviews*, vol. 53. 2016. doi: 10.1016/j.rser.2015.08.062.

[180] J. Seo, B. Yun, J. Park, J. Park, M. Shin, and S. Park, "Prediction of instantaneous real-world emissions from diesel light-duty vehicles based on an integrated artificial neural network and vehicle dynamics model," *Science of the Total Environment*, vol. 786, 2021, doi: 10.1016/j.scitotenv.2021.147359.

[181] M. Keller, S. Hausberger, C. Matzer, P. Wüthrich, and B. Notter, "HBEFA Version 3.3," *Background documentation, Berne*, vol. 12, 2017.

[182] J. (Jason) So, N. Motamedidehkordi, Y. Wu, F. Busch, and K. Choi, "Estimating emissions based on the integration of microscopic traffic simulation and vehicle dynamics model," *Int J Sustain Transp*, vol. 12, no. 4, 2018, doi: 10.1080/15568318.2017.1363328.

[183] European Environment Agency (EEA), *Air quality in Europe - 2020 report*, no. No 09/2020. 2020.

[184] Euronews, "Which cities in the European Union are worst for air pollution?," *Euronews*, 2021. https://www.euronews.com/2021/06/17/cities-in-poland-and-italy-rank-bottom-in-europe-for-air-quality

[185] A. de Marco *et al.*, "Impacts of air pollution on human and ecosystem health, and implications for the National Emission Ceilings Directive: Insights from Italy," *Environ Int*, vol. 125, 2019, doi: 10.1016/j.envint.2019.01.064.

[186] UNWTO, "World Tourism Barometer," *UNWTO*, vol. 18, no. 1, 2020.

[187] Statista, "Number of international tourists´ arrivals in the Italian region of Trentino-South Tyrol in 2016, by province," *Statista*, 2016. https://www.statista.com/statistics/703156/international-tourists-arrivals-in-trentino-south-tyrol-by-province-italy/

[188] IQAIR, "Air quality in Trento," *IQAIR*, 2021. https://www.iqair.com/italy/trentino-alto-adige/trento

[189] F. Dalrì, "Smog in città, Trento una delle più inquinate per biossido di azoto," *Trento Today*, 2022. https://www.trentotoday.it/attualita/inquinamento_aria-trento.html#:~:text=Nel capoluogo trentino%2C nel 2021,tre volte il limite previsto.

[190] Provincia Autonoma di Trento, "Monossido di carbonio," *Provincia Autonoma di Trento*, 2022. http://www.appa.provincia.tn.it/aria/qualita_aria_sezione/documentazione_divulgativa_aria/-Inquinanti_principali/pagina23.html

[191] M. Rahimi, D. Bortoluzzi, and F. Biral, "Impacts of Vehicle Speed and Number of Heavy Vehicles on Emissions and Fuel Consumption in Sensitive Locations," *Transp Res Rec*, p. 03611981221137586, Nov. 2022, doi: 10.1177/03611981221137586.

[192] J. D. Sterman, *Systems Thinking and Modeling for a Complex World*, vol. 34, no. 1. 2004.

[193] J. Banks, J. S. Carson II, B. L. Nelson, and D. M. Nicol, *Discrete event system simulation, 5th Edition*, 5th ed. Pearson, 2009.